SOME EFFECTS OF HISTORY ON TURBULENT FLOW.

by

Brian E. Lee , B. Sc.

1969

Thesis submitted to the University of Leicester

for the Degree of Doctor of Philosophy.

ProQuest Number: U622467

All rights reserved

INFORMATION TO ALL USERS
The quality of this reproduction is dependent upon the quality of the copy submitted.

In the unlikely event that the author did not send a complete manuscript
and there are missing pages, these will be noted. Also, if material had to be removed,
a note will indicate the deletion.
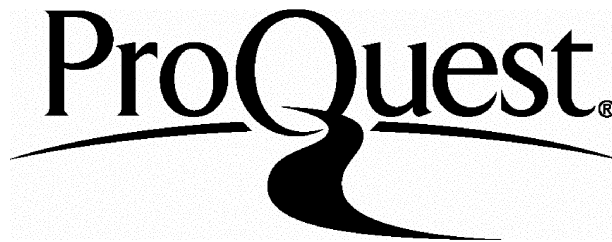
ProQuest U622467

Published by ProQuest LLC(2015). Copyright of the Dissertation is held by the Author.

ProQuest LLC
789 East Eisenhower Parkway
P.O. Box 1346
Ann Arbor, MI 48106-1346

SUMMARY

Few physical phenomena can be adequately described without reference to their histories. This maxim applies not only to the field of experimental engineering but throughout academic disciplines to geography , biology , human relations and almost every sphere of physical activity. With reference to the field of fluid dynamics the interpretation of this statement means that few real flow situations can be described solely in terms of local values and relationships and that the previous history of the flow must be taken into account. An example of this is the work of Cockrell , Diamond and Jones (1) * , who showed that for a given diffuser , the performance varied even though the inlet boundary layer thickness parameters were maintained constant , and inferred that the manner in which the boundary layers had been produced has an appreciable effect on diffuser performance.

This thesis has three major objectives. The first is to use our knowledge of flow history to provide an explanation of the ' overshoot ' phenomenon experienced by the growth of the boundary layer thickness parameters in duct flow. This manifests itself by the manner in which a thickness parameter grows until it reaches a stationary point , whereupon it subsequently decreases.

The second objective is to attempt to expand our knowledge of flow history effects by simulating a mean velocity profile at the duct entry and observing the subsequent development in both this and the turbulence parameters of the flow. This second objective has practical applications in the production of atmospheric boundary layers and other shear flows for the purpose of model

* Figures in brackets refer to reference listing.

testing.

The third objective is to use the experimental results obtain--ed from duct flow in the auxiliary equation of an integral method of boundary layer calculation. This then should provide a realistic allowance for the flow history effects. Since the lack of any allowance of flow history effects is very often a major failing of the use of integral techniques it is possible in this instance to attempt to assess the overall usefulness of such a method.

In addition to these major objectives , appendices are presented on the experimental behaviour of the local relationships, often used in calculation methods , between the turbulent shear stresses and the mean velocity profile. The distributions of these mixing lengths and eddy viscosities are compared with some of the formulations available in the literature.

A description of the experimental facilities is given which includes a section on the use of hot wire anemometers for the measurement of turbulence. Some of the likely sources of error encountered here , together with their possible magnitudes , are also presented.

Acknowledgements.

No man is an island , and clearly the work contained in this thesis has required the help and co-operation of a large number of people.

First and foremost I would like to thank the Science Research Council for its support in 1965/1966 and the University of Leicester subsequent to this. Furthermore , I am grateful to Professor McLellen , Head of the Department of Engineering , for permitting the work to proceed and for his encouragement and help particularly where finance was concerned.

I would like to thank my colleagues , Colin Tory , Colin Bradley , John Moorman , Barry Miller and Ken Haywood for the helpful discussions we have had and for their encouragement.

The technicians are the life blood of any laboratory and my thanks go out to those here who have helped make my ideas possible. To Colin Harris , Rod Smith and Eric Hooley my thanks for their help in the laboratory with many major and minor tasks , to Dick Sexton who produced the anemometer mountings , to the work shop staff and the carpenters for parts of the rig and to the computer assistants for their help with the data reduction programmes. My thanks also to the Drawing Office staff for their help with the design of the wire grid mounting and for the drawings and graphs in this thesis.

To my wife my thanks not only for typing this thesis but for her steadfast support and encouragement throughout the period of my research at Leicester.

Finally and most of all I would like to thank my supervisor

David Cockrell for all he has taught me and for all the help I have had from him since we first met.

CONTENTS

List of Figures.

Notation.

A_1) functions of n defined in Equation (5.2.13.)
B_1)

B width of duct

C_f Coefficient of friction

d diameter of hot wire sensor

D average height of roughness elements

E instantaneous fluctuating voltage output of hot wire anemometer bridge

f Fanning friction factor

F_x Forces acting on the fluid in the x direction

h half height of duct

H height of duct = 2h

H shape factor of velocity profile

head loss in Equation (4.3.3.)

K a constant

ℓ length of active section of hot wire sensor

ℓ_{PR} Prandtl mixing length defined in Equation (A.1.5.)

L duct length from inlet

L_e length of inlet region

n variable parameter in power law velocity profile description

p pressure

$\overline{q^2}$ sum of mean squares of fluctuating velocity components

R hot wire anemometer operating resistance

R_e Reynolds Number

S slope of hot wire anemometer calibration curve

u ,v,w instantaneous fluctuating velocities in the x , y and z directions respectively

u_* friction velocity

U,V,W	local mean velocities in the x,y and z directions respectively
$\bar{U}$	bulk mean velocity
Umax	maximum velocity across duct
V	hot wire anemometer bridge D.C. voltage (Chapter 2)
U_E	effective velocity experienced by a hot wire anemometer
x,y,z	co-ordinate directions , see Fig.2.3.

δ	physical thickness of boundary layer
δ_{95}	boundary layer thickness when U = 95% Umax
δ^{*}	displacement thickness of boundary layer
θ	momentum thickness of boundary layer
τ	shear stress
λ	microscale of turbulence
ρ	density
μ	dynamic viscosity
ϑ	kinematic viscosity
ϵ_m	eddy viscosity

Subscripts

o	wind-off condition in hot wire anemometer equations
r.m.s.	root mean square value
d	conditions in the equilibrium region
w	wall conditions
c	duct centreline conditions
$\delta/2$	conditions halfway across the velocity profile after the inlet region

Since the figures in this thesis have not been converted to Metric Units the following conversion factors may be found useful.

Length 1 foot = 0.305 m

     1 inch = 2.54 cms

Density 1 lb/ft^3 = 16.02 Kg/m^3

Kinematic Viscosity

     1 ft^2/sec = 0.093 m^2/sec

CHAPTER 1.

INTRODUCTION.

1.1. Flow History.

There are probably few physical situations in which history
is not at least partly accountable for the value of any one of
the parameters which describe the system. Although it is often
very much simpler to predict the value of a given quantity in
terms of other parameters describing the system at a given point in
space and time , it is usually only an approximation to do so.
However in a complex physical situation it is difficult enough
to form relationships between local parameters and the problem of
forming relationships for parameters in terms of their histories
is often almost impossible.

This is the situation which exists now in turbulent fluid
flow , particularly in boundary layers. We have a complex physical
situation in which inadequate local relations exist between its
descriptive parameters , also we are aware that the history of
some of these is important , but which ones and in what
circumstances is still uncertain.

One of the basic difficulties in any analysis of turbulent
boundary layer behaviour is the relation of the turbulent shear
stresses to the mean flow. Since most attempts to solve the
turbulent boundary layer problem are based on knowledge concerning
the behaviour of laminar boundary layers , where the shear stress

is linearly related to the derivative of velocity , these attempts
tend to be centred round the assumption that the turbulent stresses
are a function only of the local velocity profile. Using this
assumption and experimental data , the turbulent shear stresses
are then expressed in the form of an eddy viscosity or mixing
length correlated in terms of local properties. However as more
measurements of turbulence become available the assumption of
this form of local relationship is being questioned , since it
appears that the flow history as well as the local mean velocity
profile play a part in determining the shear stress distribution.

In a review of turbulent boundary layer calculation methods
Rotta (2) states , " Actually the shear stress distribution is
also affected by the previous history. No proposals for the shape
parameter equation which make proper allowance for this circumst-
-ance have yet been made. But , at least , one knows now for
certain that the insufficiency of the present calculation methods
originate here , and any attempt at a positive improvement must
start at this point. "

This dependence of the turbulent shear stress distribution
was first found by Jacobs (3) who experimented with flow over
a change in wall roughness. He found the shear stress gradient
in the outer part of the boundary layer retained the value it had
over the previous wall roughness for a considerable distance
after the change , whereas the wall shear stress changed almost
immediately to its new value. This effect has also been found to
be caused by a sudden change in pressure gradient. Physically,
a sudden change in pressure gradient produces a sudden change in
$\frac{\partial U}{\partial x}$ throughout the boundary layer , resulting in a sudden change
in $\frac{\partial U}{\partial y}$, and the rate of production of turbulent energy.

The change in intensity and shear stress then follows. Near the wall the scale of turbulence is small enough for the adjustment to take place almost immediately so that the inner part of the boundary layer is locally in equilibrium. In the outer part of the boundary layer , however , most of the turbulent energy resides in large scale turbulence , which is considered to have a longer lifetime and it is this which is responsible for the slow adjustment of the turbulent intensities and shear stresses.

In the flows in which the dominant factors do not vary significantly in the direction of the flow it is possible to correlate the entire boundary layer distribution in terms of local conditions. However such simple correlations break down when the flow conditions vary. The motions which cause the shear forces originate at the wall and are diffused into the stream by the action of turbulence. As this diffusion occurs relative to the moving fluid , the shear at any point in the boundary layer has its origins at a point on the surface upstream of its present location. Thus the shear stresses in the outer part of the bound- -ary layer are governed by history , whilst near a solid surface local conditions prevail.

1. 2. Scope of the present work.

Arising from this realization that in different flow conditions the flow history will affect the relationship between the mean flow and the turbulence , this thesis attempts to provide answers to the following three questions :-

(i) Is it possible to use what we know about flow history to provide a full explanation of the common two - dimensional duct flow situation ?

(ii) Using Clauser's ' black box ' analogy can we alter one of the inputs to the two - dimensional turbulent boundary layer and use the responses to expand on our ideas of the effects of flow history ?

(iii) Can we find out some of the limitations which the effect of flow history puts on an integral method of boundary layer calculation ?

These questions will be briefly discussed immediately and will be dealt with more deeply in subsequent chapters.

1.2.1. Duct Flows.

The way in which a flow develops down a long , straight , constant cross - section rectangular duct is not as widely documented or understood as one might suppose. Indeed , the very terms used in describing flow regimes in such a duct are widely used to mean different things. The term ' fully developed ' is sometimes taken to mean a duct flow where the boundary layers may , by some criteria , be said to have just met ; whereas in

other cases it is taken to mean a duct flow whose parameters do not change as observations are made further downstream. Sometimes only parameters based on the mean velocity distribution are consi- -dered whilst at other times turbulence parameters are taken into account. The problem which arises when one attempts to say where the boundary layers growing from opposite walls of the duct meet is also confusing. When one considers the knowledge currently available concerning the conditions at the outer edge of the boundary layer it is plainly incorrect to refer to a point where boundary layers meet , but more realistic to refer to a region in which , due to the intermittent nature of the outer flow , the boundary layers meet from time to time. Then as one progresses downstream the value of the intermittency of the flow , (i.e. the fractional time the fluid is non - turbulent) , on the duct centre - line will eventually decrease until only patches of totally enclosed irrotational fluid are accountable. Even to talk about the existence of a potential core composed of irrotat- -ional fluid is occasionally misleading , since in most experimen- -tal rigs the uniform flow region between boundary layers growing on opposite walls often bears a small , but definite amount of turbulence due to honeycombs and grids upstream of the working section.

The published evidence of work on flows in rectangular ducts is confined principally to three topics. First there are those investigations on the nature of the secondary flows in the corners of a rectangular duct. Secondly , work on the way in which the flow develops for a short distance downstream of the entry , and finally those publications dealing with the state of

the flow which the authors claim to be fully - developed. The first topic has been well documented and it is not the intention of this thesis to discuss this work. However there does seem to be a dearth of information about what happens to the flow between the material covered in the second topic and that in the third. It is a common assumption to presume that the governing flow parameters reach their final constant value in the region where the boundary layers meet. We do know though that the shear stress in the outer part of the flow is influenced by history and has its origin at the wall upstream of its present position. Thus in the region where the boundary layers meet , the shear stress may well not yet have reached its final value. It is for this reason that the parameters describing the state of the flow continue to change. This study is developped further in Chapter 3.

1.2.2.   Simulated Flow Conditions.

Clauser (4) has compared the problem of the growth of a turbulent boundary layer to a black box , containing an unknown response system into which a number of inputs can be fed. The outputs from the box then indicate the behaviour of its inner mechanism. As long as the mechanism of the box is hidden from us the only way to become aquainted with its response to any input functions that may be generated is to learn by experience, i.e. to try to correlate the observed output functions with the inputs for a number of examples. Such experimental results should at least enable us to describe the principal properties of the system qualitatively.

If we allow the flow to proceed unimpeded down a rectangular duct then eventually a stable situation will prevail providing there are no changes in wall roughness , cross - sectional geometry or pressure gradient. In this stable flow situation we can then regard the distributions of mean velocity , shear stress , intensity and scale of turbulence as being mutually compatible. If we consider these compatible distributions of parameters as inputs to the turbulent boundary layer , then by reproducing some of them and allowing the others to alter in a known manner we will , by observation of the outputs (i.e. the distribution of parameters at a later stage in the flow's development) , be able to build up a knowledge of the system.

Chapter 4 contains a description of the effects of simulating velocity profiles at the entry to the duct. Four cases are given of different methods of simulation of the mean velocity profile which would occur at the end of the duct if the flow were permitted to develop naturally.

The results of this work are of interest not only for the more basic reasons of understanding the mechanisms of turbulence but because they have a definite practical purpose. The conditions necessary for the simulation of naturally-occuring flows , partic- -ularly the production of atmospheric velocity profiles in which to perform tests on models , are still the subject of debate and good experimental evidence is vital to the formulation of accepted codes of practice.

1.2.3. Turbulent Boundary Layer Calculation.

As we have seen , one of the limiting factors in the succes-
-ful development of turbulent boundary layer calculation methods
is in the use we are able to make of flow history in the formulation
of auxiliary equations. Furthermore , despite recent advances ,
the use of the earlier integral forms of calculation is still
fairly widespread; the drawbacks of integral calculation methods
being more in the physics incorporated into the constituent
equations than in the equations themselves.

It was decided to use an integral calculation method which
by virtue of the particular form of auxiliary equation , incorpora-
-tes both the value of the shear stress at a point halfway across
the boundary layer and the slope of the shear stress at the duct
centreline. Instead of using an equation to describe the behaviour
of the shear stress distribution , use is made of the duct flow
experimental data. In this way it is possible to feed in the true
effects of flow history on the shear stress distribution and
observe their effect on a typical integral calculation method.

This analysis is extended in Chapter 5.

1.2.4. Local Relationships.

Despite their disadvantages (see Batchelor (5) for example)
local relationships between shear stress and mean velocity dist-
-ributions are still in use in calculation methods in the form of
mixing length and eddy viscosity theories. Since the experimental
data was readily available it was considered a useful exercise to

compare the manner in which these local relationships developed
with those formulations in use.   This comparison is presented in
Appendices 1 and 2.

Chapter 2.

Experimental Facilities.

2.1. The Wind Tunnel.

The wind tunnel in which the tests were performed is shown
pictorially in Fig. 2.1 and schematically in Fig. 2.2. The
major criterion for its design was that its maximum overall length
was to be no more than 70 feet , that it was to be powered by a
fan already available and that it was to be produced economically.
The major design was therefore the working length and the inlet
contraction. After some initial difficulties with the design of
the inlet contraction the flow in the working section was shown
to be straight and smooth , and symmetrical , to within 3% ,
both about the x,y and x,z planes. (The co - ordinate system is
shown in Fig. 2.3.) Furthermore the flow was shown to be two -
dimensional for at least $z = H/4$ either side of the y axis even
for maximum sidewall boundary layer growth.

2.1.1. The Working Length.

The fan which would be used to drive the tunnel had a
capacity of approximately 4000 cubic feet per minute and since it
was considered desirable to attain speeds of the order of 200 feet
per second to facilitate ease of velocity measurement , this
limited the cross sectional area to the order of 1/3rd square
feet. Furthermore it was considered that a height of at least 4
inches was necessary to enable measurements to be made near the
wall , and thus the width required was 12 inches. The cross
sectional shape was rectangular since it was desired to produce

Fig. 2.1   The Wind Tunnel

24" DIA.

36" 6" 28" 9" 54" 12" 66" 46' 12" 12" 12" 6" 54"

8" DIA.

4"

¢

MEASURING STATIONS

SILENCER   FAN   ANNULAR   RECTANGULAR DUCT 12" × 4"   INLET CONTRACTION
                  DIFFUSER   6·25:1

FLOW   CANVAS   CHANGE OF
CONTROL   RING   SECTION
VANE   12"×4" to 8" DIA.
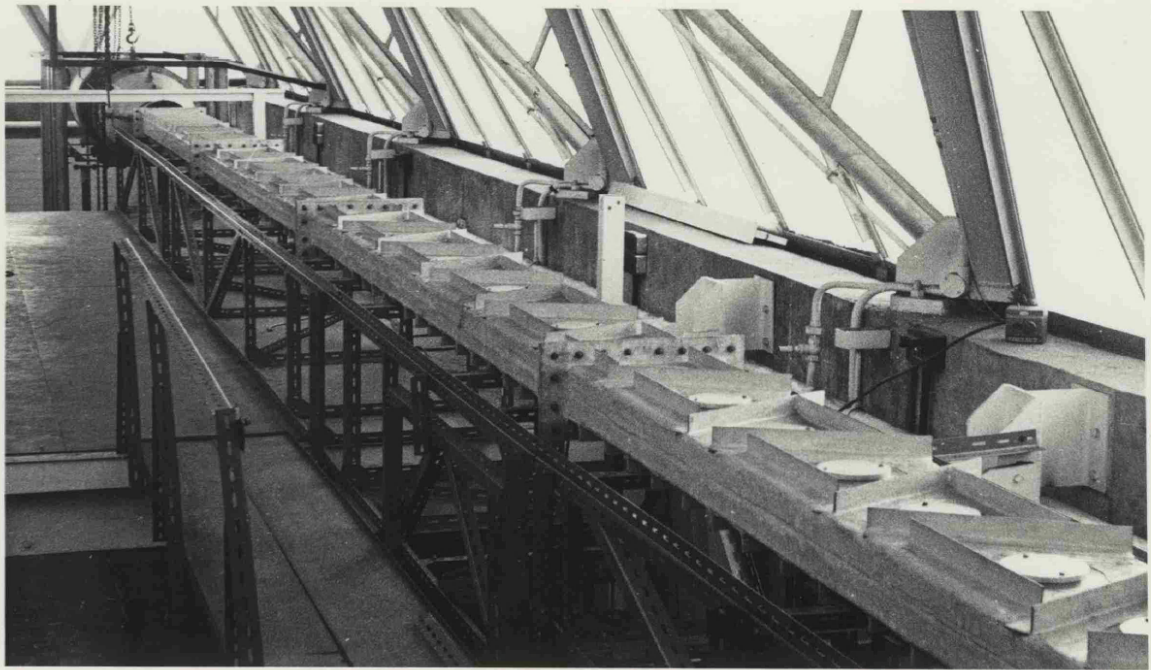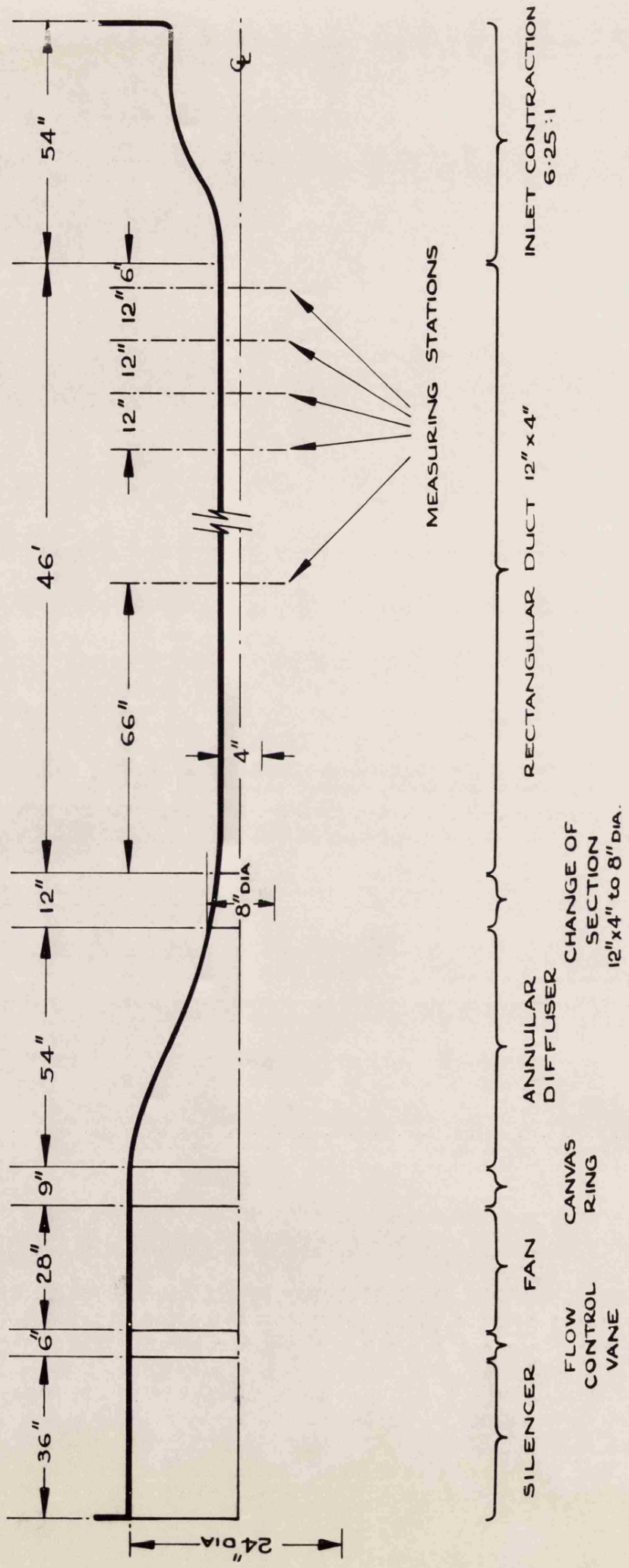
FIG.2.2. WIND TUNNEL
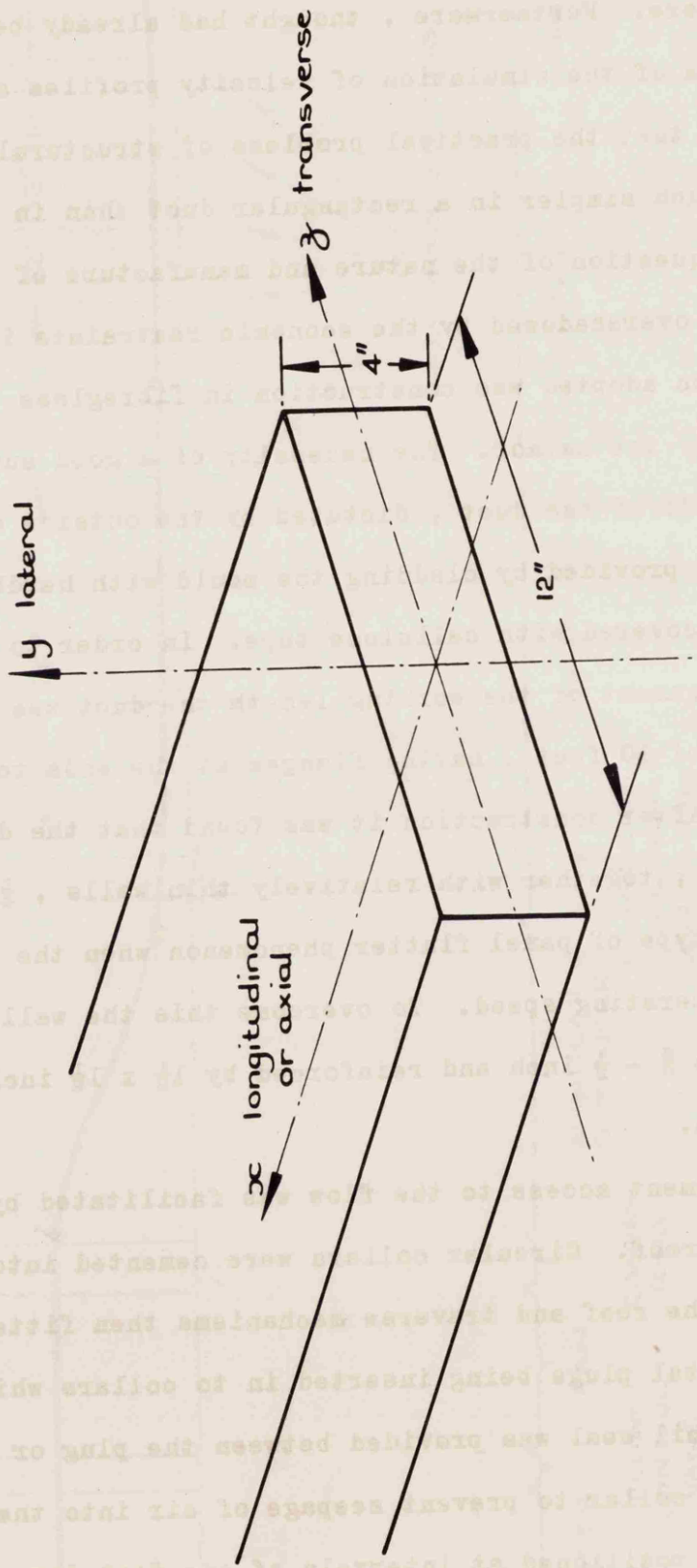
FIG.2.3.CO-ORDINATE SYSTEM FOR DUCT.

results in a two - dimensional flow which could complement results from axisymmetric flow situations being obtained both at Leicester and elsewhere. Furthermore , thought had already been given to the problem of the simulation of velocity profiles and it was considered that the practical problems of structural support would be much simpler in a rectangular duct than in a pipe.

The question of the nature and manufacture of the working length was overshadowed by the economic restraints imposed and the solution adopted was construction in fibreglass to be performed by the author. The necessity of a good surface finish on the inside of the duct , dictated by the outside of the wooden mould , was provided by cladding the mould with hardboard which was itself covered with cellulose tape. In order to ensure correct alignment of the working length the duct was constructed in lengths of 10 feet , having flanges at the ends to be bolted together. After construction it was found that the dimensions of the duct , together with relatively thin walls , $\frac{1}{4}$ inch , produced a type of panel flutter phenomenon when the tunnel was run up to operating speed. To overcome this the walls were thickened to $\frac{3}{8}$ - $\frac{1}{2}$ inch and reinforced by $1\frac{1}{2}$ x $1\frac{1}{2}$ inch slotted angle - iron.

Instrument access to the flow was facilitated by openings in the duct roof. Circular collars were cemented into place flush with the roof and traverse mechanisms then fitted into these collars , metal plugs being inserted in to collars which were not in use. An oil seal was provided between the plug or traverse base and the collar to prevent seepage of air into the duct. The collars were positioned at intervals of one foot down the length,

$Re = 2.86 \times 10^5$

$U_{\overline{C}} = 130 \text{ ft/sec}$

95 105 115 120 125

$U = 125 \text{ ft/sec}$
120
115
105
95

2"

5"
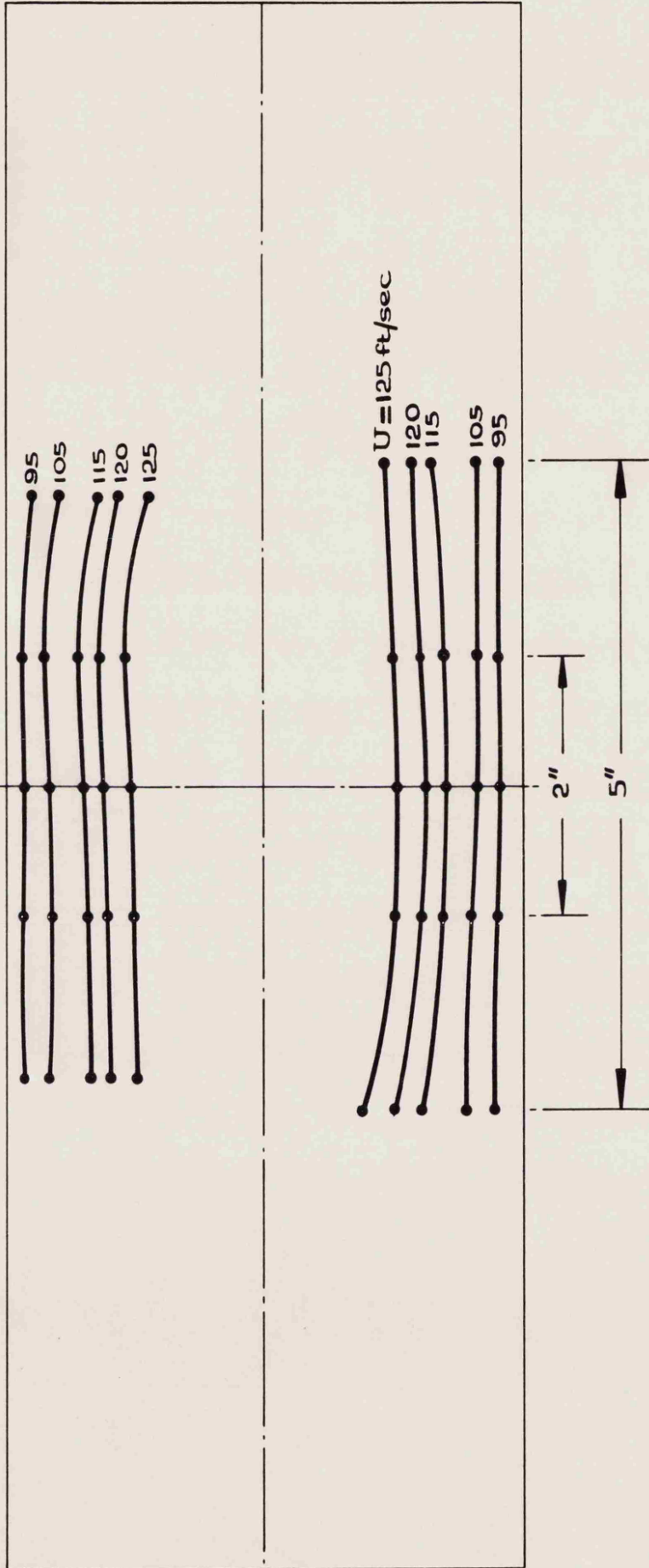
FIG. 2.4. CONTOURS OF CONSTANT AXIAL VELOCITY

$\underline{L/H = 22}$

$Re = 2.86 \times 10^5$

$U_{\!\!\!C} = 133.5\,ft/sec$

95
105
115
120
125

$U = 130\,ft/sec$

125
120
115
105
95

2"

5"
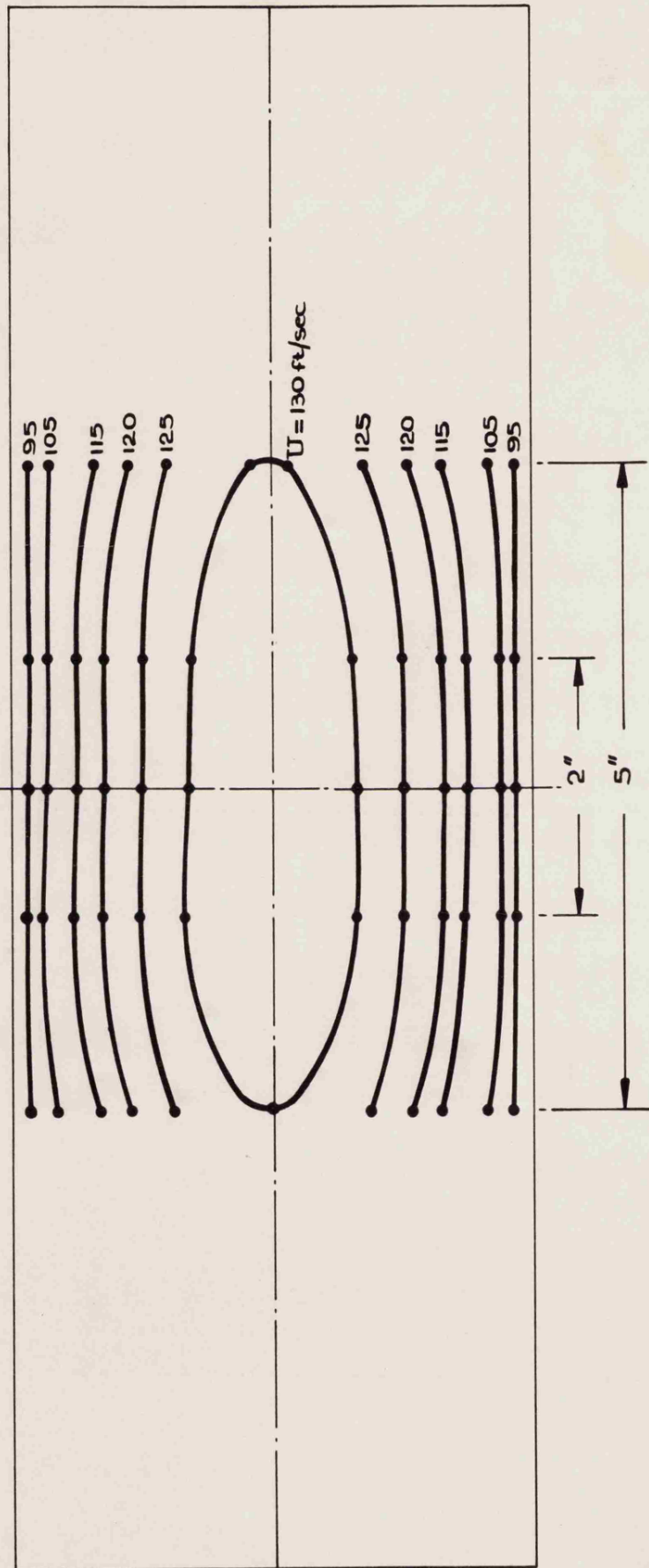
FIG.2.5.CONTOURS OF CONSTANT AXIAL VELOCITY

$\dfrac{L}{H} = 121$

$U_{\rlap{=}\mathcal{L}} = 51 \cdot 8$ ft/sec.

$Re = 6 \times 10^4$

$U/U_{\rlap{=}\mathcal{L}} = \cdot 98$

$\cdot 94$ $\cdot 90$ $\cdot 80$ $\cdot 70$
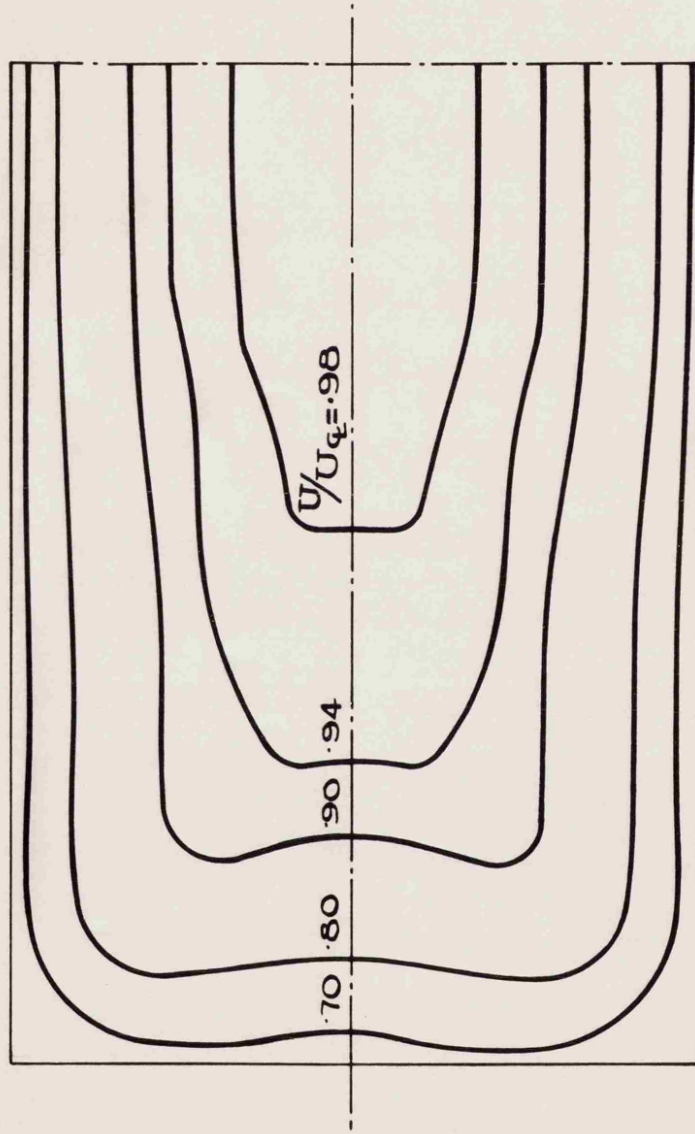
FIG.2.6. CONTOURS OF CONSTANT AXIAL VELOCITY IN 3:1 ASPECT

RATIO DUCT AFTER 'HOAGLAND'

NOTE: NUMBERS ON CURVES ARE VALUES OF $\dfrac{V_{sec}}{U_{\ell}}$
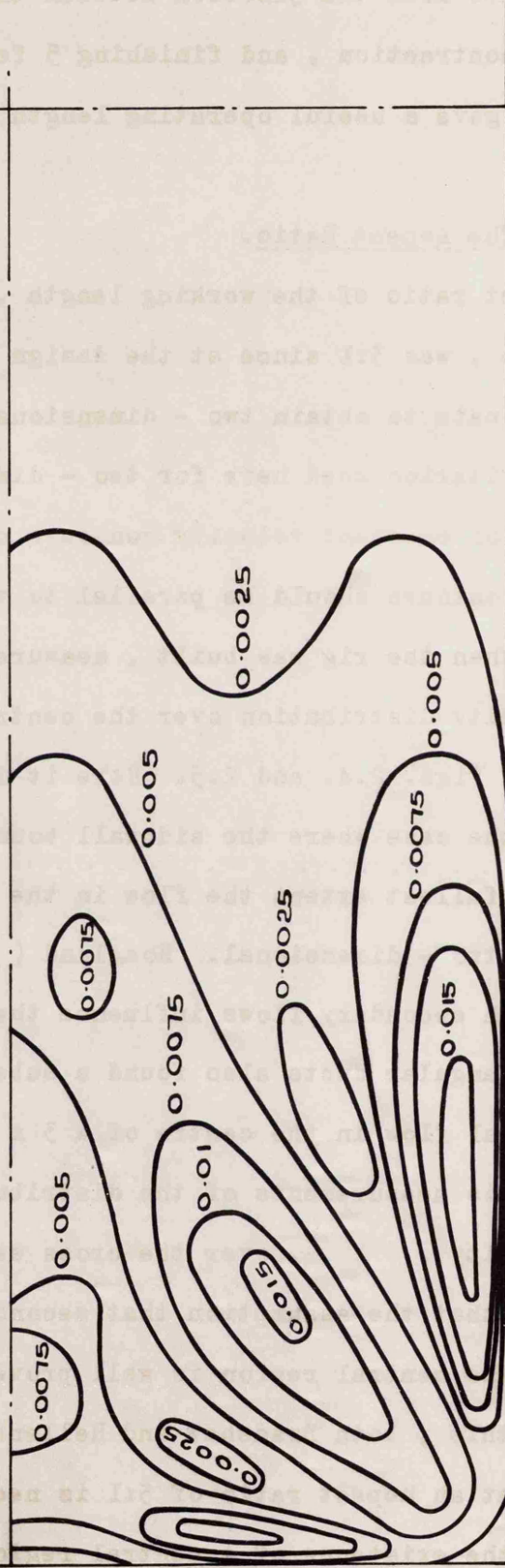
FIG.2.7. CONTOURS OF CONSTANT SECONDARY VELOCITY FOR 3 × 1 ASPECT RATIO DUCT AFTER 'HOAGLAND'

starting 6 inches from the junction between the working length

and the inlet contraction , and finishing 5 feet 6 inches from

the end. This gave a useful operating length of 121 equivalent

duct heights.

2.1.2. The Aspect Ratio.

The aspect ratio of the working length , i.e. ratio of duct

height to width , was 3:1 since at the design stage this was

considered adequate to obtain two - dimensional flow in the central

region. The criterion used here for two - dimensional flow is

that on a plot of constant velocity contours over the cross

section , the contours should be parallel to the floor and roof

of the duct. When the rig was built , measurements were made of

the axial velocity distribution over the central region of the

cross section , Figs. 2.4. and 2.5. Here it is possible to see

that even for the case where the sidewall boundary layers have

grown to their fullest extent the flow in the central two inches

of the duct is two - dimensional. Hoagland (6) who examined

the way in which secondary flows influence the primary flow in

square and rectangular ducts also found a substantial region of

two - dimensional flow in the centre of a 3 x 1 aspect ratio duct,

Fig. 2.6. By his measurements of the distribution of lateral

secondary velocity , V_{sec} , over the cross section , (Fig. 2.7),

it is apparent that the assumption that secondary velocities are

negligible in the central region is well proven.

Despite this , both Bradshaw and Hellens (7) and Tracy (8)

have stated that an aspect ratio of 5:1 is necessary before the

assumption of the existence of a central region of two -

dimensional flow can be substantiated in the case of developed

boundary layers. The solution of this apparent conflict is that
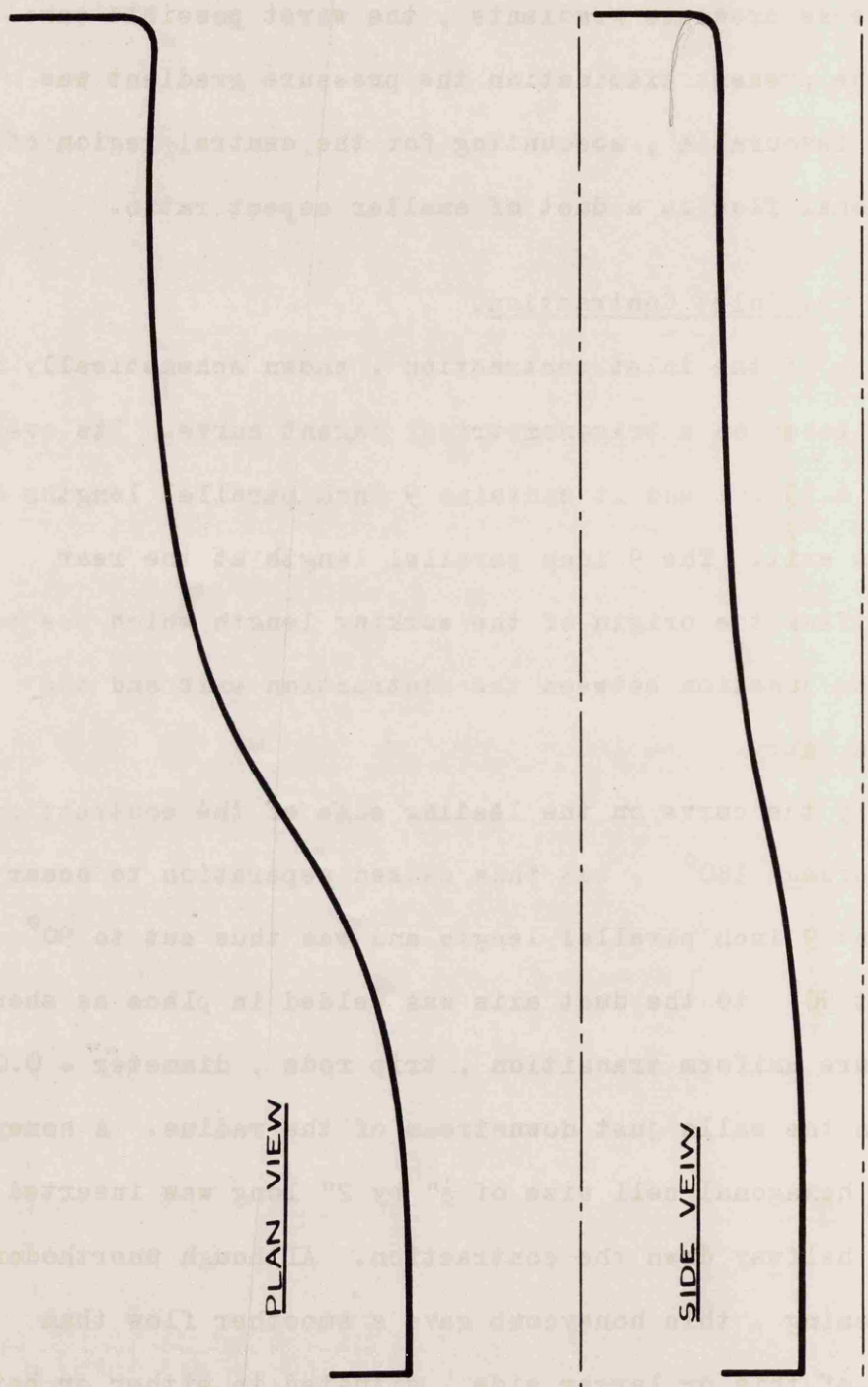
PLAN VIEW

SIDE VEIW

FIG.2.8.INLET CONTRACTION

Bradshaw and Tracy have both stated the criterion which must be
followed to avoid excessive sidewall boundary layer growth effects
in strong adverse pressure gradients , the worst possible case.
However in the present examination the pressure gradient was
both mild and favourable , accounting for the central region of
two - dimensional flow in a duct of smaller aspect ratio.

2.1.3. The Inlet Contraction.

The shape of the inlet contraction , shown schematically in
Fig. 2.8 , is based on a trigonometrical tagent curve. Its overall
area ratio is 6.25 : 1 and it contains 9 inch parallel lengths at
both inlet and exit. The 9 inch parallel length at the rear
somewhat falsifies the origin of the working length which has been
taken to be the junction between the contraction exit and the
working length entry.

Initially the curve on the leading edge of the contraction
turned back through 180° , but this caused separation to occur
along the front 9 inch parallel length and was thus cut to 90°
and a plate at 90° to the duct axis was welded in place as shown.
Also , to ensure uniform transition , trip rods , diameter = 0.036"
were placed on the walls just downstream of the radius. A honey -
comb , having hexagonal cell size of $\frac{1}{2}$" by 2" long was inserted
at a position halfway down the contraction. Although unorthodox
in its positioning , this honeycomb gave a smoother flow than
any honeycomb of this or larger size , situated in either or both
of the upstream or downstream 9 inch parallel lengths.

2.1.1. Fan and Speed Control.

The fan, made by Woods of Colchester , was 24 inch diameter
aerofoil fan and was driven by a constant speed induction motor.

Had the means been available , speed control would best be produced electrically using a Ward-Leonard system. Instead accurate speed control was effected by means of a series of shutter vanes operated by lever arms , situated between the fan and the silencer. Throughout the tests the tunnel was run at a constant overall pressure drop , measured using the static pressure tappings. This method of testing had the implication that as the local pressure drop over the devices used for simulating a mean velocity profile varied , then the mass flow and Reynolds Number also varied slightly but not significantly.

2.2. The Traverse Mechanisms.

In order to save time and with the idea of fully automating the data recording system at a later date a decision was made to automatically traverse the hot wire anemometers used for measuring the flow parameters. Photographs of the traverse mechanism are shown in Fig. 2.9.

The traverse mechanism was powered by a 6 volt motor which drives a lead screw , moving a threaded block to which a length of hypodermic tubing is attached. This hypodermic tubing runs through a hole in the base of the mechanism fitting into one of the metal collars in the duct roof. The hot wire anemometer was then attach- -ed to the end of the tubing. The only restraint then on the shortest distance of the probe from the duct wall is its own geometry.

The 6 volt motor was driven by a pulse circuit , making it possible to traverse the duct in steps of 1/40th of an inch and to dwell in between these steps for any required length of time.

A manual mechanism was also available to traverse the duct with separate pitot and static tubes. This had the advantage that in areas of particular interest readings could be taken close together while in the outer region of the flow the distance between readings could be lengthened. Measurement of the probe position was made possible by the use of a vernier depth gauge.
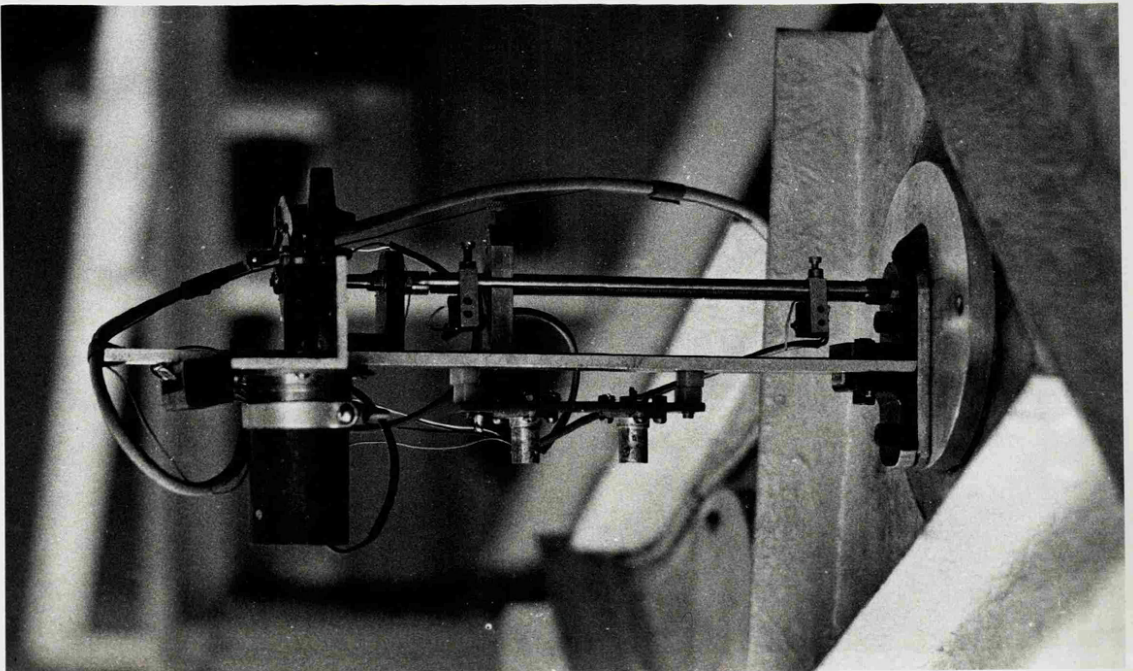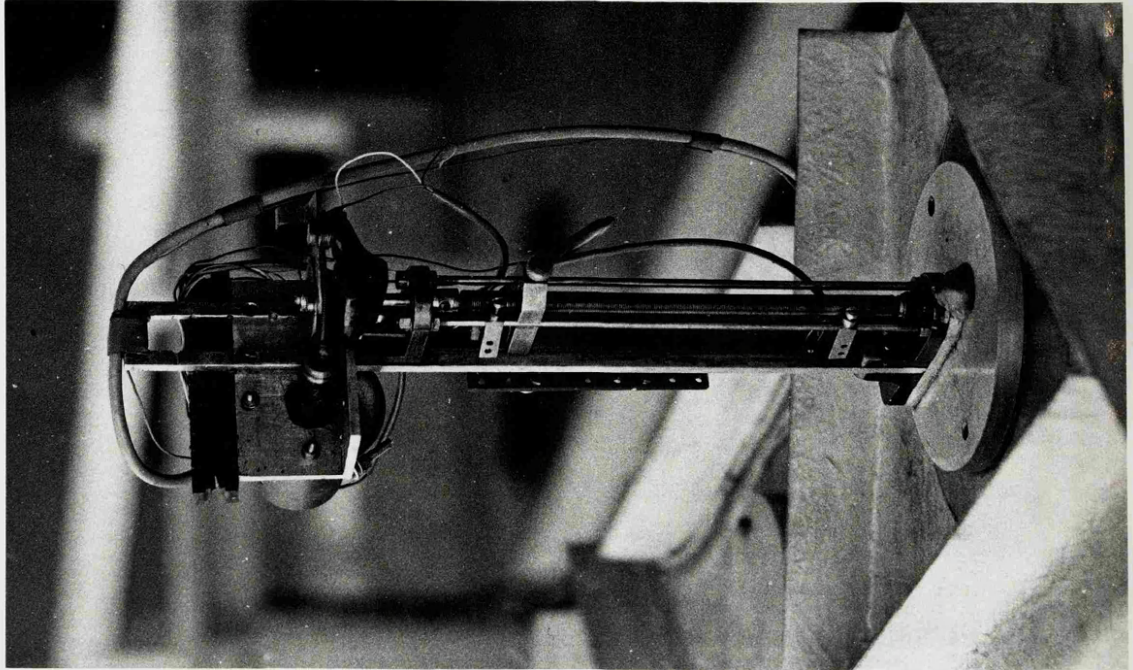
Fig. 2.9   The Traverse Mechanism

2.3. Flow Measurement.

2.3.1. Measurement of Mean Velocities.

Measurements of the mean velocity profiles across the duct were made using separate pitot and static tubes. These were manufactured from stainless steel hypodermic tubing having an outside diameter of 0.050 inches. In the design of the static tube, use was made of the recommendations of Pankhurst and Holder (9) for the tip radius and the siting of the static holes. These tubes were used in conjunction with an inclined spirit manometer.

Initially the tubes were calibrated against a standard N. P. L. Pitot – Static tube and no departure from a 1 to 1 correlation was detected.

Since one of the purposes of making these mean velocity traverses was to determine the values of the displacement and momentum thicknesses of the boundary layers , a data reduction computer programme was written to evaluate these. As a check on the programme's accuracy a number of standard power laws with exponents varying from $\frac{1}{2}$ to 1/12 were fed in as data and the computer results compared with the theoretical solution. In the determination of displacement thickness the error was zero at an exponent of 1/2 and a maximum of $2\frac{1}{2}\%$ at an exponent of 1/12; whilst in the determination of momentum thickness no error was detectable in results taken to three significant figures.

One of the sources of error involved in the use of pitot tubes for making measurements in turbulent boundary layers is the effect of the intensity of turbulence $\sqrt{\overline{u^2}}$. Following Goldstein (10) we can deduce that the pitot tube senses the sum of the

velocity heads , corresponding to the correct mean velocity and
root mean square intensity i.e.

$$\Delta P_{indicated} = \rho/_2 \left(U^2 + \overline{u^2} \right)$$ (2.1)

Thus in regions of high turbulence intensity the pitot tube
appears to read high. For example , in an airstream where
U = 100 ft./sec and turbulence intensity is 10% the error in
ΔP is 1%. Situations in which this example are typical are
known to exist near the wall and immediately behind some of the
mechanisms used for simulating a velocity profile.

2.3.2. Measurement of Turbulence Parameters.

Turbulence can be likened to a series of random vibrations
extended over a wide frequency range , in air this range being
typically 2 Hz to 15KHz at the Reynolds Number conditions at which
the tests were performed. Instruments designed to detect and
measure phenomena over such a range must possess low inertia ,
have small sensing heads (ideally a point) , produce repeatable
results and be robust. Apart from its fragility the hot wire
anemometer satisfies these requirements and since the signal is
electrically sensed data can be recorded , stored and processed
easily.

The priciple of operation is that of heat transfer from the
heated cylinder formed by the wire. Under still conditions the
wire adopts an equilibrium temperature dependent on heat input ,
free convection and radiative heat transfer. As the fluid is
caused to flow over the wire , forced convection occurs lowering
the temperature of the wire and hence its resistance. In a

constant temperature anemometer system , the reduced resistance causes the bridge to go out of balance , whence a feedback circuit comes into effect raising the resistance to its original value. The power required to do this is a measure of the fluid velocity. The merits of both this constant temperature system and the alternative constant current system have been comprehensively reviewed by Cooper and Tulin (11).

For the measurements of turbulence made in the experimental programme , a DISA 55AOI Constant Temperature anemometer was used in conjunction with DISA 55A53 Straight Wire Probe Elements and DISA 55A54 Slant Wire Probe Elements. It was not found necessary to include additional metering devices other than those incorporated in the 55AOI.

Basically the measurement of turbulence is based on the slope of the bridge voltage versus flow velocity calibration curve , S , which by definition we may express as

$$S = \frac{dV}{dU} \qquad (2.2.)$$

where V is the bridge D.C. voltage and U is the mean velocity.

Assuming that King's Law (the existence of a linear relation between the electrical power input to the transducer and the square root of the flow velocity) , is true we can write:

$$\frac{V^2}{R} = \alpha + \beta \sqrt{U} \qquad (2.3.)$$

or

$$\frac{V^2}{R} = \frac{V_o^2}{R} + \beta \sqrt{U} \qquad (2.4)$$

where R is the probe operating resistance and V_0 is the bridge

D.C. voltage for zero flow conditions.

Differentiating (2.3.)

$$\frac{2V}{R} \frac{dV}{dU} = \frac{\beta}{2\sqrt{U}}$$

$$\therefore \quad \frac{dV}{dU} = \beta \frac{R}{4 V\sqrt{U}} \tag{2.5.}$$

Combining (2.2.) and (2.5.) we get

$$S \approx \beta \frac{R}{4V\sqrt{U}}$$

but from (2.4.)

$$\sqrt{U} = \left(V^2 - V_0^2\right) \frac{1}{\beta R}$$

$$\therefore \quad S = \frac{\left(V^2 - V_0^2\right)}{4 V U} \tag{2.6.}$$

A knowledge of the factors in this equation enables measurements of turbulence quantities to be made without the necessity for individual calibration of each wire used.

If a wire were placed in a position A in the (x, y) plane at 45° to each axis then by linearizing its response equation and neglecting squares and products we could write the fluctuating part of the response equation thus:

$$E_A \text{ r.m.s.} = \sqrt{S_A^2 \left(u + v\right)^2} \tag{2.7}$$

where S_A is a function of the wire itself and its operating condition, as described in equation (2.6), as well as its orientation.

If we then took the same wire and placed it in position B by turning it through 90° in the plane (x,y) so that it was again 45° to each axis , similarly we could write the fluctuating part of its response equation as

$$E_B \text{ r.m.s.} = \sqrt{S_B^2 (u - v)^2} \tag{2.8}$$

Now since we have the same wire at the same point with its orientation to the flow direction set at $+45^\circ$ and -45° we can write

$$S_A = S_B = \frac{(V_A^2 - V_{oA}^2)}{4V_A U} \tag{2.9}$$

where V_A is the bridge D.C. voltage when the wire is in position A. By squaring and subtracting Equations (2.7) and (2.8)

$$\overline{uv} = \frac{(E_{A r.m.s.})^2 - (E_{B r.m.s.})^2}{4 S_A^2}$$

and on substitution of Equation (2.9) we get

$$\overline{uv} = \left\{ (E_{A r.m.s.})^2 - (E_{B r.m.s.})^2 \right\} \cdot \frac{4 V_A^2 . U^2}{(V_A^2 - V_{oA}^2)^2} \tag{2.10}$$

Since U is known at points across the duct from the pitot and static tube measurements and $E_{A r.m.s.}$, $E_{B r.m.s.}$, V_A and V_{oA} are known from the meter readings on the anemometer bridge we are able to determine $\overline{uv}$ directly in $(ft./sec)^2$. Furthermore , if we merely required the ratio $\frac{\overline{uv}}{U^2}$ it would not be necessary to make pitot readings and static tube readings at all.

If we were now to take a straight wire and place it normal to the flow in either of the y or z axes in position C , the fluctuating part of its response equation could be written

$$E_{c\ r.m.s.} = \sqrt{S_c^2\ \overline{u^2}} \tag{2.11}$$

where

$$S_c = \frac{V_c^2 - V_{o_c}^2}{4\ V_c\ U}$$

Thus we can write the longitudinal intensity of turbulence as a percentage of the local mean flow velocity U , i.e.

$$\frac{\sqrt{\overline{u^2}}}{U}\ \%_o = E_{c\ r.m.s.}\ .\ \frac{4\ V_c}{\left(V_c^2 - V_{o_c}^2\right)} \times 100 \tag{2.12}$$

In order to determine the lateral (y direction) intensity of turbulence it is necessary to utilize the information gained from all three wire positions. By squaring and adding (2.7) and (2.8) we get

$$\left\{\left(E_{A\ r.m.s.}\right)^2 + \left(E_{B\ r.m.s.}\right)^2\right\}\frac{1}{2S_A^2} = \overline{u^2 + v^2} \tag{2.13}$$

Squaring (2.11) and subtracting from (2.13) yields

$$\overline{v^2} = \frac{1}{2S_A^2}\left\{\left(E_{A\ r.m.s.}\right)^2 + \left(E_{B\ r.m.s.}\right)^2\right\} - \frac{\left(E_{c\ r.m.s.}\right)^2}{S_c^2} \tag{2.14}$$

and on substitution of S_A and S_C we get ,

$$\frac{\sqrt{\bar{u^2}}}{U} \, \%_o = \left\{ \frac{8 V_A^2}{(V_A^2 - V_{oA}^2)^2} \left(E_{A \, r.m.s.}^2 + E_{B \, r.m.s.}^2 \right) - \frac{16 V_c^2 E_{c \, r.m.s.}^2}{(V_c^2 - V_{oc}^2)^2} \right\} \times 100 \quad (2.15)$$

It should be noted that all measurements of the percentage
intensity of turbulence are based on the local value of the mean
velocity and not the bulk mean velocity $\overline{U}$ or the maximum velocity
U max. A data reduction computer programme was used to reduce
the values of E , V , V_0 and U to the required form i.e. the $\overline{uv}$
correlation and the percentage intensities of turbulence.

Brief measurements of the spectrum of the longitudinal
intensity of turbulence were made with the help of the English
Electric Company's Mechanical Engineering Laboratory , using an
Ampex Tape Recorder and subsequently analysing the recorded
information on an analogue computer.

2.3.3. Errors in the Measurement of Turbulence.

The complete story on how errors arise in the measurement of
turbulence is the subject of a multitude of publications. The
aim of this present section is only to give a brief description of
how some major errors can arise and the way in which their effects
can be minimized where possible. It also indicates the degree of
reliability present in the measurements made in subsequent
chapters.

(a) Errors caused by ambient temperature fluctuations.

The operating procedure followed when using DISA anemometers
is first to determine the resistance of the probe when it is cold
and in zero airflow. A suitable overheat ratio, 1.7 in this case,
is chosen according to the type of probe in use to give maximum
sensitivity. Then the arm of the bridge which balances the probe

is set to the appropriate overheat resistance , causing the probe
to come into operation in its heated form. Should a change in the
ambient temperature occur this will cause the effective overheat
ratio to alter and hence the operating temperature will also change.
In an attempt to minimize this effect , the cold resistance was
determined at the start of each traverse and the balance arm
resistances set accordingly to give the correct overheat ratio.
Furthermore the wind tunnel was run up for at least half an hour
before any measurements were made in order to acheive equilibrium
between the inside of the working length and the surrounding air.
Despite these precautions it would be possible for errors to arise
due to changes in the ambient temperature during the time required
to make a traverse. These errors are thought to be very small
since no evidence of their effect was ever found.

    (b) <u>Errors Caused due to heat loss by wall proximity</u>.

Errors in measurements made by hot wire anemometers can be
caused by the proximity of the probe to the wall. This causes
heat conduction through the fluid to the wall , giving false low
readings. However such errors are generally considered negligible
when the probe is more than 20 wire diameters from the wall. In
the case of the present tests the measurements made closest to the
wall were at $y = 0.05$ inches which is approximately 220 wire
diameters , and thus this effect was neglected.

    (c) <u>Errors due to drift of wires caused by dust</u>.

The manufacturing method of hot wire elements can be divided
into 3 main groups. The most common method(the one which DISA
employ) is to weld drawn tungsten wire to needle points a fixed
distance apart. Secondly there is a method in which the ends of
a drawn tungsten wire are copper plated leaving a bare section in

the centre. These ends are then soft soldered to cupro - nickel

supports. Thirdly there is the Wollaston process whereby the whole

wire is plated and then the centre section is etched away with

nitric acid. In the first two cases the sensing section of the

probe is smooth drawn wire whilst in the third case the surface

of the sensor is gouged and pitted by the action of the etching

agent. While no airflow can be free of dust particles down to a

size below that of the wire diameter , the amount of dust present

will depend largely on the immediate enviroment of the airflow

source , i.e. the laboratory , and to a lesser extent the general

environment i.e. urban or rural areas. Thus if one recognizes the

inevitable presence of dust then the screening and filtration of

the airflow is very much a subjective precaution. The way in

which dust affects a hot wire is firstly by impact , in which

mechanical stresses are set up which alter the wire resistance ,

and secondly by dust settling on the wire surface and and altering

its thermal properties. Hence the nature of the wire surface is

all important in the consideration of how dust will settle and

cling to it.

Collis (12) who used Wollaston wires in an urban environ -
-ment has reported a diminution of wire sensitivity due to dust

at the rate of $\frac{1}{2}\%$ per minute for the first half hour of a run at

100 feet per second airflow velocity. Dryden and Kuethe (13)

reported the rate of diminution of sensitivity to be 0.28% per

minute over $1\frac{1}{2}$ hours at an airflow velocity of 110 feet per

second , using smooth drawn wires. Although it is not specifically

mentioned it is assumed that the rate of diminution of sensitivity

is not a linear function of time but increases with increasing

time. Based on figures of this order , a traverse taking 10

minutes could give a decrease in sensitivity of the order of 2%
in the worst case.

In these tests all the wires used had smooth drawn surfaces
and as a further precaution the wires were washed in filtered
trichloroethelene before each traverse.

(d) <u>Errors due to high turbulence intensity</u>.

In writing down the response equation of a hot wire anemometer
it is generally assumed that the relative turbulence intensity is
small , in order to make possible a linearization of the response
equation to turbulence fluctuations. However it is of practical
importance to know at what intensity level such a linearization
begins to induce unacceptable errors. Hinze (14) produces an
elegant theoretical analysis of this effect but reaches the
decision that insufficient information of turbulence structures is
available to apply it fully .   However , he does give a guide that
the error involved in turbulence measurements in high intensity
airflows is of the order of half the percentage intensity level
i.e. the error in the measurement of turbulence level of 10% is of
the order of 5% too high.

(e) <u>Errors due to end effects</u>.

In general the wire supports of a probe are large compared
with the wire itself and their thermal inertia can be assumed
infinite by comparison. Because of the temperature difference
between the wire and its supports , a cooling effect is exerted
on the wire by conduction to the supports. This cooling reduces
the effective length of the wire and led Bethov (15) to introduce
the concept of cold length i.e. that part of the wire near the
supports which is effectively inactive. His conclusions were
that a ratio of this cold length to the total length of 0.10 is

adequate for good results and that this requires the length to diameter ratio (1/d) of the wire to be at least 100.

In the present tests the 1/d ratio of the probes used was 100 , but an unpublished communication with the probe manufacturers states that the probe design is such as to minimize errors from this source.

(f) <u>Errors due to finite wire length.</u>

The use of a wire of finite length involves errors arising from the integration of velocity fluctuations along its length. This causes an under estimate of the contribution from eddies of a length scale the same as or of smaller order than the wire length. More detail of this type of error is given by Frenkiel (16) , who states that the size of error incurred using a wire of length ℓ in an airflow whose microscale is λ , is of the order of

$$- \frac{\ell^2}{6\lambda^2}$$

Measurements made in the present tests using a DISA Correlator to determine λ indicate that errors arising from this source are negligible.

(g) <u>Errors due to the directional sensitivity of inclined</u>
  <u>wires.</u>

The validity of the cosine law for describing the directional sensitivity of hot wires has often been doubted. An alternative expression is

$$U_E^2 = U^2 \left(\cos^2\alpha + k \sin^2\alpha \right)$$

(2.16)

Where U_E is the effective velocity , U is the flow velocity , α is the inclination of the wire to the flow and K a function

thought to depend on velocity and the length to diameter ratio of the wire.

In a detailed investigation on measurements made by inclined wires Champagne (17) indicates that for wires of the type used in the present tests a value of K = 0.25 would be realistic and that this could produce errors in the measurement of $\overline{uv}$ and $\frac{\sqrt{\overline{v^2}}}{U}$ % of the order of 10% too low.

However various values of this factor K are given in the literature. Hinze (14) gives it as between 0.1 and 0.3 depending on velocity (K increasing as the velocity decreases) . Webster (18) determined K to be 0.2 but his results showed no systematic dependence either on velocity or l/d ratio. Both Dueller (19) and Schubauer and Klebanoff (20) have shown that for inclinations of less than 70° , K is zero and Chu (21) is reported to have found no deviation from the cosine law at all.

ERRORS

MAJOR CAUSES

DIRECTIONAL SENSITIVITY OF INCLINED WIRES

possible error in $\sqrt{\overline{v^2}}$% and $\overline{uv}$ of 10% low

HIGH TURBULENCE INTENSITY

possible error in $\sqrt{\overline{u^2}}$% , $\sqrt{\overline{v^2}}$% and $\overline{uv}$ of 5% high

MINOR CAUSES

AMBIENT TEMPERATURE FLUCTUATIONS

WALL PROXIMITY

DRIFT CAUSED BY DUST

FINITE WIRE LENGTH

END EFFECTS
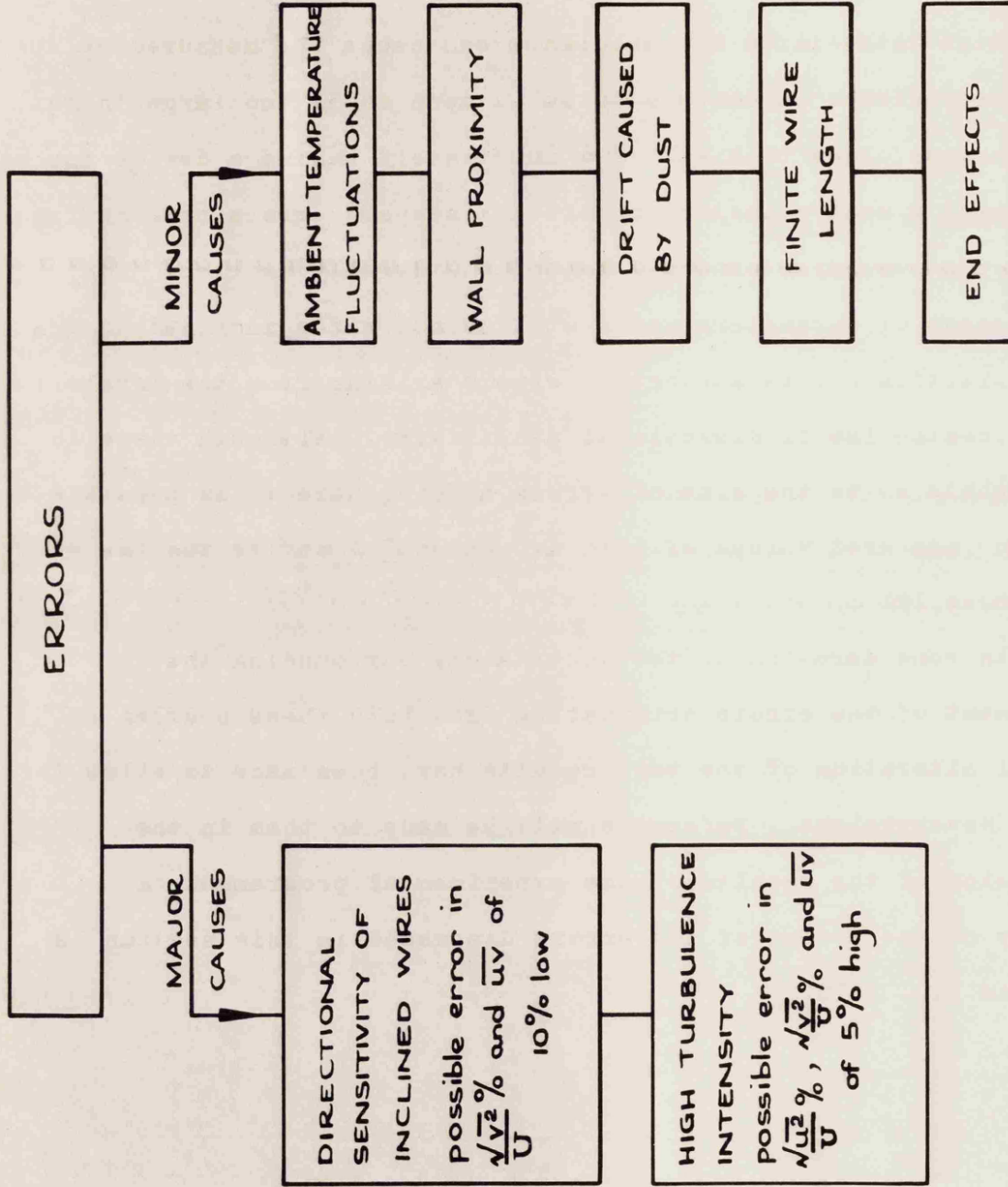
FIG. 2.10. SOURCES OF ERROR INVOLVED IN MEASURING TURBULENCE WITH HOT WIRE ANEMOMETERS

The conclusions that may be drawn from this brief survey of
the errors involved in the use of hot wire anemometers are that
there are two primary sources to be taken into account in results
from the test programme.

High intensities of turbulence can cause the measured values
of the turbulence parameters to be as much as 5% too large in the
flow regions close to a wall and immediately behind a device for
simulating a mean velocity profile. Elsewhere errors arising from
this source would be expected to be considerably smaller. The
measurement of parameters which utilize hot wires inclined to the
flow direction may be subject to errors arising from the invalidity
of the cosine law of directional sensitivity. Although there is
some debate as to the size of errors arising here it is possible
that the measured values of both $\overline{uv}$ and $\frac{\sqrt{\overline{u^2}}}{U}$ % may be too low by
as much as 10% .

In consideration of the uncertainty surrounding the
assessment of the errors originating from both these sources no
overall alteration of the test results have been made to allow for
them. Nevertheless , reference will be made to them in the
discussion of the results of the experimental programme. A
summary of the effect of the errors discussed in this section is
shown in Fig. 2.10.

Chapter 3.

Duct Flow.

The manner in which flows , particularly those that are turbulent , develop downstream in a pipe or duct is at present the subject of some conjecture. Partially the reason for this is the difficulty of performing adequate experiments which may be used as a comparison with the various theories available. The incomplete state of knowledge about boundary layer transition , from laminar to turbulent flow , alone presents practical problems , as does our assumptions concerning the nature of the flow boundaries and the central core.

Since anomalies exist in the terminology used in the various publications on pipe and duct flows it should be pointed out that the term ' developing flow ' implies flow up to the point at which the values of all the flow parameters cease to change with increasing distance downstream. It does not mean flow up to the point or region where the boundary layers may be said to have met. The term ' equilibrium flow ' is taken to mean the flow at any point down - stream of the position where the flow parameters cease to change with distance. The ' inlet flow region ' is that length from inlet to the region where the boundary layers merge.

In this chapter it is intended to present some ideas about the way that the effects of flow history can be used to explain the development of the mean flow in a duct.

3.1. The prediction of developing flows.

Various theories exist for the purpose of predicting the
development of mean flow parameters , but to date none of them can
give an entirely satisfactory comparison with the relatively sparse
experimental data available.

One of the best known of the earlier attempts to predict the
development of turbulent boundary layers in pipes and ducts is that
derived for the development of boundary layers on a flat plate at
zero incidence with constant free stream velocity , which is
presented by Schlichting (22).
Here he writes

$$\delta = 0.37 . x . Re_x^{-1/5}$$
  3.1.1.

where δ is the height of the boundary layer , x is the distance
from the leading edge of the plate and Re_x is the Reynolds Number
based on x and the free stream velocity. If this is now applied to
the developing flow in a pipe or duct of height H , the length
required for the boundary layers to meet (δ = H/2) from inlet
may be expressed

$$\frac{L_e}{H} = 1.33 \, Re_L^{1/5}$$
  3.1.2.

where now the Reynolds Number is based on L_e , the length of the
inlet region.

The original equation from which this is developed is for
flow over a flat plate at zero incidence and the data required for
its formulation concerning the values of wall shear stress were
taken from measurements of equilibrium flow in a pipe where a

1/7th power law velocity profile was assumed. The validity of its
application back to developing boundary layers in pipes is doubtful,
since it is based on a constant free stream velocity , whilst free
stream flow in the entry region of pipe accelerates. Thus equation
3.1.2. is liable to under - estimate the length of the inlet region.

More recently other theories have appeared in the literature,
again with the purpose of predicting flow development downstream of
a pipe or duct inlet. The method by Ross (23) yields the relative
momentum thickness of the boundary layer at any point up to 10
diameters downstream of a pipe entry and uses this to compute the
accompanying pressure drop and head loss. The analytical prediction
of the length of the inlet region , by Lakshamana (24) requires
that a known inlet velocity profile develop into a known end
velocity profile but with the drawback that both specified profiles
should have non - zero first derivatives at the wall , thus limiting
its usefulness to non - uniform inlet velocity profiles only.
Bowlus and Brighton (25) have also produced a theory predicting
the length of the inlet region requiring the use of the integral
continuity and momentum relationships and the assumption that the
wall boundary layer can , everywhere , be fitted by a 1/7th Power
Law velocity profile. In a prediction method at present being
developed by Cockrell (26) he uses an integral method of boundary
layer prediction incorporating an entrainment equation dependant on
the boundary layer turbulence , originally developed by Hirst and
Reynolds (27) . He concludes that probably the most significant
result is that no single relation can be given between the length
from inlet to the point where the boundary layers merge and the
Reynolds Number. His analysis shows that the initial entrainment
rate , which is a measure of the boundary layer turbulence near

inlet , is more important than the Reynolds Number. A comparison
of his predictions with the experimental results of Barbin and
Jones (28) for developing flow in a pipe is good , however only
an approximate correlation is made with the results of Comte –
Belliot (29) for duct flow after the boundary layers have merged.

3.2. The nature of the inlet region flow.

In their experimental study of developing pipe flow , Barbin
and Jones (28) state that following the disappearance of the free
stream , further changes in the velocity profile and distribution
of turbulence parameters occur before an equilibrium condition is
reached. In his discussion on this paper , Brenkert says he would
expect the velocity profile to change as the turbulent shear stress
approaches its equilibrium value and that it would be interesting
to find out what happens further down the pipe.

In an effort to try to set down what influences the nature
of the developing flow in a pipe or duct , use is made of one of
Schubauer's classical papers (30). Here he states that it is
generally known that the velocity distribution in a flat plate
boundary layer differs from that found in equilibrium pipe or duct
flow , the difference becoming more distinct at high Reynolds
Numbers. The pipe and duct flow velocity profiles obey the
logarithmic law to a fair degree of approximation whereas the
boundary layer profiles show a deviation from this for $y/\delta > 0.2$,
where δ is the physical thickness of the boundary layer. This
difference in the behaviour of the two types of flow is attributed
to intermittency , i.e. the irregular outer limit of the boundary
layer envelope , which is present in flat plate boundary layer
flow and absent in equilibrium pipe or duct flow. The effect of
this intermittency is shown to influence not only the shape of the
mean velocity profile but also the distribution of turbulent
energy.

For developing flow in a duct both of these flow situations
are present. Initially the thin inlet boundary layer will exhibit
intermittent effects in its outer region not too dissimilar from

those of a flat plate boundary layer , whilst in the equilibrium

flow region no intermittency will be present (discounting totally

enclosed regions of irrotational flow formed by the merging of two

intermittent regions). Since it is known from Schubauer's work

that these two types of flow have different mean velocity profiles

associated with them it is quite natural that one should expect a

change from one type of flow to the other i.e. in the region between

the boundary layers merging and the onset of equilibrium flow.

Schubauer also reported a difference in the distribution of

turbulent energy of the two flow types. However when the boundary

layer distribution is divided by the intermittency factor (the

ratio of time the fluid is non - turbulent to the total time) the

two distributions become similar. This point could be deduced from

Barbin and Jones (28) results in which they observe a sudden

increase in turbulence intensity when the boundary layers begin to

merge. Had they divided their results by the intermittency factor

at each point this supposed sudden increase would have been less

apparent.
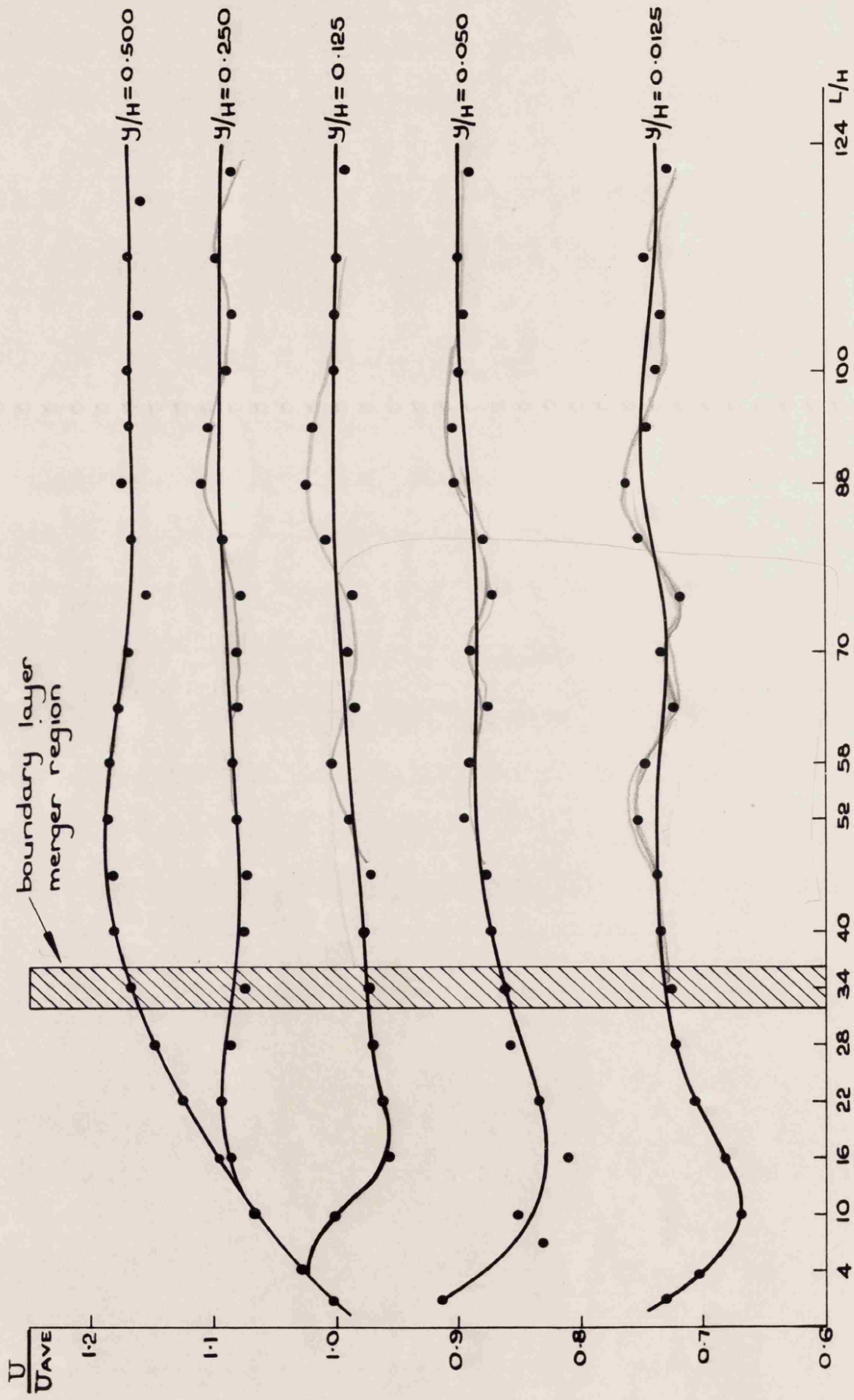
FIG. 3.1. DEVELOPMENT OF MEAN VELOCITY DISTRIBUTION IN DUCT FLOW
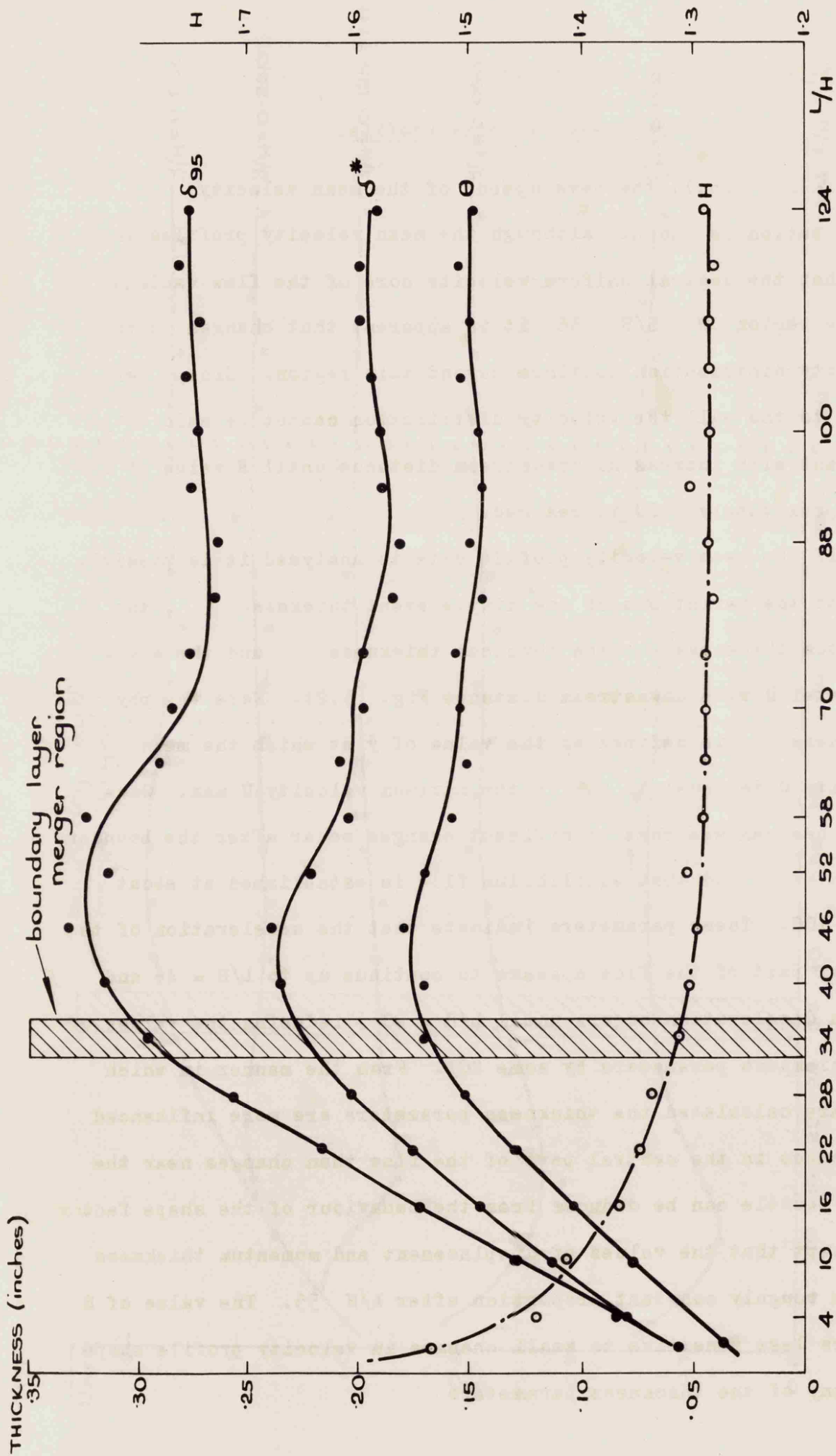
FIG.3.2. DEVELOPMENT OF MEAN VELOCITY PROFILE PARAMETERS IN DUCT FLOW

3.3. Experimental Results.

3.3.1. The Mean Velocity Profile.

In Fig. (3.1) the development of the mean velocity distribution is shown. Although the mean velocity profiles indicat--ed that the central uniform velocity core of the flow vanished in the region $32 < L/H < 36$ it is apparent that changes in the velocity distribution continue beyond this region. Except very close to the wall the velocity distribution cannot be said to be constant with increasing downstream distance until a value of L/H of approximately 100 is reached.

If the mean velocity profile data is analysed it is possible to plot the variations of the displacement thickness δ^{*}, the momentum thickness θ, the physical thickness δ_{95} and the shape parameter H with downstream distance Fig. (3.2). Here the physical thickness δ_{95} is defined as the value of y at which the mean velocity U is equal to 95% of the maximum velocity U max. Once again one can see that significant changes occur after the boundary layers merge and that equilibrium flow is established at about L/H = 100. These parameters indicate that the acceleration of the central part of the flow appears to continue up to L/H = 46 and then a deceleration occurs until L/H = 90 , reducing the values of the thickness parameters by some 20%. From the manner in which they are calculated the thickness parameters are more influenced by changes in the central part of the flow than changes near the wall. Little can be deduced from the behaviour of the shape factor H except that the values of displacement and momentum thickness are in roughly constant proportion after L/H ≈ 55. The value of H appears less sensitive to small changes in velocity profile shape than any of the thickness parameters.

3.3.2. The wall shear stress.

Since the results of measurements of the turbulent shear stresses ($-\overline{uv}$) are non - dimensionalized by the square of the fric--tion velocity for the equilibrium region u_{*d}^2

where $$u_{*d} = \sqrt{\frac{\tau_{wd}}{\rho}}$$ 3.2.1.

it would be pertinent to describe the measurement of τ_{wd} at this point. It is the value of the wall shear stress in the equilibrium region which has been used since various investigators have shown that the value of τ_w decreases from its value at the duct entry to its constant value some distance downstream. However in none of the reports has τ_w taken longer than L/H $\simeq$ 15 to reach its final value , such measurements being reported by Holdhusen (31) , Barbin and Jones (28) and Bowlus and Brighton (25) .

Measurement of the wall shear stress was made by the following methods.

(i) The Moody Chart.

This chart of Reynolds Number against friction factor was used assuming the duct to conform to the smooth pipe curve.

for $\overline{U}$ = 115 ft/sec.

H = 0.333 ft.

λ = 1.54 x 10^{-4} ft^2/sec.

then Re = 2.48 x 10^5

This gives f = 0.0145

and since $$f = 4\tau_w / \tfrac{1}{2}\rho \overline{U}^2$$ (3.2.2)

then τ_{wd} = 0.056 lb/ft^2

This then gives , from 3.2.1.

$$u_{*d}^2 = 24.04 \text{ ft}^2/\text{sec}^2$$

(ii) The Pressure Drop Relationship.

On assuming that the only net forces acting on the fluid in the equilibrium flow region are the pressure drop and the wall shear stress then it is possible to write.

$$\frac{dp}{dx} = \frac{d\tau}{dy}$$

(3.2.3)

For a rectangular duct of height H and breadth B this can be rewritten

$$\frac{\Delta p}{\Delta l} = 2\tau_w \cdot \frac{(H+B)}{H.B}$$

(3.2.4)

This gives the value of τ_{w_d} as

$$\tau_{w_d} = 0.0546 \text{ lb/ft}^2$$

and a value of friction velocity of

$$u_{*d}^2 = 23.44 \text{ ft}^2/\text{sec}^2$$

(iii) The Logarithmic Law.

If the validity of the logarithmic law of velocity distribution for equilibrium flow in pipes is assumed correct for points near the wall , then by measuring the mean flow velocity it is possible to compute a value for the friction velocity. From Prandtl (32) the following equation was used

$$U = u_* \left\{ 5.75 \log_{10} \frac{y u_*}{\tfrac{\nu}{2}} + 5.5 \right\}$$

(3.2.5)

This gave a value of $u_{*d}^2 = 23.6 \text{ ft}^2/\text{sec}^2$

(iv) The Ludweig - Tillman Skin Friction Relationship (33)

This relationship , based on experimental observation of flow over a flat plate , is as follows

$$C_f = 0.246 \cdot 10^{-0.678H} \cdot Re_\theta^{-0.268}$$ 3.2.6.

where Re_θ is the Reynolds Number based on the boundary layer momentum thickness.

Since

$$u_* = U \sqrt{\frac{C_f}{2}}$$ 3.2.7.

u_{*d}^2 was determined to be

$$u_{*d}^2 = 22.82 \ ft^2/sec^2$$

(v) The Schultz-Grunow Skin Friction Relationship (34)

This relationship, also based on flat plate flow observations states

$$C_f = \frac{0.0334}{(\log_{10} Re_\theta)^{1.838}}$$ 3.2.8.

Using this , the friction velocity is

$$u_{*d}^2 = 23.55 \ ft^2/sec^2$$

Since the accuracy of none of these results would be expected to be better than about 5% they were averaged to give the value used to non-dimensionalize the turbulent shear stresses. This average value is

$$u_{*d}^2 = 23.5 \ ft^2/sec^2$$
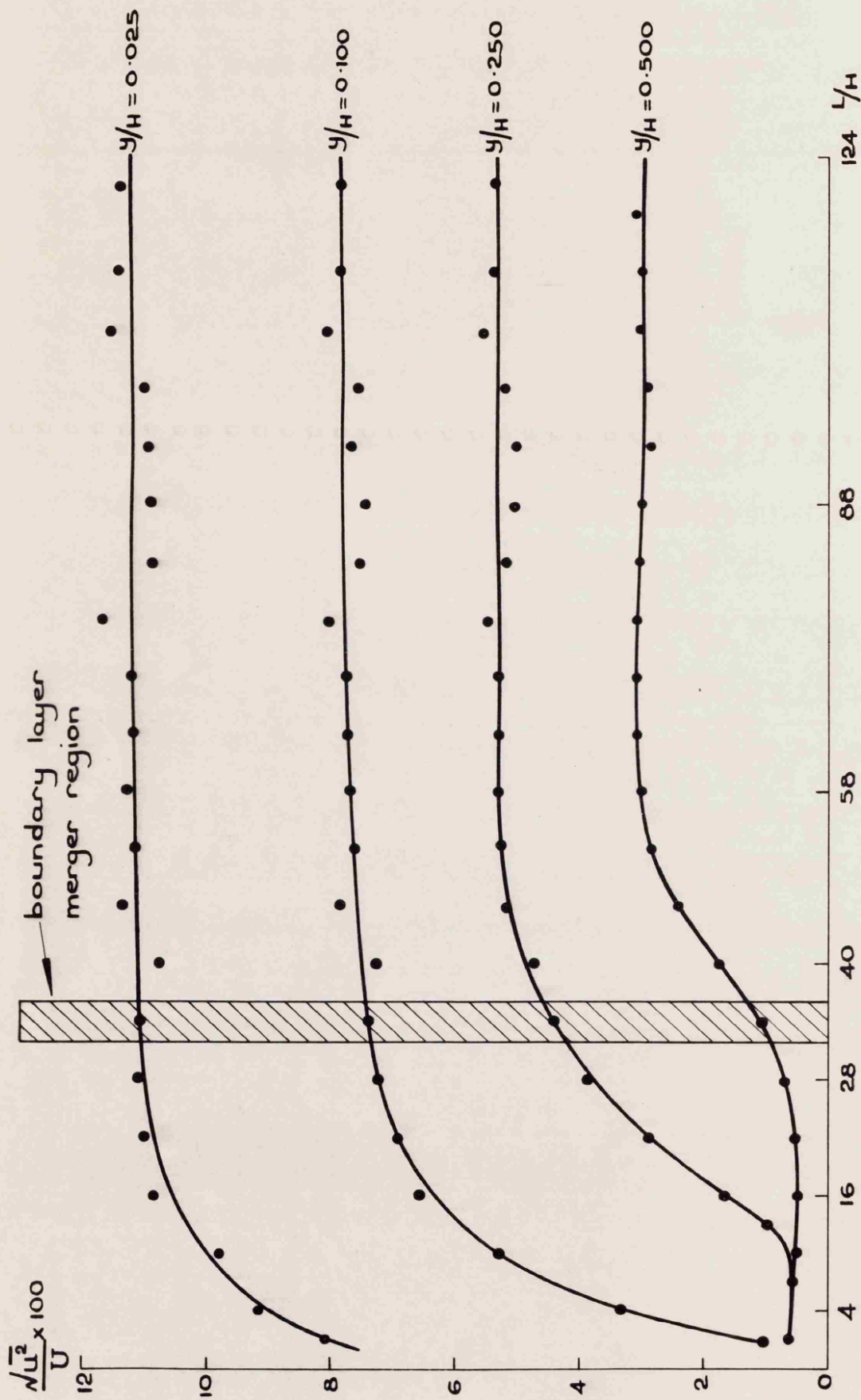
FIG.3.3. DEVELOPMENT OF LONGITUDINAL INTENSITY OF TURBULENCE IN DUCT FLOW
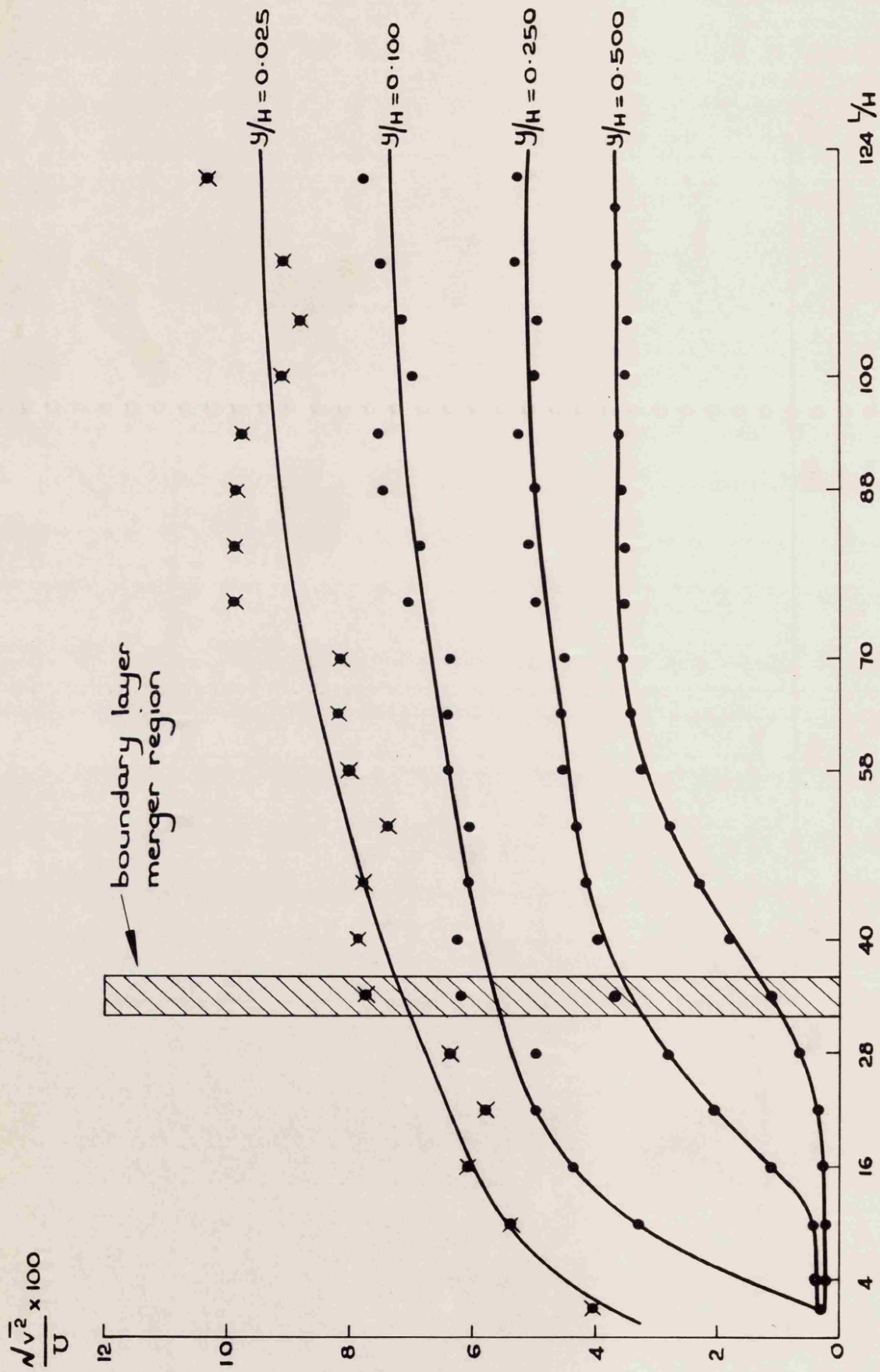
FIG.3.4. DEVELOPMENT OF LATERAL INTENSITY OF TURBULENCE IN DUCT FLOW
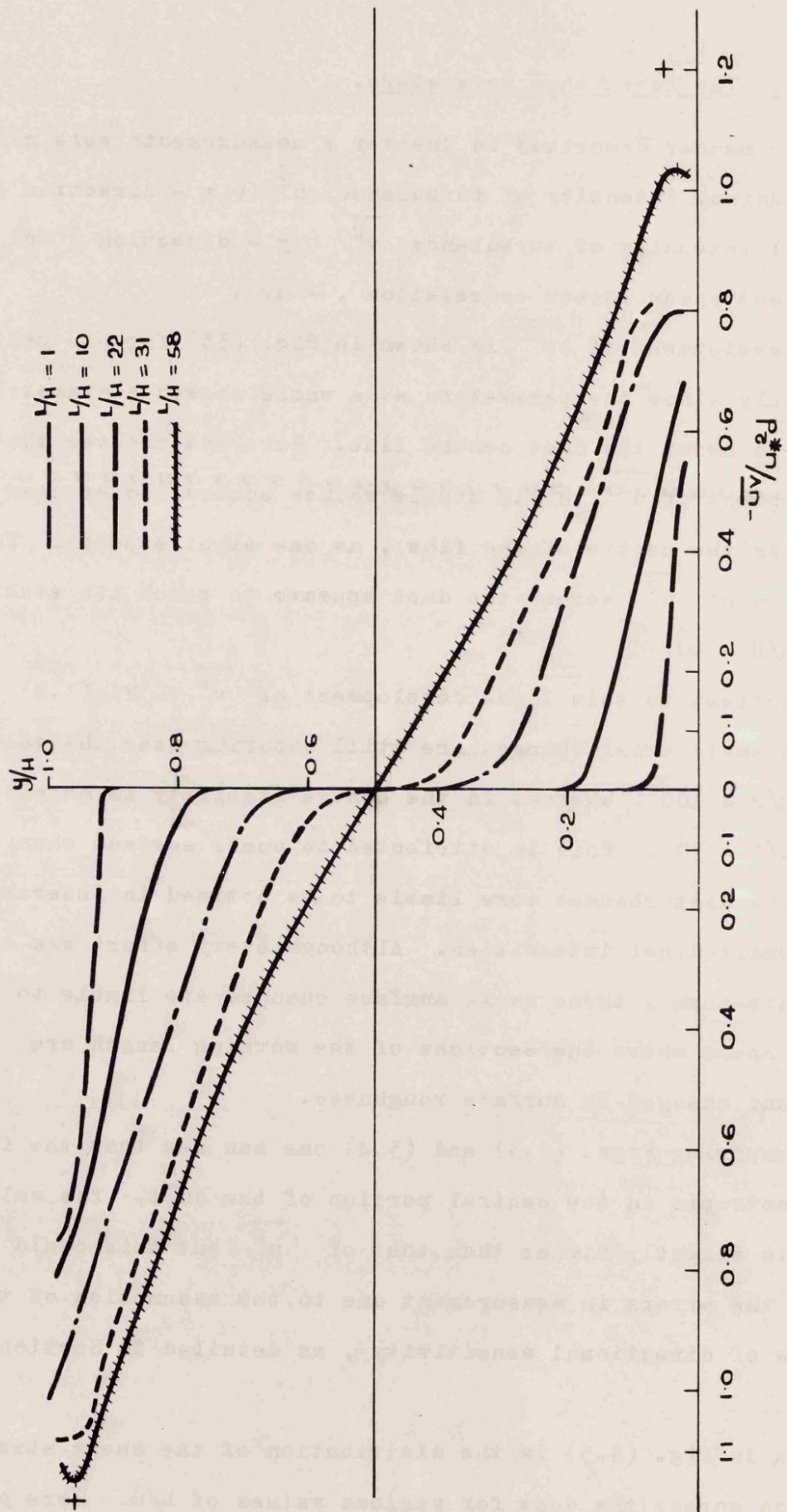
FIG.3.5. TURBULENT SHEAR STRESS DISTRIBUTION IN DUCT FLOW

3.3.3. The Turbulence Parameters.

In the manner described in Chapter 2 measurements were made of the longitudinal intensity of turbulence $\sqrt{\overline{u^2}}$ (x - direction) , the lateral intensity of turbulence $\sqrt{\overline{v^2}}$ (y - direction) and the turbulent shear stress correlation , $-\overline{uv}$.

The development of $\sqrt{\overline{u^2}}$ is shown in Fig. (3.3) for one half of the duct only since the parameters as a whole showed a symmetrical distribution about the duct centre line. Here one can see that the development of $\sqrt{\overline{u^2}}$ to its stable values occurs sooner near the wall than in the centre of the flow , as one might expect . The distribution of $\sqrt{\overline{u^2}}$ across the duct appears to reach its stabilized value by L/H = 60.

By contrast to this , the development of $\sqrt{\overline{v^2}}$, Fig(3.4) , shows that small order changes are still occuring near the wall up to about L/H = 100 , whereas in the centre stability is obtained by about L/H = 70 . This is attributed to small surface changes causing flow disturbances more liable to be noticed in lateral than in longitudinal intensities. Although every effort was made to eliminate them , these small surface changes are liable to be causeddby steps where the sections of the working length are joined , and changes in surface roughness.

By comparing Figs. (3.3) and (3.4) one can see that the flow is near isotropic in the central portion of the duct. The value of $\sqrt{\overline{v^2}}$ is slightly higher than that of $\sqrt{\overline{u^2}}$ but this could well be due to the errors in measurement due to the assumption of the cosine law of directional sensitivity , as detailed in Section 2.3.3.

Shown in Fig. (3.5) is the distribution of the shear stress correlation across the duct for various values of L/H. Here one
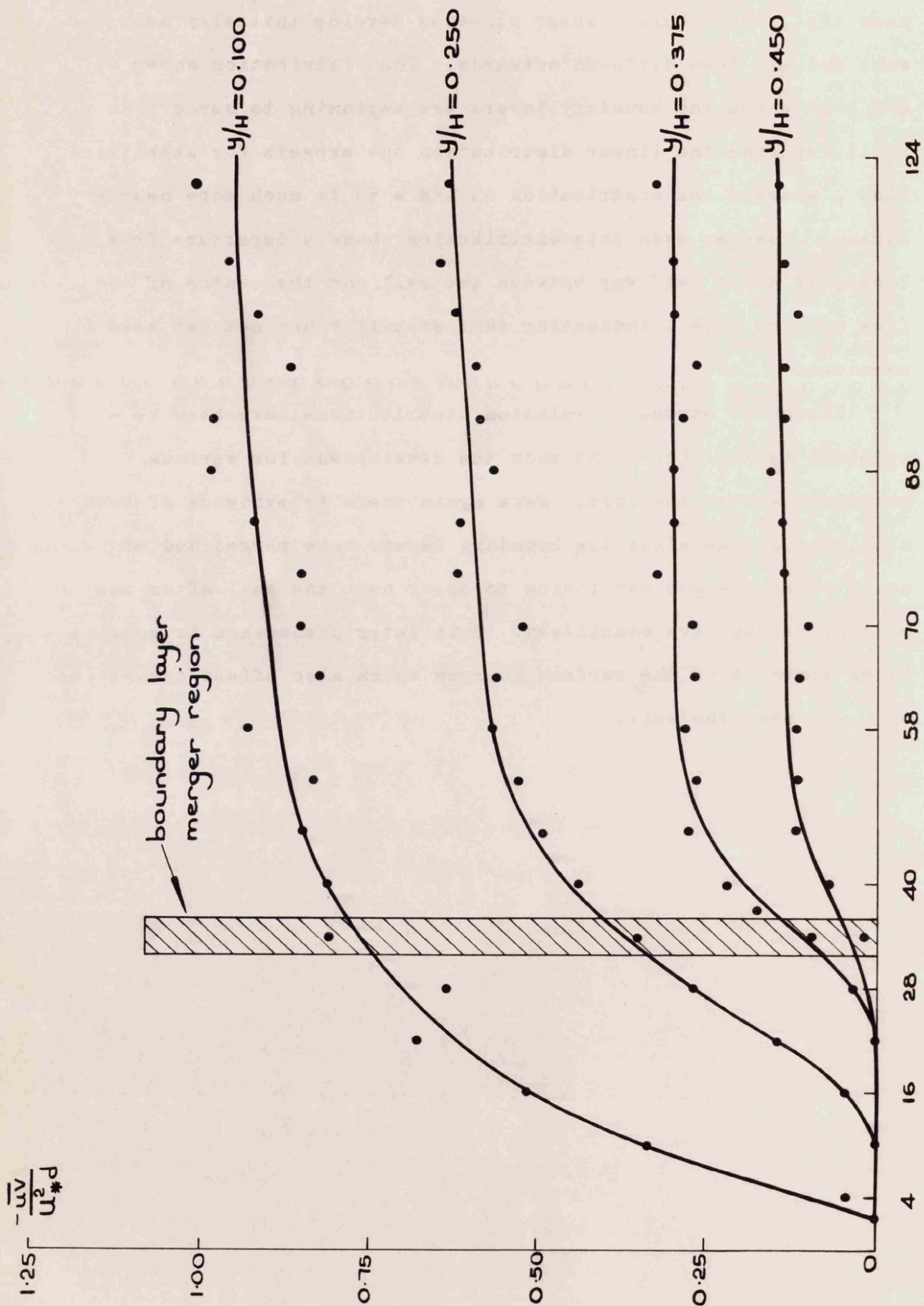
FIG. 3.6. DEVELOPMENT OF TURBULENT SHEAR STRESSES IN DUCT FLOW

sees that the turbulent shear stresses develop initially near the wall and are then diffused outwards. The distribution shown at L/H = 31 where the boundary layers are beginning to merge , is still far from the linear distribution one expects for stabilised flow , whereas the distribution at L/H = 58 is much more nearly linear. However even this distribution shows a departure from linearity about half way between the wall and the centre of the flow on each side , indicating that stability has not yet been acheived.

The shear stress correlation distributions have been re - -plotted in Fig. (3.6) to show the development for various positions across the duct. Here again there is evidence of both continued change after the boundary layers have merged and of small order changes continuing to occur near the wall after the central values have stabilised. This later phenomenon is considered to be a result of the surface changes which also affect the values of $\sqrt{\overline{v^2}}$ near the wall.
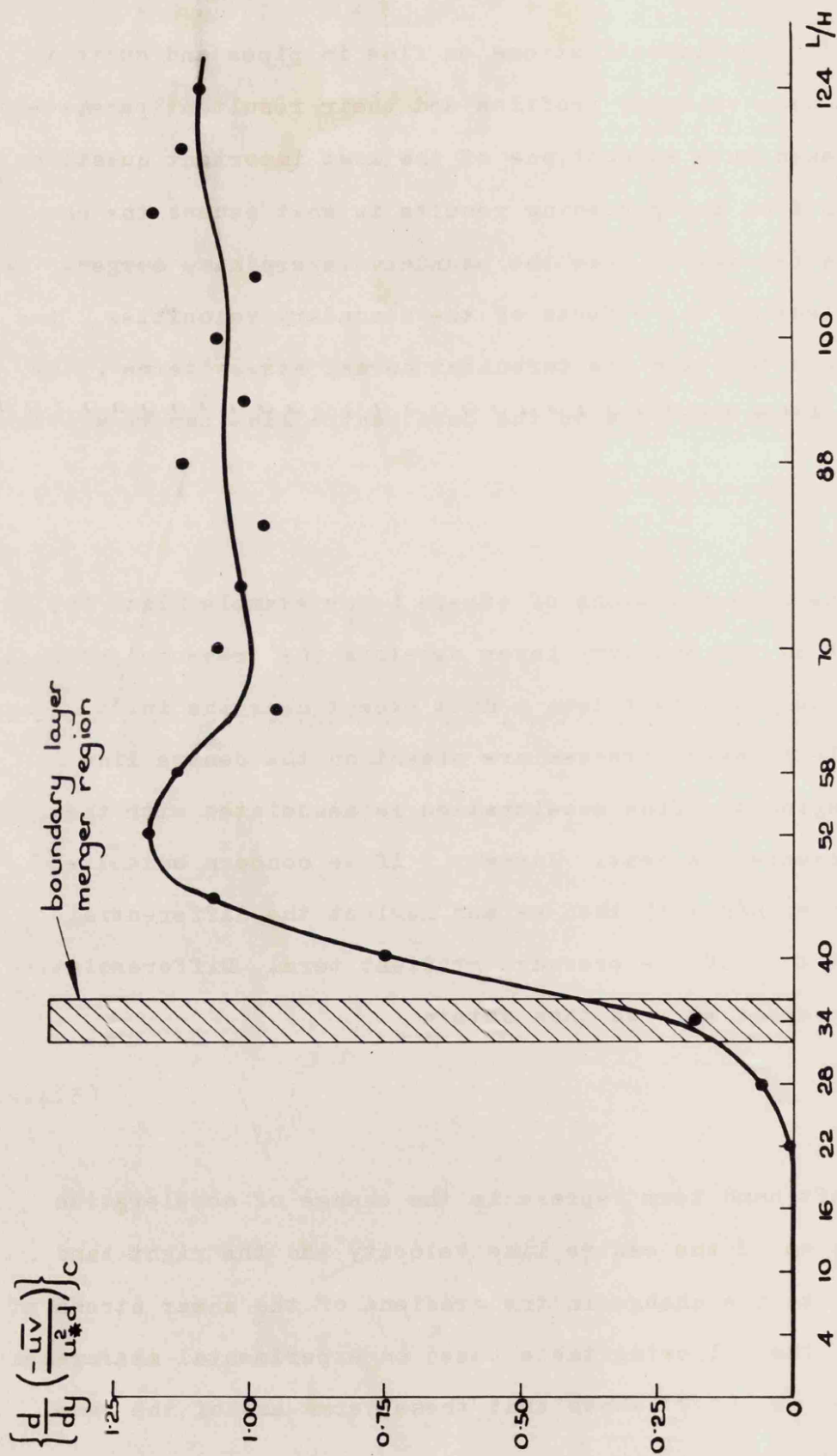
FIG.3.7.TURBULENT SHEAR STRESS GRADIENT ON DUCT CENTRE LINE

3.4. Discussion.

Since in many investigations on flow in pipes and ducts it is only the mean velocity profiles and their resultant parameters which are taken into account, one of the most important questions which arises from the preceding results is what causes the change of thickness parameters once the boundary layers have merged.

By neglecting the effects of the secondary velocities , the viscous stress term and the turbulent normal stress terms , the momentum equation for flow on the duct centre line can be written

$$U_{max} \frac{\partial U_{max}}{\partial x} = -\frac{1}{\rho} \frac{dp}{dx} + \left\{ \frac{\partial}{\partial y} \left(-\overline{uv} \right) \right\}_c \qquad (3.4.1)$$

From the investigations of others (for example Olson (35)) we know that as the boundary layer develops the pressure gradient is approximately constant down a duct except near the inlet , thus since turbulent shear stresses are absent on the centre line in the inlet region the flow acceleration is associated with the changing pressure gradient. However , if we concern ourselves with flow after L/H = 15 then we can neglect the differential with respect to x of the pressure gradient term. Differentiating 3.4.1 with respect to x we then obtain

$$\frac{\partial}{\partial x} \left\{ U_{max} \frac{\partial U_{max}}{\partial x} \right\} = \frac{\partial}{\partial x} \left\{ \frac{\partial}{\partial y} \left(-\overline{uv} \right) \right\}_c \qquad (3.4.2)$$

where the left hand term represents the change of acceleration or deceleration of the centre line velocity and the right hand term represents the change in the gradient of the shear stress at the centre. The following table based on experimental measurements derived from Fig. (3.7) shows that these terms are of the same order of size

L/H	l.h.s.	r.h.s.
34	39 ft/sec^2/ft	34 ft/sec^2/ft
43	36 "	32 "
61	25 "	28 "

Table 1 - Size of Terms in Equation 3.4.2.

The development of the gradient of the shear stress on the duct centre line is shown in Fig. (3.7). Here we see that up to L/H = 22 it is zero since the turbulent shear stresses have not yet grown out from the wall sufficiently to influence it. From L/H = 22 to L/H = 50 it increases up to a value beyond that expected of a linear shear stress distribution. At this point it then decreased to its predicted value at about L/H = 70 whence it remains substantially the same but oscillates about 5% either side of the mean line.

From information here on the behaviour of the turbulent shear stress gradient and using equation 3.4.2. it should be possible to deduce the way in which the central region of the flow will accelerate or decelerate.

As the gradient increases up to about L/H = 50 so we would expect the central velocity to accelerate up to this point and then as it decreases from L/H = 50 to L/H = 70 we would expect this to be accompanied by a deceleration of the central velocity.

If reference is made to Fig. (3.1) , the development of U/$\overline{U}$, for the value y/H = 0.500 then one can see that this is what does happen. Furthermore if we refer to the development of the thickness parameters presented in Fig.(3.2) we can see this trend repeated here , more prominent in S_{qs} than in S^* and θ

since this is more influenced by the centre region's behaviour than the other two.

Thus we see now that the mechanism behind the continued change of the mean velocity profile once the boundary layers have merged is the distribution of the turbulence shear stress , and note that it is the gradient and not their absolute values which is important. Since the shear stresses in the centre of the flow have their origins upstream of their present position , their values in the region where the boundary layers merge will not be compatible with the state of development of the mean velocity profile , and they will continue to increase. Thus any attempt to use local relationships between the mean velocity profile and the turbulence shear stresses in a situation of this nature cannot be entirely succesful.

Chapter 4.

Simulated Flow Conditions.

As we have seen in the previous chapter , if the flow is
allowed to develop unimpededdown a long rectangular duct then
eventually a stable situation is reached , in which the flow
parameters remain constant with increasing distance. In this stable
or equilibrium flow region these parameters can be thought of as
being mutually compatible. If one of the flow parameters is
reproduced in its stable form at the duct entry then by observing
the subsequent behaviour of this and other parameters we will be
able to build up a knowledge of the way in which such parameters
are interrelated. This chapter contains a description of the
effects of simulating mean velocity profiles at the duct entry ,
in which three different types of simulation device were used.

The results of this work are of practical interest to the
field of industrial aerodynamics concerned with model testing in
'unnatural' flows i.e. flows which by virtue of their parameter
distributions , usually the mean velocity profile , cannot be
produced by the natural growth of boundary layers on flat plates
and in pipes. A particularly important aspect of this is the
reproduction of atmospheric boundary layers for the purpose of
testing architectural , structural and vehicular models. Thus a
parallel purpose of this chapter will be an explanation of some of
the methods of 'artificially' producing flows and a discussion
of some of the consequences of the means of production.

4.1. Introduction.

It is perhaps not clear at the moment , why we should be concerned with the consequences of a method of natural flow simulation. The reason for this is that there are a number of practical methods which might be utilised to simulate an equilibrium type of mean velocity profile , but these methods will not necessarily also simulate the compatible equilibrium distributions of other flow parameters. Thus on returning to Clauser's Black Box analogy , if we keep one input constant and allow the others to vary then the outputs of this constant input property will also vary from one case to another.

Practically then , we are concerned with the means of producing velocity profiles and the observation of the changes which take place both in them and in the turbulence structure of the flow as it proceeds downstream.

In his comment on the paper by Baines and Peterson (36) , in which they tested a theoretical analysis of flow through square mesh grids and perforated plates , Eisenberg asks how far downstream it is necessary to go before the velocity profile becomes stabilized . Furthermore , he notes that it is not clear that screens used for boundary layer production will yield the same characteristics (i.e. shear stress distribution) as natural boundary layers , nor is it clear that such boundary layers will continue to grow in the manner of a boundary layer starting from the leading edge of a flat plate.

In this statement we have the problems of the consequences of artificial production of mean velocity profiles concisely stated. Intuitively,and with no reference to other published work, Eisenberg

is suggesting that the manner in which a boundary layer is produced
has an important effect on its subsequent development. As we have
seen in the previous chapter the development of a flow is influenced
by a delicate relationship between the distribution of mean velocity
and turbulent shear stress. Thus to reproduce the equilibrium
distribution of mean velocity and a random distribution of shear
stress will produce a flow whose further development will be
unstable as it proceeds downstream of the simulation mechanism.
This instability will be a function of the difference between the
equilibrium distribution of shear stress and the random distribution
produced by the velocity profile simulation mechanism.

Thus the consequences of a method of flow simulation are made
manifest in the manner in which the flow parameters change down –
–stream of the simulation mechanism. A practical example of the
importance of this is the simulation of an atmospheric boundary
layer in which a long model is to be tested. Here changes in the
flow parameters will be functions of both the effect of the model
on the flow and the stabilisation process of the boundary layer;
difficulty then arises in deciding how much of the total change is
attributable to each cause.

4.2. Methods of Velocity Profile Simulation Available.

The literature contains many accounts of methods of velocity profile simulation , and although a complete survey is not presented here , at least an account of some of the more important methods will be given.

This presentation will be split up into the different types of practical mechanisms , which may be listed as follows:-

(i)   the use of wall roughness

(ii)   a grid of rods normal to the flow

(iii)   a curved rectangular mesh screen

(iv)   a linear rectangular mesh screen angled to the flow

(v)   a system of overlapping screens normal to the flow

(vi)   shaped honeycombs

(vii)   forced mixing devices

Some of their relative advantages and disadvantages will be given in addition to some of the uses to which they have been put.

4.2.1.   The Use of Wall Roughness.

The use of wall roughness for the production of thick boundary layers if the oldest of the available techniques and is often used because of its practical simplicity. A good account of the thickening of boundary layers is given by the work of Nikuradse (37) who first introduced the idea with his sand grain experiments.

Perhaps the most frequently encountered problem requiring the use of some form of velocity profile simulation is that of producing a thick boundary layer in a situation where there is insufficient length available to grow it naturally. For this

purpose wall roughness is often used , even though it does involve
a significant , if shorter length. Franck (38) and Torrance (39)
have both used this method for the simulation of atmospheric
boundary layers for the purpose of model testing. Klebanoff and
Diehl (40) have studied the effects of the use of particle wall
roughness and a number of investigators (Logan and Jones (41) ,
Jacobs (3) etc.) have used a change in wall roughness to
demonstrate the flow history effect as described in Chapter 1.

The major advantage of its use is its practical simplicity and
its ability to yield acceptable results if the modelling laws of
Jenson and Franck (42) are adhered to. These laws are used to
describe the required technique for modelling the upstream terrain
necessary for accurate atmospheric boundary layer simulation. In
most cases of practical interest the Earth's surface is aero -
-dynamically rough so that the effect of viscosity can be neglected.
In this case the flow is entirely determined by the geometry of
the obstacles on the Earth's surface. For the regions which are
not close to an individual obstacle the flow is statistically
determined by the distribution of the roughness length , Zo ,
which is a measure of the average height of the roughness elements.
Provided that the Reynolds Number is not reduced so much that the
surface is no longer aerodynamically rough the flow in the Earth's
boundary layer can be simulated in a model provided geometrical
similarity is preserved and the roughness length , Zo , is reduced
in proportion to the geometric scale.

The basic disadvantage of this approach to the simulation of
velocity profiles is that a prohibitive wind tunnel length is
required for their development. A further drawback is the
inability of this method to produce a range of profile shapes.

4.2.2. The Use of a Grid of Rods Normal to the Flow.

The practice of using a grid consisting of varyingly spaced rods
or cylinders placed normal to the flow is probably the most
frequently used method of simulating a velocity profile. A number
of different theories exist to enable the spacing of the rods to be
calculated to produce a required shape of velocity profile , but
there is no great difference between them. The exception to this
is the theory of Brighton (43) , in which a specific distance
downstream of the grid is required for the profile to develop ,
whereas the other theories assume the profile is generated immed-
-iately downstream of the grid.

Two generalized theories of flow through non - uniform gauzes are
presented by Elder (44) and McCarthy (45) , in which the particular
case of the use of grids of rods is discussed. These are both
complex mathematical treatments of the subject and the work of
Elder has been extended by Cockrell and Lee (46) to give a more
accessible account of the practical use of his theory. Owen and
Zienkiewicz (47) present a theory for the calculation of grids
which will produce linear shear profiles in which to study the
effects of uniform vorticity flow on cylinders. This theory has
subsequently been used by Rose (48) in an attempt to produce a flow
with homogenous turbulence , and by Livesey and Turner (49) who
produce profiles having a high ratio of maximum to mean velocity in
order to study velocity profile decay. In order to study the flow
regimes in diffusers Wolf and Johnson (50) have produced a theory
for the calculation of grids to give axisymmetric and asymetric
velocity profiles. Cowdrey's (51) theory of grid spacing , given
for the simulation of atmospheric velocity profile models, is

probably the simplest available treatment both physically and mathematically. Two other uses of grids are reported , by O'Neill (52) and Brighton (53) who both adopt an empirical , trial and error method , of determining the necessary spacing of the rods.

The major advantage of this method is the practical ease with which a grid of rods can be set up in a wind tunnel combined with the fact that the required profile is thought to be generated immediately downstream of the mechanism (the validity of this and other assumptions concerning the use of grids of rods is discussed later in this chapter). Furthermore the method has the ability to produce a required velocity profile from an initial non-uniform upstream velocity profile. However it is not without disadvantages. Immediately behind the grid the velocity profile is not smooth but consists of a series of jets and wakes and consequently the displacement of a single rod can produce a serious velocity excess or defect in the required profile. Although it is generally assumed that the velocity profile upstream of a grid situated at the working length entry is uniform there is often a thin boundary layer at the wall , and this can be shown to give rise to a velocity excess downstream of the grid close to the wall. This occurs because the fluid upstream has a lower velocity and thus suffers a smaller loss in total head than the fluid in the uniform region of the velocity profile. Hence the total head downstream of the grid increases across the face of the grid , there is a velocity increase toward the wall. Examples of this can be seen in the experimental results published by Owen and Zienkiewiez (47) and Cockrell and Lee (46).

4.2.3. The Use of Curved Rectangular Mesh Screens.

The use of curved rectangular mesh screens for velocity profile
production is not common and suffers from both practical and
theoretical disadvantages.

This method has been employed by Lau (54) in order to study
temperature stratified atmospheric boundary layers as part of a
programme concerning air pollution. Lau presents a theoretical
prediction method for the necessary curvature and produces good
agreement with experiment. Baines (55) has also used this method
in a study of the pressure distributions on model buildings in an
atmospheric flow , but his curvatures were arrived at in an
empirical manner. As part of his mathematical treatment of flow
through arbitrarily shaped gauzes Elder (44) also considers the
case of the curved rectangular mesh screen , and an extension of
his work here is presented by Turner (56).

The use of this method of velocity profile production entails
some practical disadvantages concerning the structural support
required in a wind tunnel. Even if the screen is held by shaped
clamps at either side of the working section , it is often found
necessary to insert shaped stiffening rods at intervals along its
length , to ensure uniformity of curvature laterally. These
stiffening rods then produce wakes which at least are a nuisance
and can coalesce and ruin the entire flow. Furthermore , the
appearance of wrinkles in the gauze can disrupt the required
velocity profile by acting in a manner similar to lenses and
producing flow concentrations.

4.2.4. The Use of Linear Rectangular Mesh Screen Angled to the flow.

Apart from the theoretical treatment by Elder (44) , only one example of this method is known to the author , that being by Bonneville and Harper (57). This method has only a limited application due to the type and shape of profile which can be produced in this manner. The effect of screen non-uniformities here has the same disadvantages mentioned in connection with the use of curved gauzes.

4.2.5. The Use of a System of Overlapping Screens Normal to the Flow.

McCarthy (45) , as part of his treatment of a generalized theory of flow through non-uniform gauzes , considered the flow produced by a system of overlapping rectangular mesh gauzes having varying solidarity ratios. The theoretical analysis required to predict the required gauze system for a particular flow is complex but has the advantage over other methods in its ability to deal with three-dimensional flows. McCarthy used this method satisfactorily to simulate the flow pattern produced by a ship's hull in which propellers could be tested.

However there are practical disadvantages in this method of velocity profile simulation. The availability of mesh sizes dictated by the analysis may be difficult to realize and imperfec--tions in the joints between the types of mesh will produce disturbing wakes.

4.2.6. The Use of Shaped Honeycombs.

The use of shaped honeycombs , that is honeycombs having a lateral variation of cell length , has been used by Kotansky (58) to produce linear shear flow. The use of this material as a gauze for profile simulation is advantageous since it eliminates most of the structural and support problems encountered in the use of the other methods. Because of its cellular structure it is useful as a built-in flow straightener and by varying the size and shape of the cells it is possible to effect some control over the resulting turbulence structure. Its main disadvantage is the problem of machining it to produce the required shape , but this is probably best overcome by using a metal honeycomb fitted with low melting point thermoplastic polymer which can be removed when the shaping operation is completed.

4.2.7. The Use of Forced Mixing Devices.

The use of a number of forced mixing devices to alter velocity profiles and prevent flow separation is outlined by Schubauer and Spandenburg (59). They reach the conclusion that the use of forced mixing devices produces similar effects on the flow to the reduction of the pressure gradient , and the small differences in boundary layer thickness produced by different flow mixing devices are subsequently magnified as the flow develops downstream.

An earlier application of one of the devices discussed by Schubauer and Spandenburg , the vortex generator , is made by Taylor (60) who used it to prevent separation inside a diffuser.

Further use of the forced mixing device concept is made by Armitt (61) to simulate the turbulence structure of the atmospheric flows. Armitt argued that better results could be obtained for

the flow around structural models if the atmospheric turbulence was modelled and the velocity profile grew rapidly as a result of the induced mixing than if only the velocity profile was modelled with no thought for the turbulence structure. Armitt's work has since been improved by Counihan (62) who used slim wedges rather than vortex generators.

A disadvantage of the use of forced mixing devices for flow simulation lies in the difficulty of producing an adequate theoretical analysis for the resulting flow. This problem is further considered in the next section. In general however their use is on trial and error basis governed primarily by what published results exist.
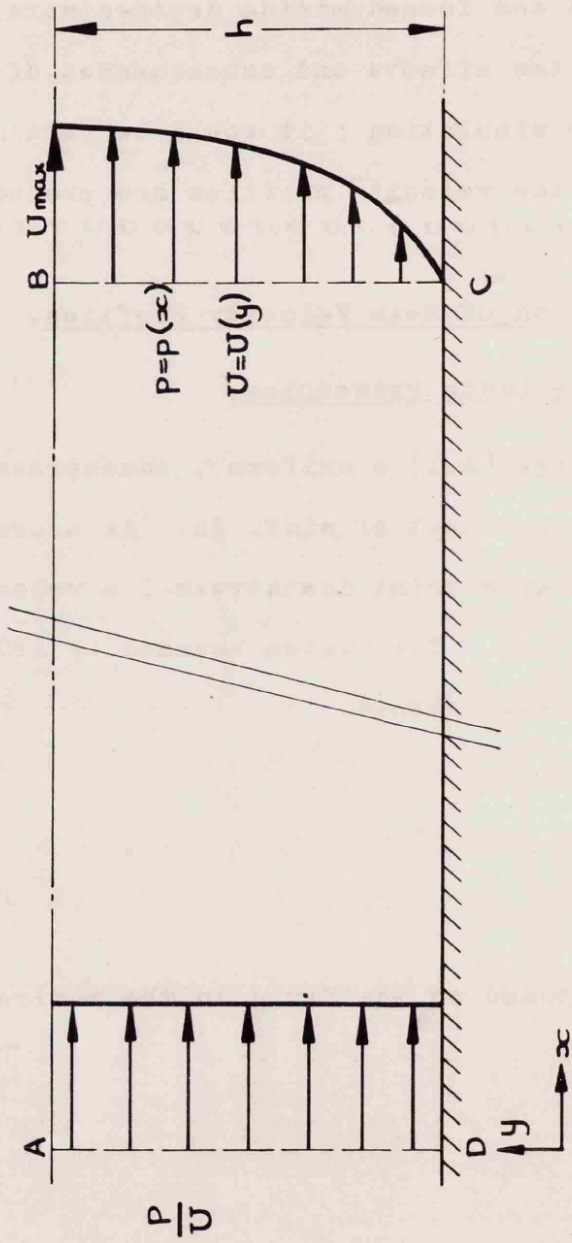
FIG. 4.1. ILLUSTRATION OF MOMENTUM PRINCIPLE

4.3. Methods of Flow Simulation Adopted.

In view of the effort required it was decided not to attempt to simulate the flow with all of the available methods but to concentrate on those most frequently utilised to model atmospheric flows. Thus a grid of rods and forced mixing devices were chosen.

In order to progress to the effects and consequences of these methods of velocity profile simulation , it would be pertinent at this point to desdribe how the velocity profiles are produced.

4.3.1. The Production of Mean Velocity Profiles.

(a) Consideration of the Basic Principles.

In the system shown in Fig. (4.1) a uniform , incompressible , two - dimensionàl flow enters a duct of width 2h. As a consequence of some constraint situated at a point downstream , a velocity profile $U = U(y)$ is established. The system bounded by ABCD must then satisfy the following requirements.

Continuity.

$$\bar{U}.h = \int_o^h U.dy \qquad\qquad 4.3.1.$$

Conservation of Momentum.

$\sum F_x$ = Total force imposed on the fluid in the x direction per unit width.

$$\left. \begin{aligned} &= \rho \left\{ \int_o^h U_{loc}^2 . dy - \bar{U}^2.h \right\} \\[2mm] &= (P - p).h + \text{thrust on walls} \\ &\qquad\quad + \text{thrust on constraint} \end{aligned} \right\} \quad 4.3.2.$$

Energy.

Along any streamline , application of Bernoulli's Equation gives

$$p(x) + \tfrac{1}{2}\rho V_R^2 = H$$

where V_R is the resultant velocity in the direction of the streamline.

On the grounds of symmetry , AB in Fig. (4.1) is a streamline and thus

$$P + \tfrac{1}{2}\rho \bar{U}^2 = p + \tfrac{1}{2}\rho U_{max}^2 + \Delta H \qquad 4.3.3.$$

Equilibrium.

When the mean velocity profile is in equilibrium the total force acting on the fluid is zero , i.e.

$$\textstyle\sum F_x = 0 \qquad\qquad 4.3.4.$$

As an illustration of these principles , consider a boundary layer growing along DC and let $\dfrac{\delta(x)}{h}$ be small. The centreline velocity is given by

$$U_{max}(x) = \bar{U}\left\{ \frac{h}{h - \delta^*(x)} \right\}$$

where δ^* is the boundary layer displacement thickness.

Since ΔH is negligible (where $\dfrac{\delta(x)}{h}$ is small) by application of Equation 4.3.3 along the centreline

$$p(x) = P - \tfrac{1}{2}\rho \bar{U}^2 . \frac{\delta^*(x)\left\{ 2h - \delta^*(x) \right\}}{\left\{ h - \delta^*(x) \right\}} \qquad 4.3.5.$$

and thus from Equation 4.3.2.

$$\sum F_x = \{P - p(x)\} \cdot h - \int_0^x \tau_w \cdot dx$$

$$= -\rho \bar{U}^2 \cdot \theta(x) \qquad\qquad 4.3.6.$$

where θ is the boundary layer momentum thickness.

The contribution of the pressure term is to accelerate the flow near the centreline where the shear forces are small. However , near the wall shear fordes dominate , thus preventing an acceleration of the flow. Consequently a velocity profile is formed.

Now consider the problem where x has increased so that $\frac{\delta(x)}{h}$ is no longer small. As an example let $\delta(x) = h$, so that the boundary layer just fills the duct. Since AB constitutes a stream - line , the rate of change of momentum can no longer be considered to be $-\rho \bar{U}^2 \cdot \theta(x)$ but Equation 4.3.6. becomes

$$\sum F_x = \{P - p(x)\} \cdot h - \int_0^x \tau_w \cdot dx = \rho \left\{ \int_0^h U^2 \, dy - \bar{U}^2 \cdot h \right\}$$

If the boundary layer can be represented by a power law

$$\frac{U}{U_{max}} = (y/h)^{1/n}$$

then from equation 4.3.1

$$U_{max} = \left(\frac{n+1}{n}\right) \bar{U}$$

and hence F_x is given by

$$\sum F_x = \{P - p(x)\} \cdot h - \int_0^x \tau_w \cdot dx = \rho \bar{U}^2 \cdot h \cdot \frac{1}{n(n+2)} \qquad 4.3.7.$$

To determine the drag imposed by the wall consider Equation 4.3.5. in the case of the production of a power law profile boundary layer.
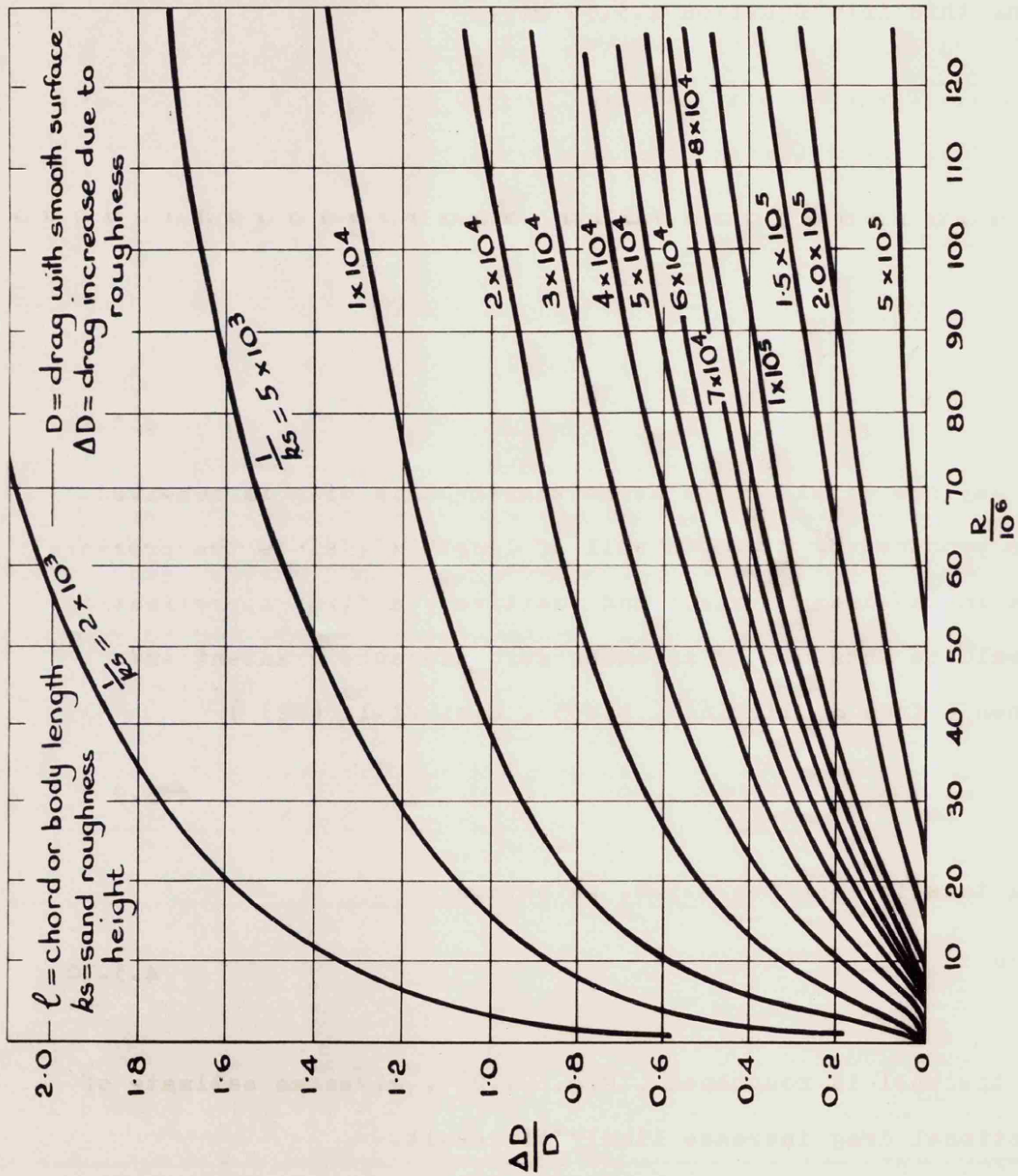
FIG. 4.2. FRACTIONAL INCREASE OF DRAG (BASED ON NIKURADE'S MEASUREMENTS)

Since $\dfrac{\delta^*(x)}{h}$ is given by

$$\frac{\delta^*(x)}{h} = \frac{1}{(1+n)}$$

the equation reduces to

$$P - P(x) = \tfrac{1}{2}\rho\,\overline{U}^2\left\{\frac{2n+1}{n^2}\right\}$$

Inserting this into Equation 4.3.7. gives

$$\int_0^x \tau_w \cdot dx = \rho\,\overline{U}^2 h\left\{\frac{2n+1}{2n^2} - \frac{1}{n(n+2)}\right\}$$

$$= \rho\,\overline{U}^2\,h\left\{\frac{(2n+1)(n+2) - 2n}{2n^2(n+2)}\right\}$$

$$= \rho\,\overline{U}^2\,h\cdot\left\{\frac{2n^2 + 3n + 2}{2n^2(n+2)}\right\}$$

$$4.3.8.$$

We may now consider the means whereby this drag is acheived. If it is produced by a smooth wall of length x , since the pressure gradient in the duct is small and positive , a first approximation for x could be obtained by assuming zero pressure gradient and n = 7 when (from Schlicting , p.433 , Eqn. 21.12 (22))

$$\int_0^x \tau_w \cdot dx = 0.0128\,\rho\,U_{max}^2 \cdot x \cdot \left(\frac{U_{max}\,\delta}{\nu}\right)^{-1/4}$$

$$4.3.9$$

Equating this to equation 4.3.8. we obtain

$$\frac{x}{h} = \left(\frac{\overline{U}.h}{\nu}\right)^{1/4} \cdot \left\{\frac{2n^2 + 3n + 2}{2n^2(n+2)}\right\} \cdot \frac{1}{0.029}$$

$$4.3.10$$

If the wall is roughened , Fig. (4.2) , gives an estimate of the fractional drag increase likely to result.

If $\dfrac{\Delta D}{D}$ = 2.0 , at a maximum roughness height , the drag in equation 4.3.9. will be increased threefold and a typical value of

$\dfrac{x}{h}$ to produce a 1/7th power law profile at a Reynolds Number of

3.10^5 will be reduced from the value given by Equation 4.3.10 of

88.5 to 73.6.

Further reduction in length is possible by still further

increasing the drag (for instance introducing a step obstruction

to the flow). In all cases the normal turbulent mixing process

will ensure the characteristic power law shape , consisting of a

near constant velocity profile except in the region close to the

wall. Since diffusion by turbulent mixing occurs comparitively

slowly it may be necessary to hasten the mixing process by the

introduction of vortex generators downstream of the step.

(b) Profile Produced by Constraints.

As we have seen in the previous chapter it takes time for the

linear shear stress distribution , characteristic of equilibrium

flows , to establish itself. Hence , unless the devices chosen to

produce the resistance to the flow are able to create the necessary

shear stresses then the required linear distribution must develop

outwards from the wall. Thus devices like the step considered

above will produce a velocity profile having the correct momentum

thickness but are unlikely to be in equilibrium. It is for this

reason that devices such as the vortex generator have been used to

introduce the flow resistance. Such devices are capable of producing

a finite , if incorrectly shaped , distribution of shear stress ,

and even this is sufficient to interact with the mean flow ,

decelerating it and causing rapid boundary layer growth.

Thus there are two interrelated features of simulated velocity

profiles , (i) there must be the means to produce a momentum defect

(ii) there must also be the means to produce a linear shear stress

distribution if the profile is to be in equilibrium.

(c) **Profile Produced by Grids of Rods.**

The characteristic argument in the formulation of a mathematical
model for the design of these grids is to neglect the production
of shear stresses and to assume no change will occur in the profile
once it has been produced. Thus the flow can be regarded as poten-
-tial both upstream and downstream of the grid.

Over the last 30 years there have been a number of approaches
to the problem of the design of graded drag producing mechanisms.
Using Weighardt's (63) relationship the non - dimensional pressure
drop , K , across the grid is related to its geometry and may be
expressed as

$$K = \frac{\Delta p}{\frac{1}{2}\rho U^2} = \frac{c\,s}{(1-s)^2} = \frac{c(1-\beta)}{\beta^2}$$

4.3.11.

where U is the relative velocity through the grid

    c is a slowly varying function of Reynolds Number

    s is the solidarity ratio

    β is the porosity of the grid

In a grid of cylindrical rods of diamter d and centreline
spacing l , s may be expressed as d/l .

In order to design the grid it is necessary to establish an
expression for K(y) in terms of the known upstream velocity profile.
Collar (64) established a method of analysis based on the Rankine-
Froude actuator disc theory. Assuming the total head to be
conserved both upstream and downstream of the grid he used the
momentum and energy principles to establish an expression for K in
terms of the upstream and downstream axial velocities. The problem
of grid design differs from actuator disc theory in that the

pressure far from the grid is not the same upstream as it is downs-

-tream and in developing the equations Collar had to consider the

evaluation of this overall pressure difference. There are

additional problems associated with satisfying continuity for flow

constrained by a duct and the method Collar adopted is criticised

by Taylor and Batchelor (65). They , and others since , introduce

distrubance velocities ,having some simple structure , into the

flow. Then using the constancy of total head postulation both

upstream and downstream of the grid they obtain the realtionship.

$$\frac{U_2}{U_1} = \frac{1 + \alpha - \alpha K}{1 + \alpha + K}$$ 4.3.12.

where U_1 is the velocity increment produced by the disturbance

velocity at an upstream station and U_2 is the corresponding

increment at a downstream station. α is the refraction of the

stream at the grid introduced by lateral flow. In this way the

behaviour of lateral flow is introduced into the analysis.

Using Equation 4.3.12 K is given from the known velocity

distribution U_1 and the required distribution U_2 once α is

known. An empirical relationship for α suggested by Taylor and

Batchelor is

$$\alpha = 1.1 \left(1 + K \right)^{-1/2}$$ 4.3.13.

Even so , the form of relationship given by Equation 4.3.12. is

still not entirely suitable for present purposes since , most

importantly , it does not permit a lateral velocity variation to be

represented.

As an attempt to improve this work , Elder (44) produced a

very general extension of the method proposed by Owen and Zienkiewicz

(47) for the production of linear shear profiles , which permitted

the consideration of arbitrarily shaped and positioned gauzes.
Elder's theory is complex and very difficult to follow but since
it seemed the most appropriate for present purposes it was adopted
in the early stages of this programme.

McCarthy (45) greatly simplified the presentation of the
problem. Using the concept of constancy of total head in the axial
direction , both upstream and downstream of the grid he further
argues that since vorticity is constant along streamlines to the
first order of small quantities the lateral total head gradient is
given by

$$\frac{dH}{dy} = \rho\, U_x \left\{ \frac{dU_{x_1}}{dy} \right\} \qquad\qquad 4.3.14.$$

where U_x is the local axial velocity and U_{x1} is the axial velocity
either a long way upstream or downstream of the grid according to
which field of flow is under consideration. Applying this
relationship at the grid , through which U_x is continuous , gives

$$\frac{1}{2} U_{x_0} \frac{dK}{dy} + K \frac{dU_{x_0}}{dy} + \frac{d}{dy}\left(U_{x_{1u}} - U_{x_{1d}} \right) = 0 \qquad 4.3.15.$$

where subscripts u and d imply upstream and downstream evaluation
respectively , if K - from equation 4.3.11 - is written as

$$\frac{\Delta H}{\frac{1}{2}\rho U_{x_0}^2}$$

where U_{xo} is the local axial velocity.

McCarthy shows that Equation 4.3.15 reduces to Equation 4.3.12.
for uniformly graded grids , but permits the design of varyingly
graded grids for flow in a duct.

At this point the mathematics of grid design have become
increasingly formidable , and are of doubtful merit. Not only is the
fundamental assumption of unchanging equilibrium shear stresses
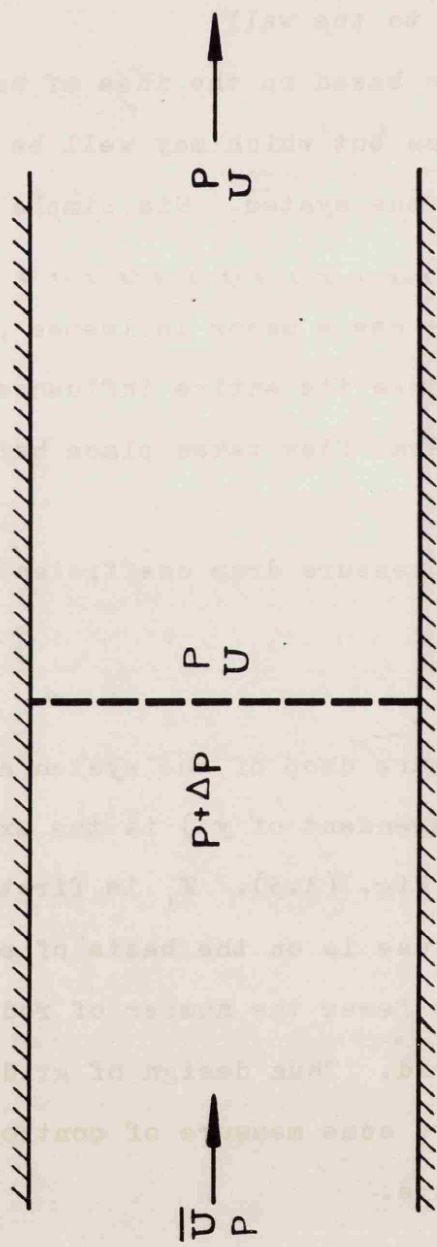
FIG.4.3.COWDREY'S GRID SYSTEM

downstream of the grid untrue (as the following experimental measurements indicate) but as Cowdrey (51) points out , in order to get solutions at all from such sophisticated approaches , linear--izing techniques have to be adopted and these are seldom valid in the region of high shear close to the wall.

Thus Cowdrey's approach is based on the idea of using simple concepts which model the physics but which may well be only approximate representations of the system. His simple concepts are:-

(i) since the grid of rods has a major influence , by blockage, on the flow ahead of it he assumes its entire influence is on the upstream flow and thus all lateral flow takes place before the grid, and

(ii) he defines a system pressure drop coefficient K_1 as

$$K_1 = \frac{P - P}{\frac{1}{2}\rho \bar{U}^2}$$

where $P - P$ is the total pressure drop of the system and $\bar{U}$ (which Cowdrey takes to be independent of y) is the axial velocity far upstream of the grid , see Fig. (4.3). K_1 is first determined arbitrarily and its successive use is on the basis of experience. The larger the value chosen the fewer the number of rods which will be required in the resulting grid. Thus design of grids having different values of K_1 may give some measure of control over the accompanying turbulence structure.

Now if the local non dimensional pressure drop , K , across the grid is defined as

$$K = \frac{\Delta P}{\frac{1}{2}\rho U^2}$$

then we can write the overall pressure drop as

$$P - \bar{P} = \frac{1}{2}\rho\left(U^2 - \bar{U}^2\right) + \frac{1}{2}\rho U^2 K$$

i.e.

$$\frac{P - \bar{P}}{\frac{1}{2}\rho\bar{U}^2} = (u^*)^2(1+K) - 1 = K_1$$

which is

$$\quad (u^*)^2 = \frac{1+K_1}{1+K} \qquad\qquad 4.3.16$$

where

$$u^* = \frac{U}{\bar{U}}$$

u* is established by the shape of the velocity profile that is required , e.g. for a linear shear profile in which

$$\bar{U}.\delta = \int_{y=0}^{y=\delta} U.dy \qquad\qquad 4.3.17$$

then

$$u^* = \frac{2y}{\delta}$$

Note that u* is not the non - dimensional velocity ratio in the required profile , for in the illustration chosen the maximum velocity is shown by continuity to be $2\bar{U}$ and not U.

Since K is established in terms of the grid structure by Equation 4.3.11 , and u* in terms of the required velocity profile by equation 4.3.17 then equation 4.3.16 can be solved to yield the required grid design.
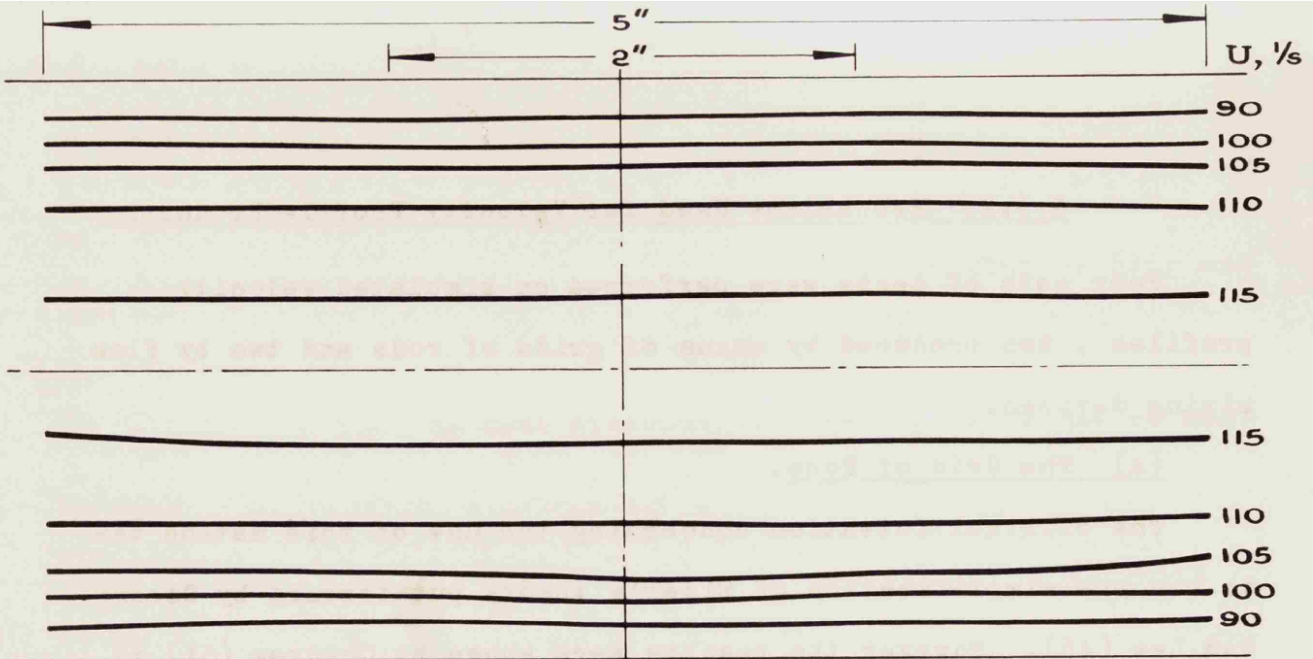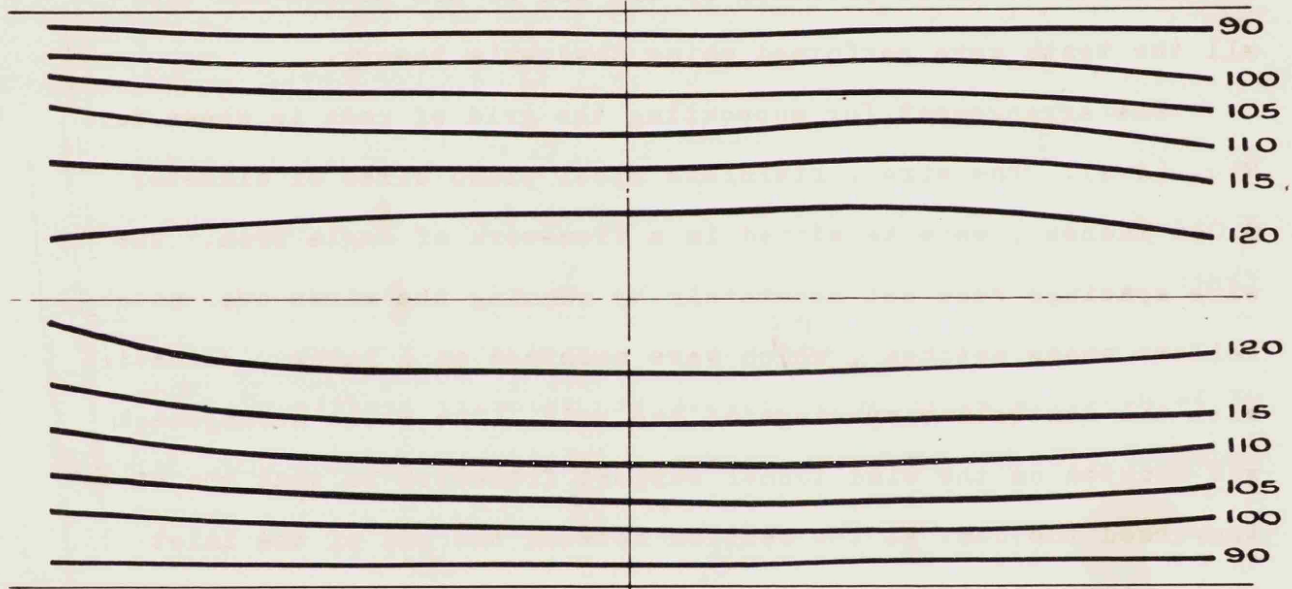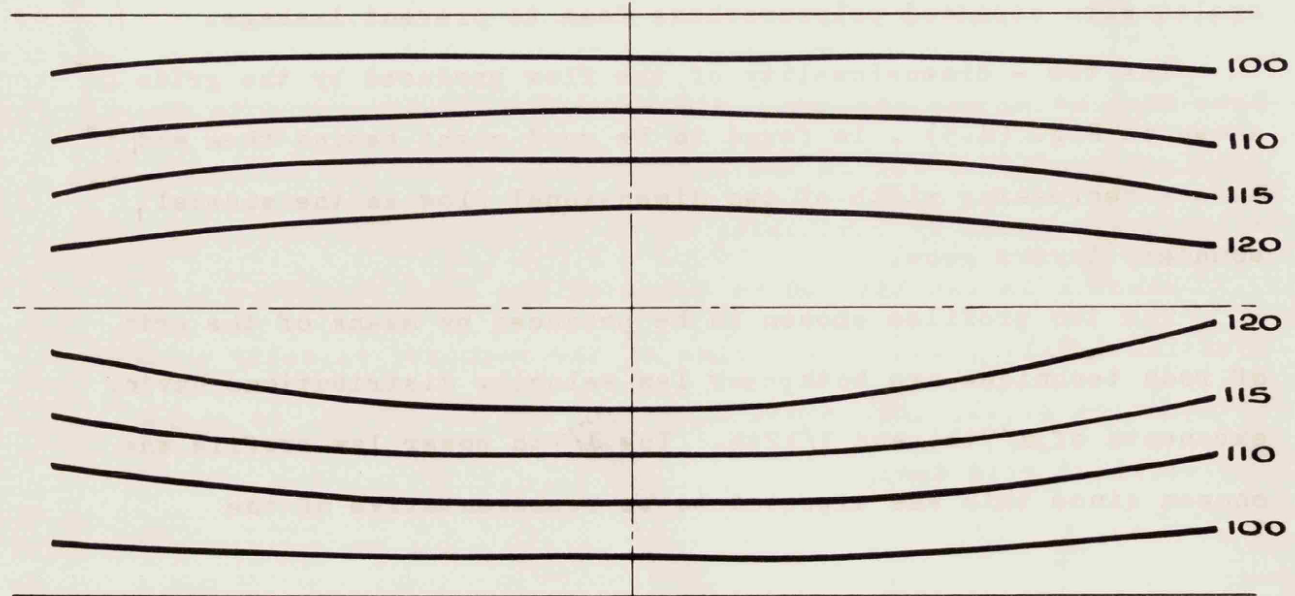
FIG.4.5. CONTOURS OF CONSTANT VELOCITY BEHIND 1/12th P.L.GRID

4.3.2. Mechanisms Used for Velocity Profile Production.

Four sets of tests were performed on simulated velocity profiles , two produced by means of grids of rods and two by flow mixing devices.

(a) The Grid of Rods.

The original intention concerning the use of this method was to use the simplification of Elder's theory put forward by Cockrell and Lee (46). However the results were shown by Cowdrey (51) to be inferior to those produced by the use of his method and thus all the tests were performed using Cowdrey's theory.

The arrangement for supporting the grid of rods is shown in Fig. (4.4). The wire , stainless steel piano wires of diameter 0.036 inches , were tensioned in a framework of angle iron. The wire spacings were set accurately by running the wires over notched rollers whose notches , which were machined on a lathe , coincided with the centreline spacings of the rods. The whole arrangement was mounted on the wind tunnel support framework so that the wires traversed the duct at the section between the end of the inlet contraction and the start of the working length. The section was sealed with expanded polyeurathene foam to prevent leakage.

The two - dimensionality of the flow produced by the grids , shown in Fig. (4.5) , is found to be good right behind them and to have a decreasing width of two dimensional flow as the sidewall boundary layers grow.

The two profiles chosen to be produced by means of the grid of rods technique are both power law velocity distributions having exponents of 1/7th. and 1/12th. The 1/7th power law profile was chosen since this was expected to be representative of the
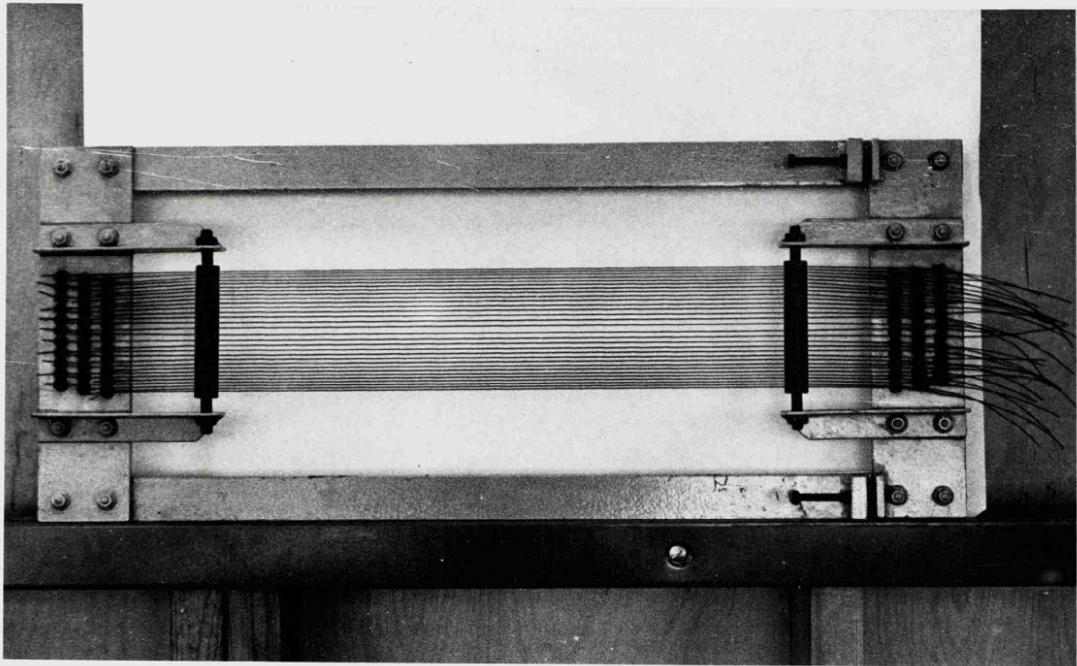
Fig. 4.4 The Wire Grid and its Support Frame

FLOW

(i)

FLOW

$1\frac{1}{2}"$

$1"$

$4"$

(ii)
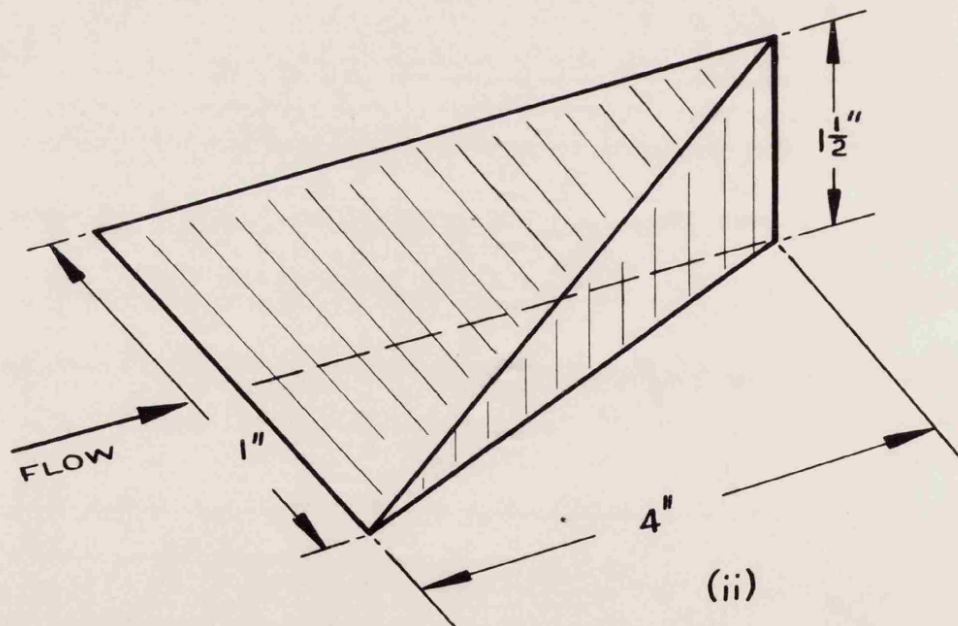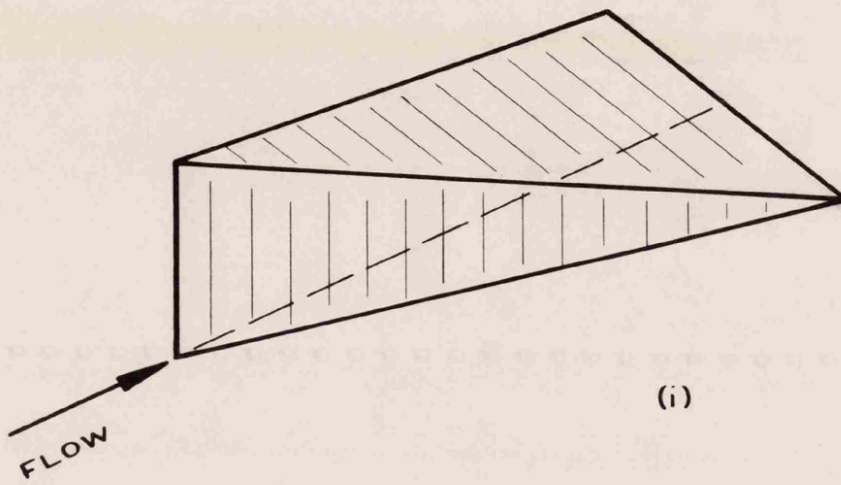
FIG.4.6. FLOW MIXING DEVICES

(i) TRIANGULAR PLOW

(ii) RAMP

FIG.4.7.POSITIONING OF RAMPS

equilibrium state of the flow at the Reynolds Number of the tests. Following preliminary tests with this grid it was found that a slight acceleration of the flow occured downstream of it and thus to observe this process more carefully a profile having a more nearly constant velocity central region was produced which would show any tendency of acceleration in greater detail. The power law exponent chosen for this purpose was 1/12.

(b) The Forced Mixing Devices.

The use of forced mixing devices in these tests is due primarily to the arguments advanced by Armitt (61). He states that in the simulation of atmospheric boundary layers the production of turbulence of the correct scale outweighs the advantages of producing the exact mean velocity profile.

Armitt's experimental facilities consisted of a small fence followed by a row of triangular vortex generators set at alternate angles to the flow. The reason for the alternate angular setting was to avoid the introduction of net vorticity in the (x , z) plane into the flow and to minimize three dimensional effects. He does note , however , that a small discrepancy in the angular setting of one vortex generator can produce annoying asymmetrical effects.

For this reason flow mixing devices which were symmetrical in themselves were chosen for the present work. The devices , chosen from an extensive list prepared by Schubauer and Spandenburg (59), were the ramp and triangular plow illustrated in Fig. (4.6). The arrangement of these devices is shown in Fig. (4.7) for the ramps on the tunnel floor. This pattern is repeated on the roof and is the same for the triangular plows.

It is noted that the ramp and the triangular plow are in fact geometrically identical but when in use merely point in opposite
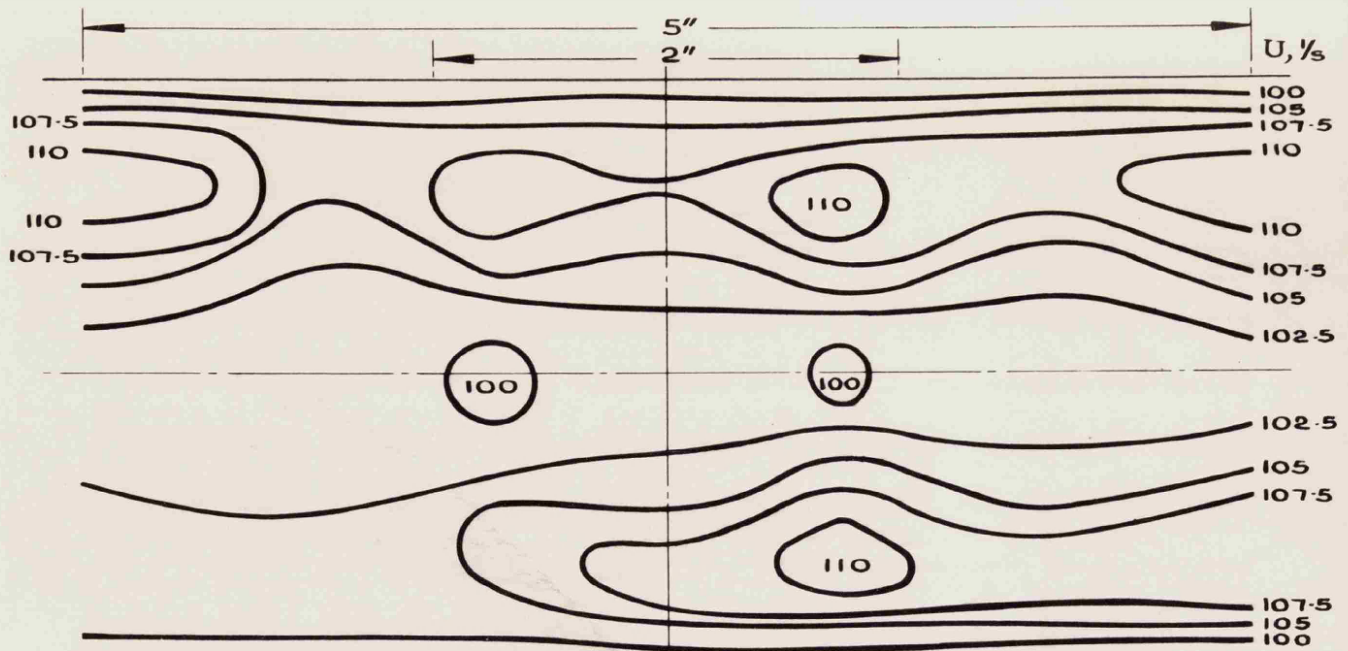
(a) L/H = 4
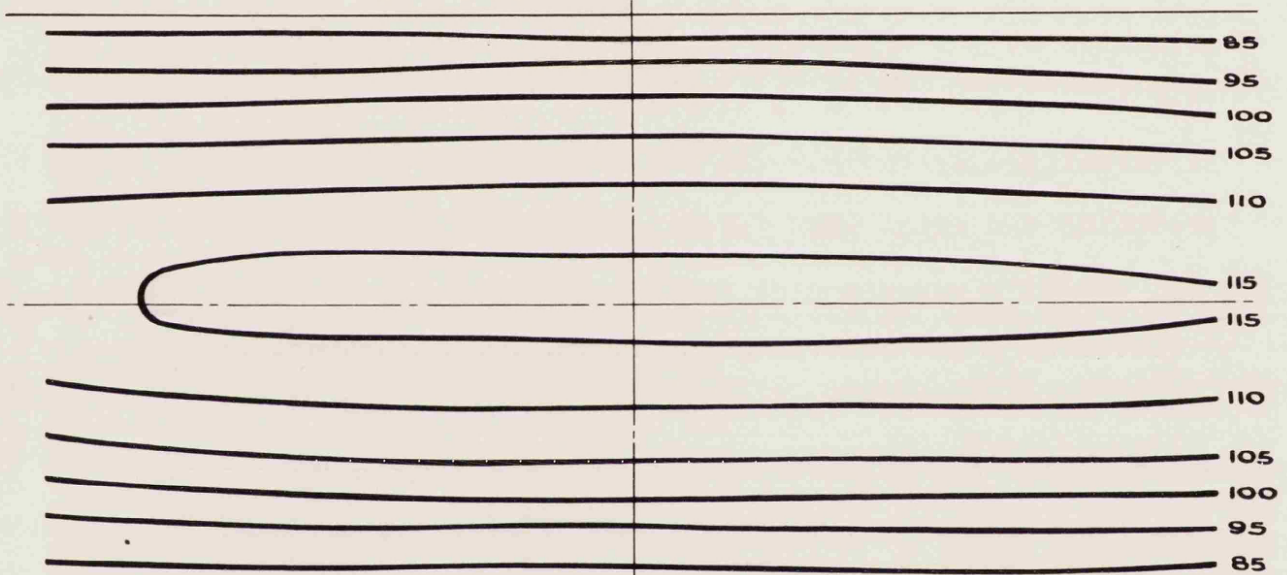
(b) L/H = 46
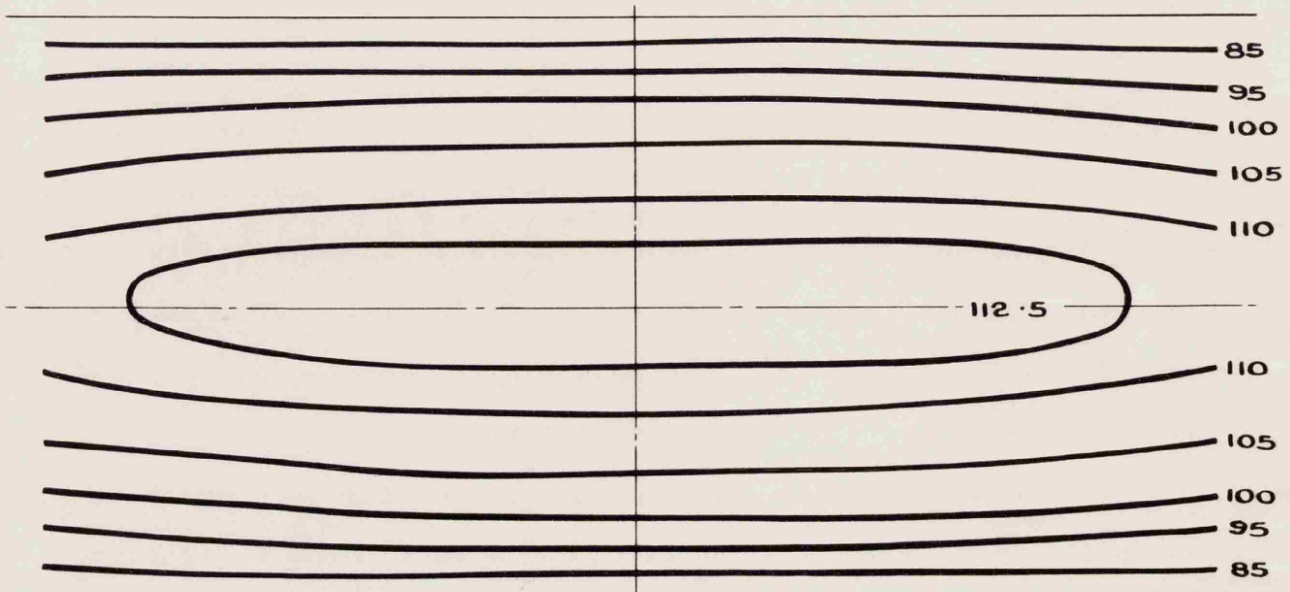
(c) L/H = 121

FIG. 4.8. CONTOURS OF CONSTANT AXIAL VELOCITY BEHIND THE TRIANGULAR PLOUGH DEVICES
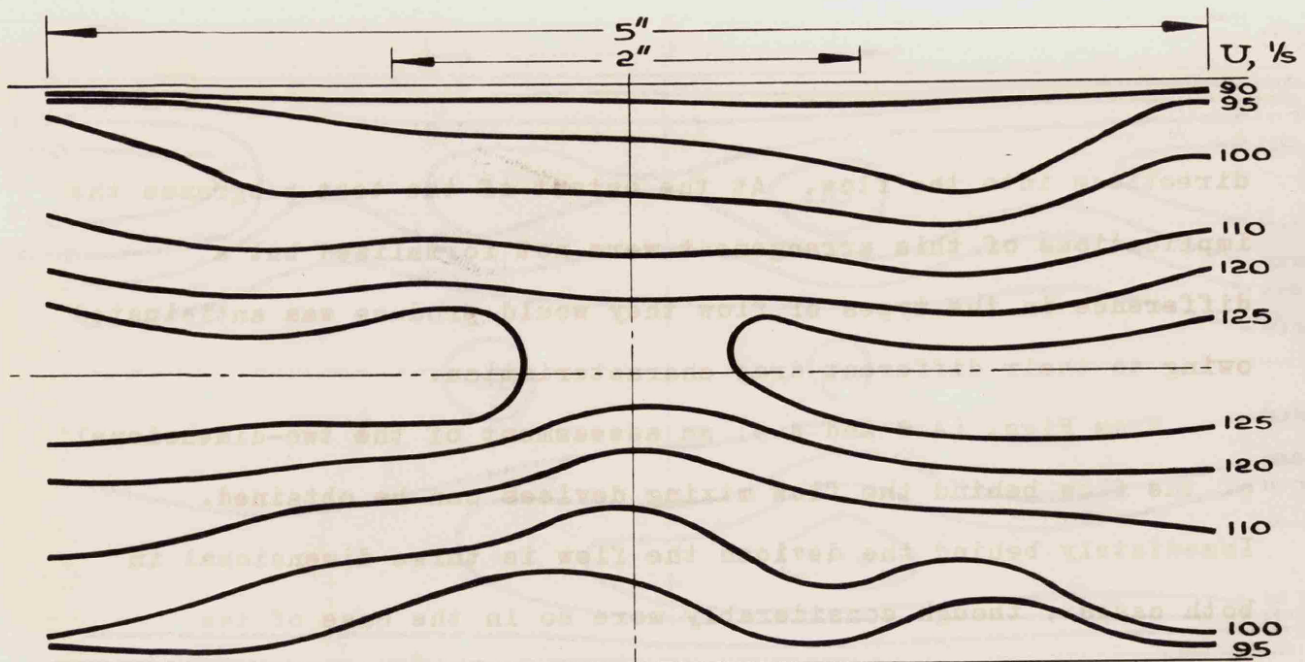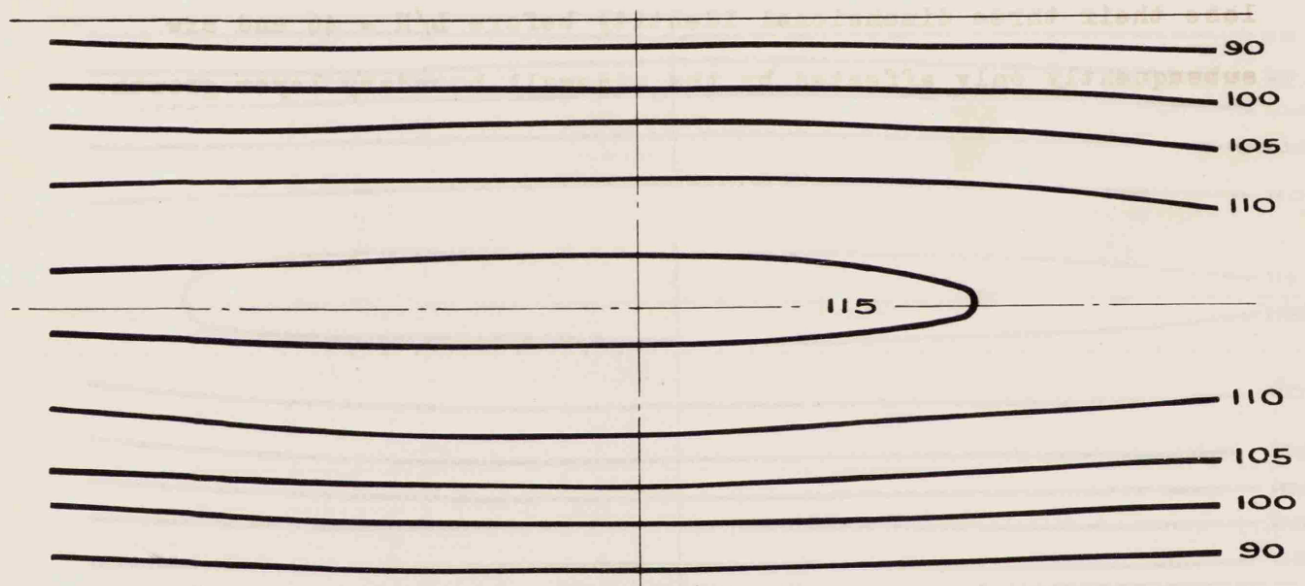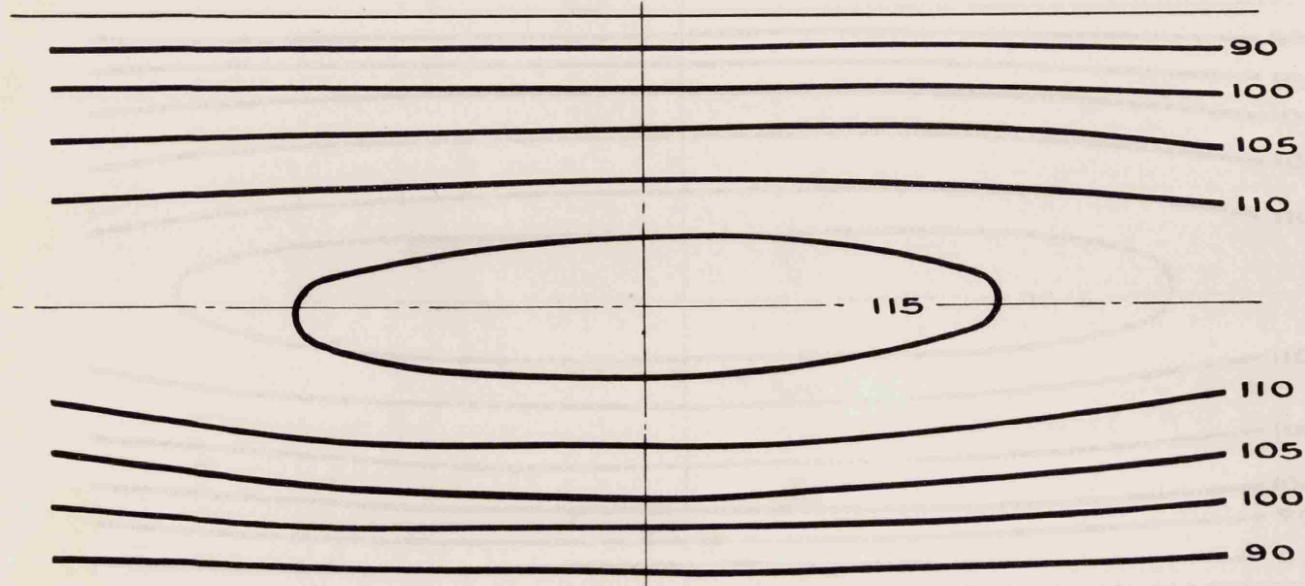
FIG.4.9. CONTOURS OF CONSTANT AXIAL VELOCITY BEHIND RAMP DEVICES

directions into the flow. At the outset of the test programme the
implications of this arrangement were not formalized but a
difference in the types of flow they would produce was anticipated
owing to their different drag characteristics.

From Figs. (4.8 and 4.9) an assessment of the two-dimensionality
of the flow behind the flow mixing devices can be obtained.
Immediately behind the devices the flow is three dimensional in
both cases , though considerably more so in the case of the
triangular plow than in the ramp. However both these flow patterns
lose their three dimensional identity before L/H = 46 and are
subsequently only affected by the sidewall boundary layer growth.
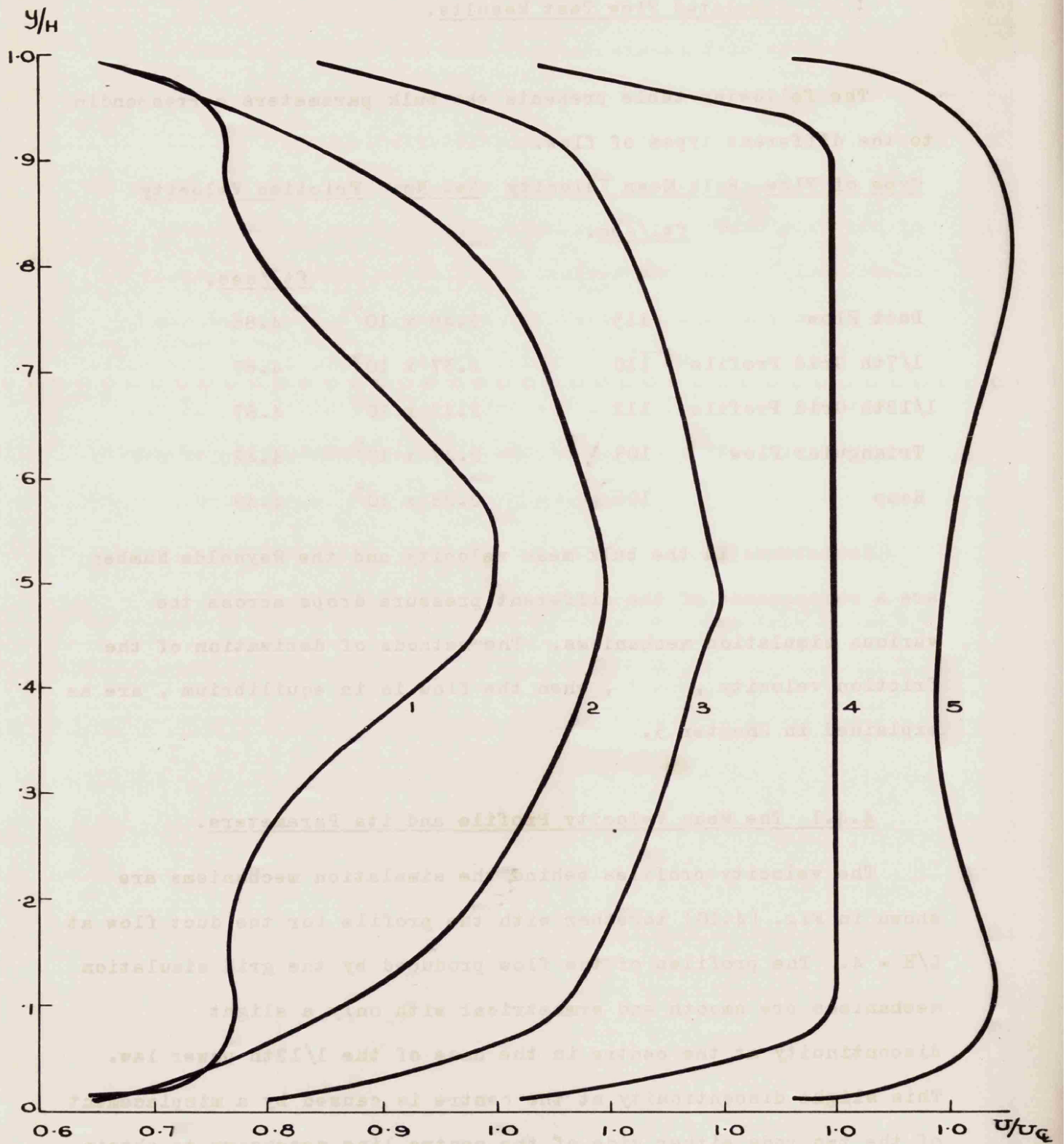
FIG.4.10.VELOCITY PROFILES IMMEDIATELY BEHIND SIMULATORS

1 — RAMP DEVICE
2 — 1/7th P.L. GRID
3 — 1/12th P.L. GRID
4 — DUCT FLOW AT L/H = 4
5 — TRIANGULAR PLOW DEVICE

4.4. Simulated Flow Test Results.

The following table presents the bulk parameters corresponding to the different types of flow.

Type of Flow	Bulk Mean Velocity ft./sec.	Re. No.	Friction Velocity U_{*d} ft./sec.
Duct Flow	115	2.48×10^5	4.86
1/7th Grid Profile	110	2.37×10^5	4.67
1/12th Grid Profile	112	2.42×10^5	4.87
Triangular Plow	105	2.47×10^5	4.42
Ramp	106	2.28×10^5	4.49

Variations in the bulk mean velocity and the Reynolds Number are a consequence of the different pressure drops across the various simulation mechanisms. The methods of derivation of the friction velocity , U_{*d} , when the flow is in equilibrium , are as explained in Chapter 3.

4.4.1 The Mean Velocity Profile and its Parameters.

The velocity profiles behind the simulation mechanisms are shown in Fig. (4.10) together with the profile for the duct flow at L/H = 4. The profiles of the flow produced by the grid simulation mechanisms are smooth and symmetrical with only a slight discontinuity at the centre in the case of the 1/12th power law. This slight discontinuity at the centre is caused by a misplacement of the two rods either side of the centre line necessary to obtain a fit in the total spacing distances across a fixed width duct. The flow behind the forced mixing devices is unusual and not
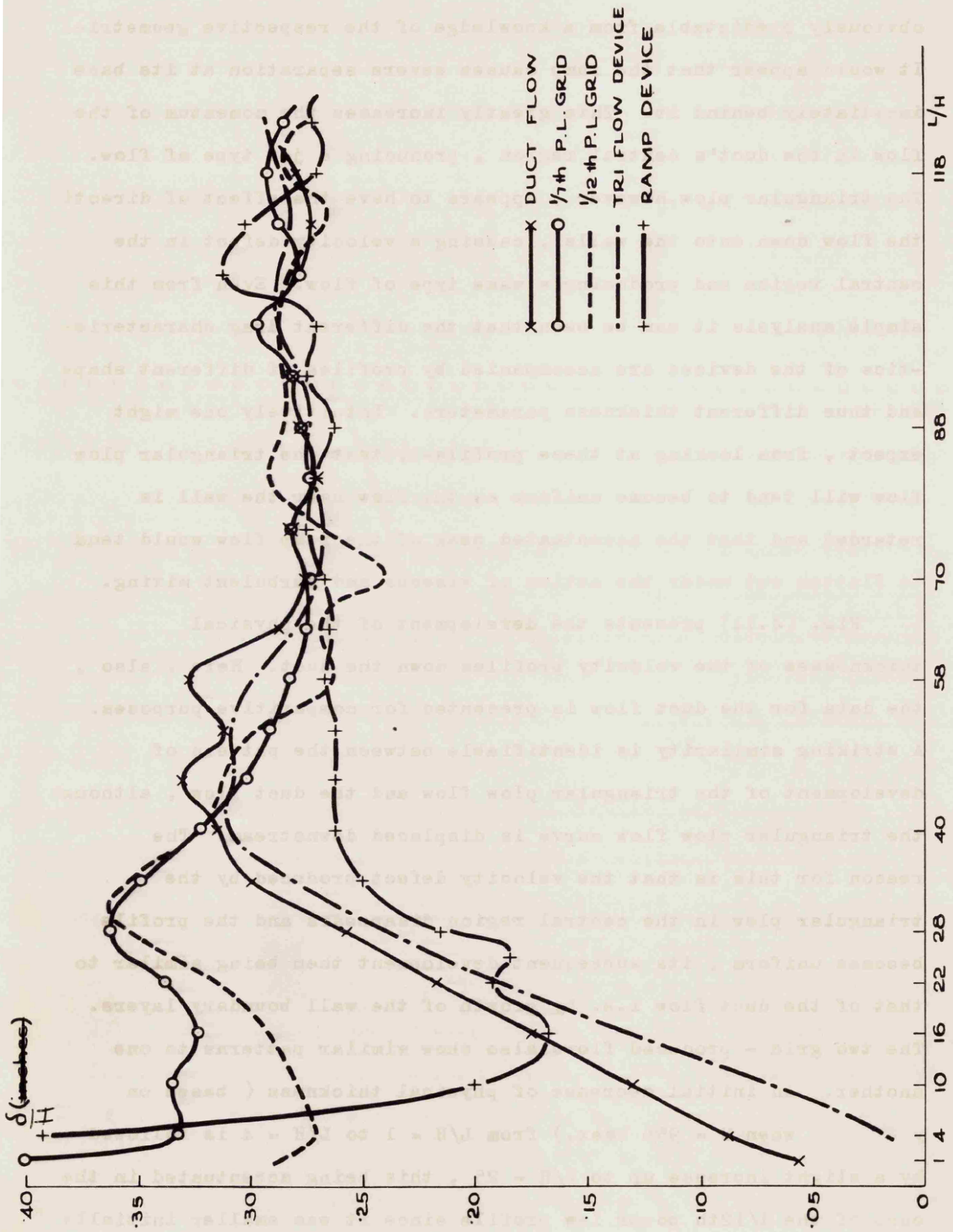
FIG. 4.11. DEVELOPMENT OF PHYSICAL THICKNESS δ WHEN $y = \delta$ $U = 95\%$ U MAX

obviously predictable from a knowledge of the respective geometries.
It would appear that the ramp causes severe separation at its base
immediately behind it. This greatly increases the momentum of the
flow in the duct's central region , producing a jet type of flow.
The triangular plow,however , appears to have the effect of directing
the flow down onto the walls , causing a velocity defect in the
central region and producing a wake type of flow. Even from this
simple analysis it can be seen that the different drag characteris-
-tics of the devices are accompanied by profiles of different shape
and thus different thickness parameters. Intuitively one might
expect , from looking at these profiles , that the triangular plow
flow will tend to become uniform as the flow near the wall is
retarded and that the accentuated peak of the ramp flow would tend
to flatten out under the action of viscous and turbulent mixing.

Fig. (4.11) presents the development of the physical
thicknesses of the velocity profiles down the duct. Here , also ,
the data for the duct flow is presented for comparitive purposes.
A striking similarity is identifiable between the pattern of
development of the triangular plow flow and the duct flow , although
the triangular plow flow curve is displaced downstream. The
reason for this is that the velocity defect produced by the
triangular plow in the central region disappears and the profile
becomes uniform , its subsequent development then being similar to
that of the duct flow i.e. by growth of the wall boundary layers.
The two grid - produced flows also show similar patterns to one
another. An initial decrease of physical thickness (based on
$y = \mathcal{S}_{95}$ when $U = 95\%$ Umax.) from $L/H = 1$ to $L/H = 4$ is followed
by a slight increase up to $L/H = 25$, this being accentuated in the
case of the 1/12th power law profile since it was smaller initially.
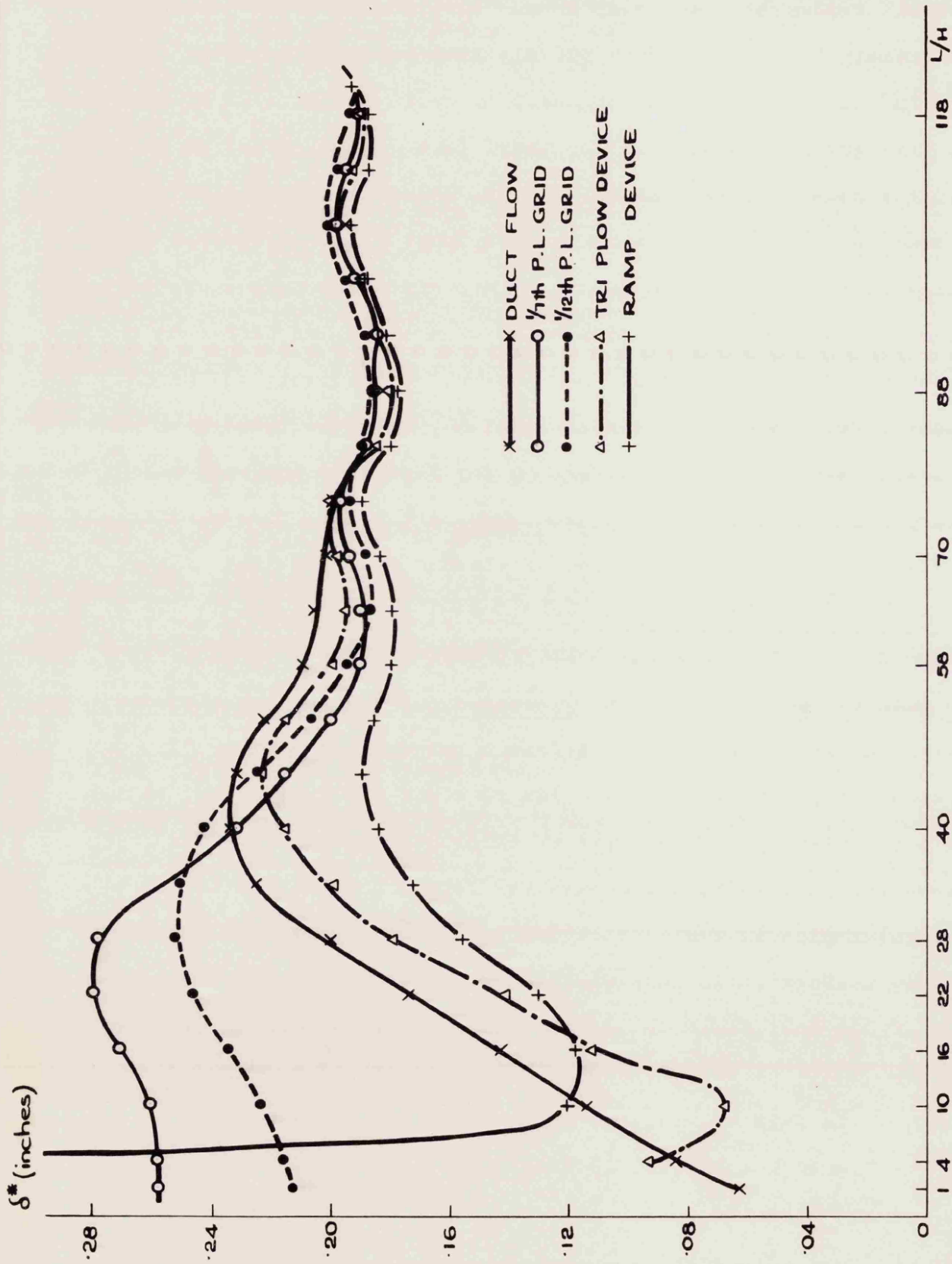
FIG. 4.12. DEVELOPMENT OF DISPLACEMENT THICKNESS δ^*

Legend:
× DUCT FLOW
○ 1/11th P.L. GRID
● 1/12th P.L. GRID
△ TRI FLOW DEVICE
+ RAMP DEVICE

δ^* (inches)

L/H

θ(inches)

·28 ·24 ·20 ·16 ·12 ·08 ·04

1 4 10 16 22 28 40 58 70 88 118 L/H

× DUCT FLOW
○ 1/7th P.L. GRID
● 1/12th P.L. GRID
△ TRI FLOW DEVICE
+ RAMP DEVICE
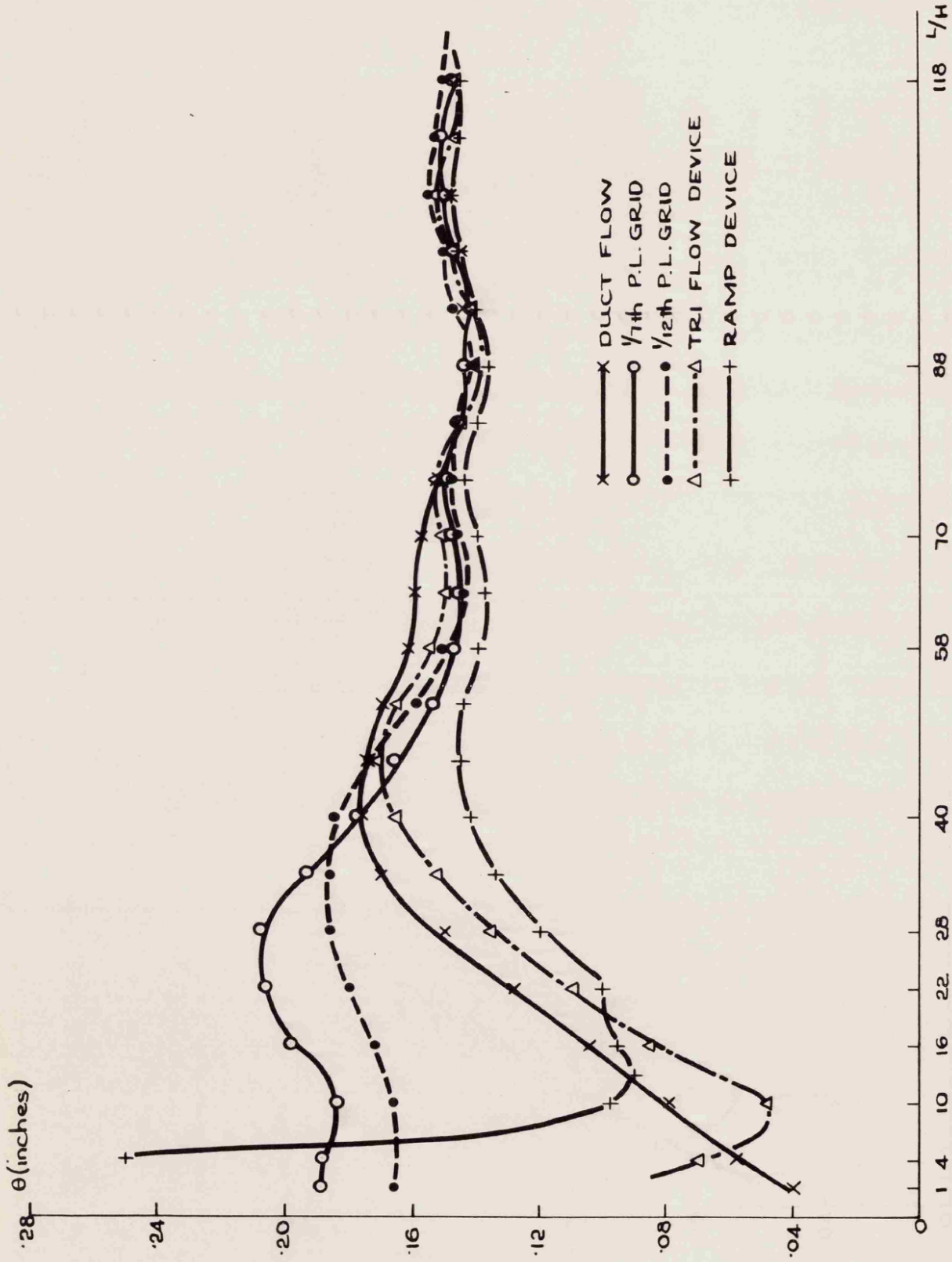
FIG.4.13. DEVELOPMENT OF MOMENTUM THICKNESS θ
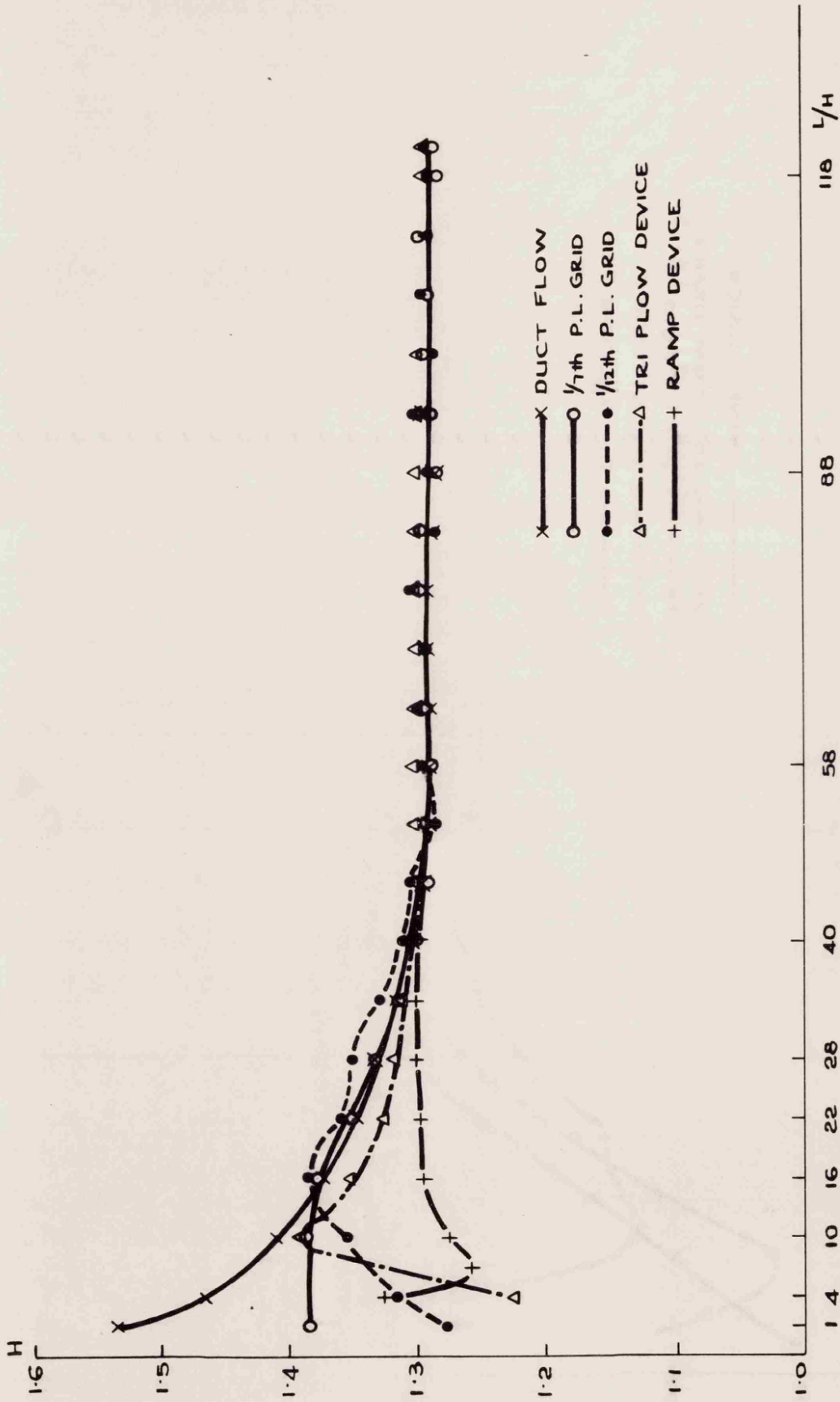
FIG. 4·14. DEVELOPMENT OF SHAPE FACTOR H

Legend:
× DUCT FLOW
○ 1/7th P.L. GRID
● 1/12th P.L. GRID
△ TRI FLOW DEVICE
+ RAMP DEVICE

Axes:
H (vertical axis): 1·0, 1·1, 1·2, 1·3, 1·4, 1·5, 1·6
L/H (horizontal axis): 4, 10, 16, 22, 28, 40, 58, 88, 118
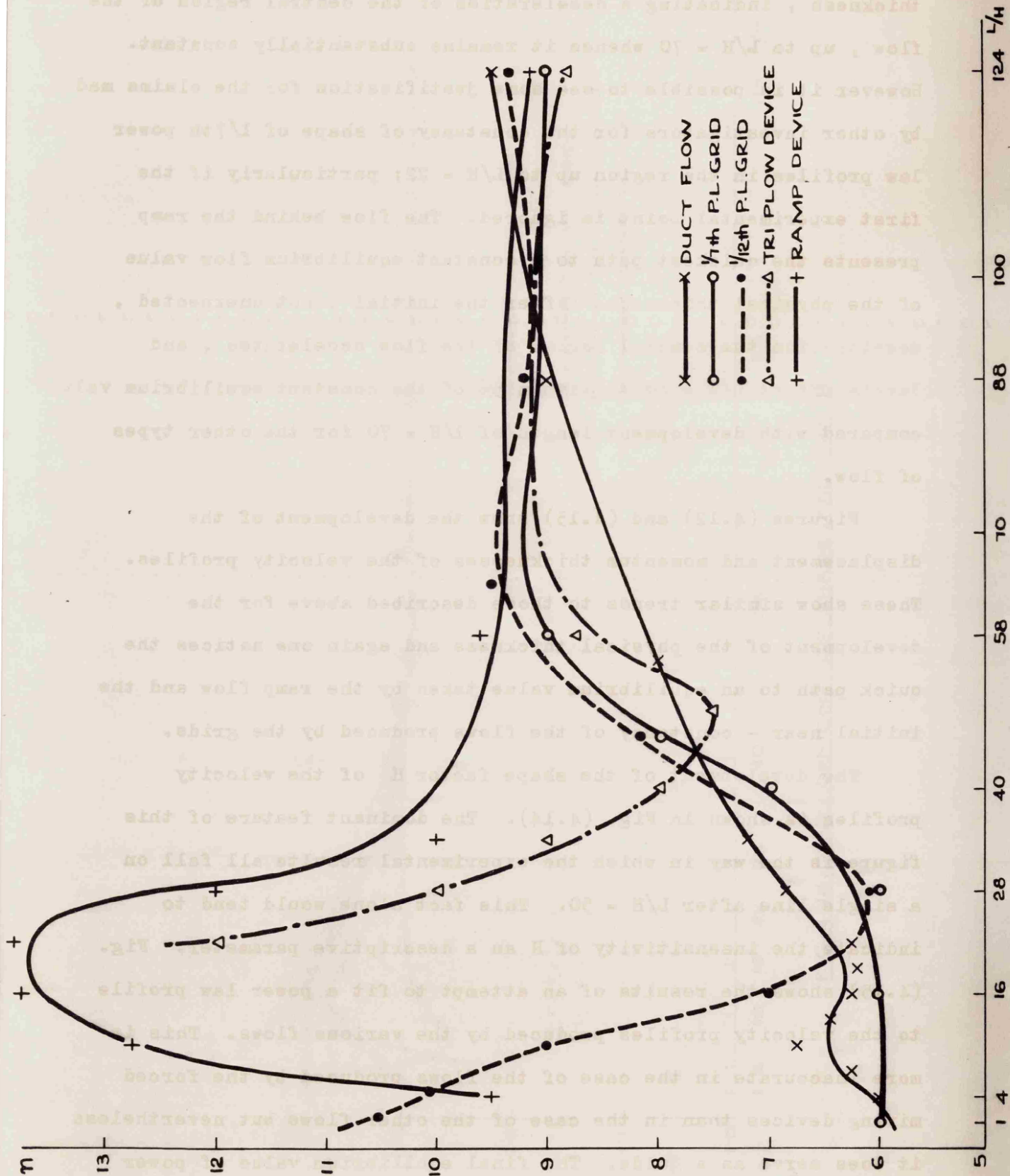
FIG.4.15.DEVELOPMENT OF POWER LAW EXPONENT η

This is then followed by a comparatively large decrease in
thickness , indicating a deceleration of the central region of the
flow , up to L/H = 70 whence it remains substantially constant.
However it is possible to see some justification for the claims made
by other investigators for the constancy of shape of 1/7th power
law profiles in the region up to L/H = 22; particularly if the
first experimental point is ignored. The flow behind the ramp
presents the quickest path to a constant equilibrium flow value
of the physical thickness. After the initial , not unexpected ,
deceleration the central region of the flow accelerates , and
levels off at L/H = 40 to within 5% of the constant equilibrium value
compared with development length of 1/H = 70 for the other types
of flow.

Figures (4.12) and (4.13) show the development of the
displacement and momentum thicknesses of the velocity profiles.
These show similar trends to those described above for the
development of the physical thickness and again one notices the
quick path to an equilibrium value taken by the ramp flow and the
initial near - constancy of the flows produced by the grids.

The development of the shape factor H of the velocity
profiles is shown in Fig. (4.14). The dominant feature of this
figure is the way in which the experimental results all fall on
a single line after L/H = 50. This fact alone would tend to
indicate the insensitivity of H as a descriptive parameter. Fig.
(4.15) shows the results of an attempt to fit a power law profile
to the velocity profiles produced by the various flows. This is
more inaccurate in the case of the flows produced by the forced
mixing devices than in the case of the other flows but nevertheless
it does serve as a guide. The final equilibrium value of power
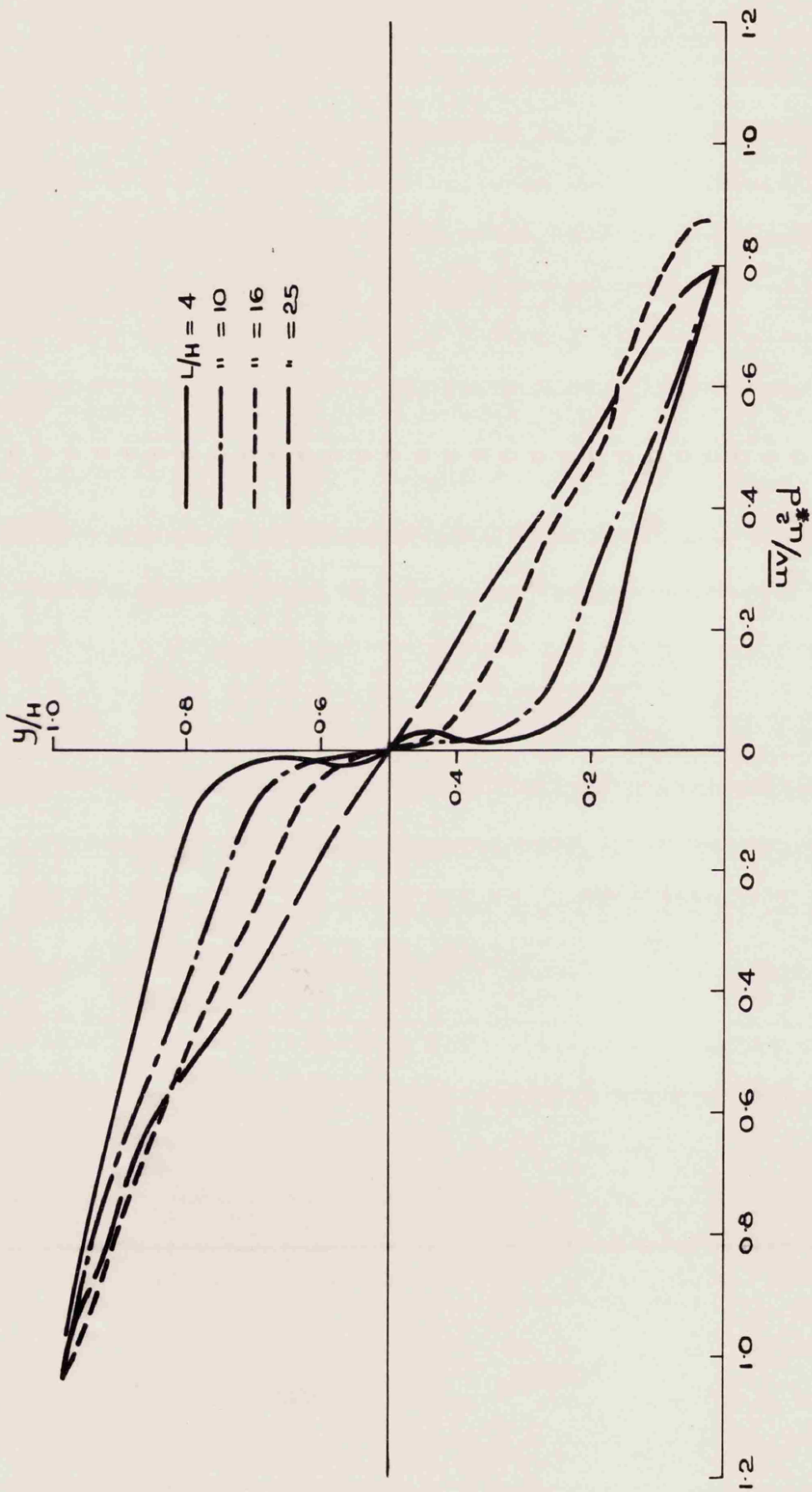
FIG.4.16.REYNOLDS STRESS DISTRIBUTION BEHIND ¼th P.L. GRID.

$x/H = 4$
$\quad " = 13$
$\quad " = 25$
$\quad " = 37$

y/H

$\overline{uv}/u_*^2$
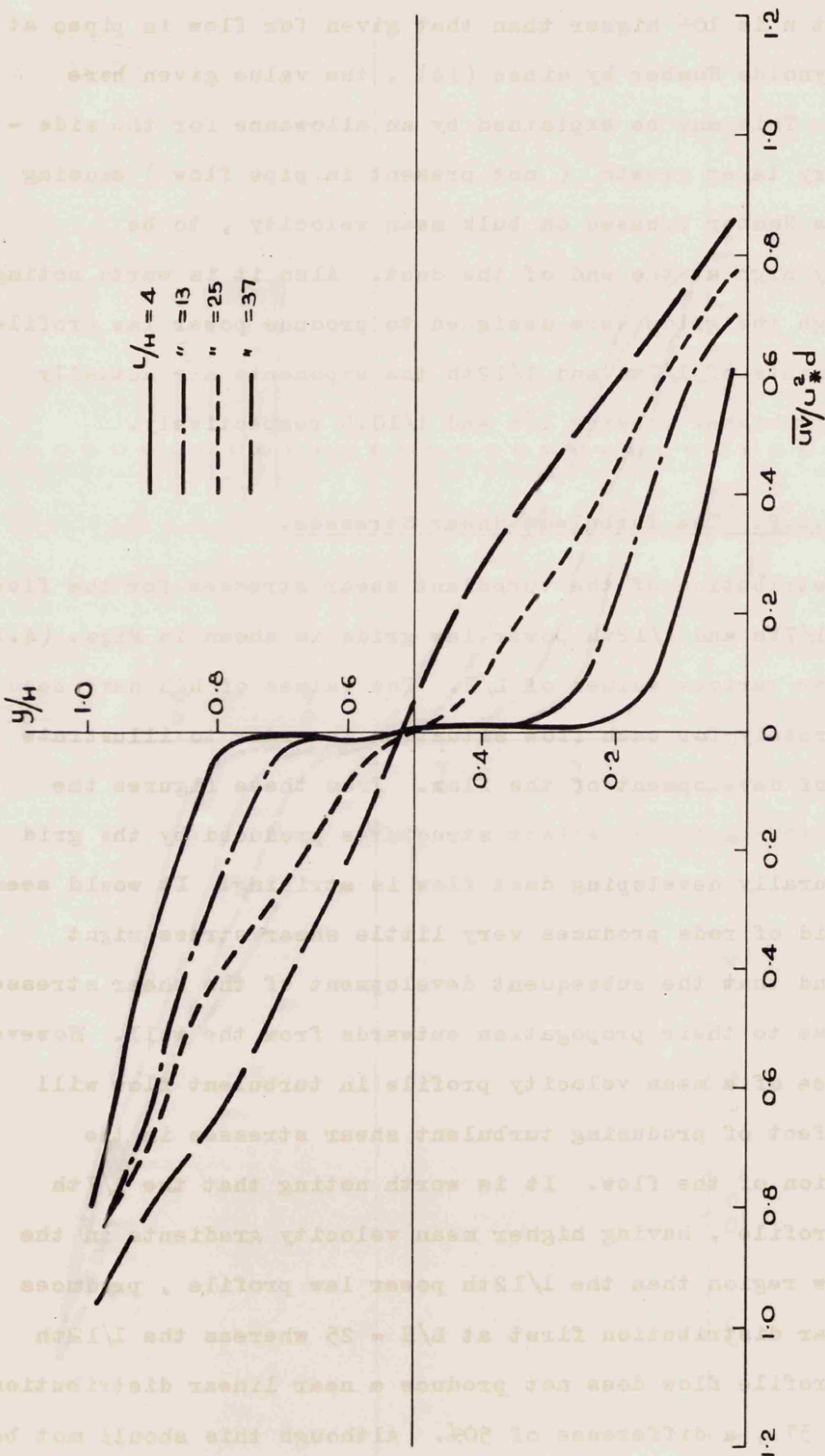
FIG. 4.17. REYNOLDS STRESS DISTRIBUTION BEHIND ⅛th P.L. GRID.

law exponent n is 10% higher than that given for flow in pipes at the same Reynolds Number by Hinze (14) , the value given here being 8.8 . This may be explained by an allowance for the side - wall boundary layer growth (not present in pipe flow) causing the Reynolds Number , based on bulk mean velocity , to be artificially high at the end of the duct. Also it is worth noting that although the grids were designed to produce power law profiles having exponents of 1/7th and 1/12th the exponents are actually both slightly higher , being 1/6 and 1/10.5 respectively.

4.4.2. The Turbulent Shear Stresses.

The distribution of the turbulent shear stresses for the flow behind the 1/7th and 1/12th power law grids is shown in Figs. (4.16) and(4.17) for various values of L/H. The values of L/H have been chosen separately for each flow situation in order to illustrate the stages of development of the flow. From these figures the similarity between the turbulent structures produced by the grid and the naturally developing duct flow is striking. It would seem that the grid of rods produces very little shear stress right behind it and that the subsequent development of the shear stresses is mainly due to their propogation outwards from the wall. However the existence of a mean velocity profile in turbulent flow will have the effect of producing turbulent shear stresses in the central region of the flow. It is worth noting that the 1/7th power law profile , having higher mean velocity gradients in the central flow region than the 1/12th power law profile , produces a near linear distribution first at L/H = 25 whereas the 1/12th power law profile flow does not produce a near linear distribution until L/H = 37 , a difference of 50%. Although this should not be
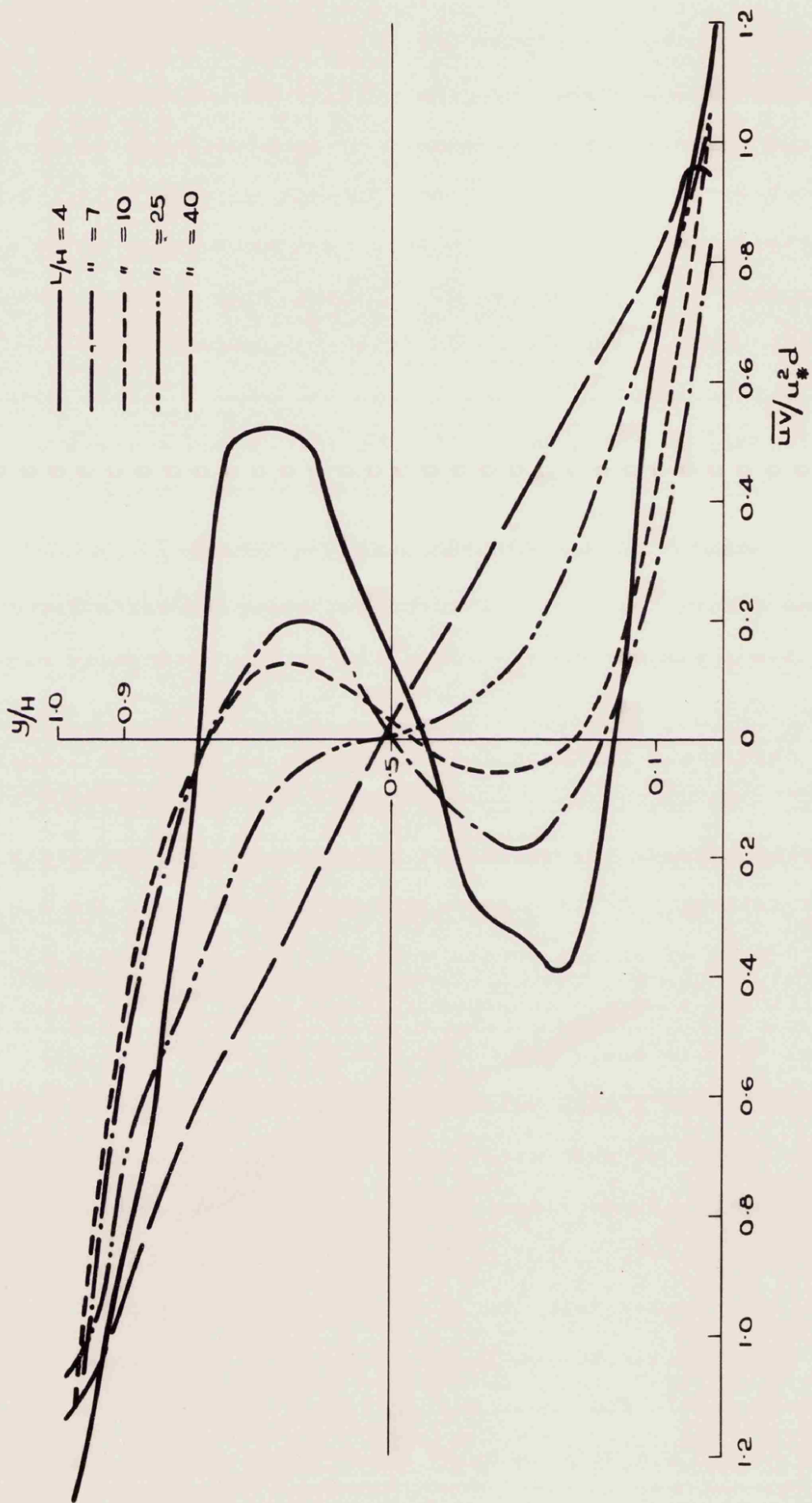
FIG.4.18.REYNOLDS STRESS DISTRIBUTION BEHIND TRIANGULAR PLOW DEVICE
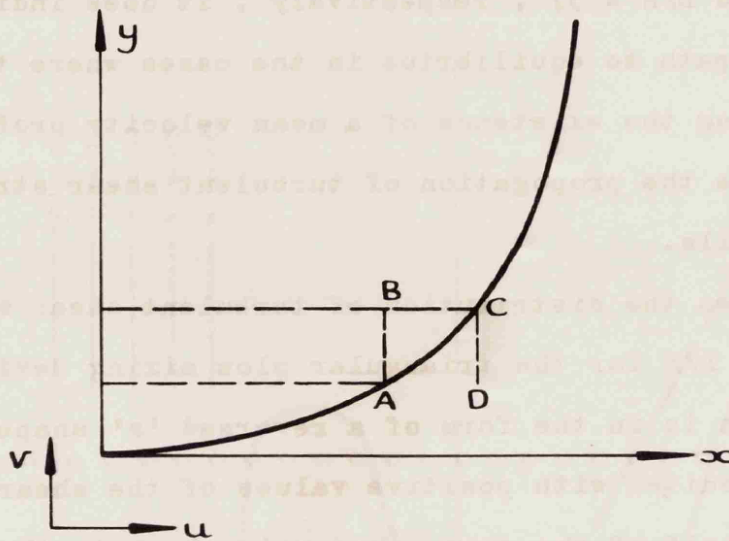
The explanation of the normal negative correlation of u and v is as follows :- If a particle of fluid moves from A to B then this must be accomplished by the particle having +ve v velocity. It will carry with it the u velocity compatible with its y position. By virtue of the velocity profile shape the u velocity at B is higher than that at A and thus the particle will have a negative u component. Thus +ve v is associated with -ve u and the reverse will be true for a particle moving from C to D. Thus any shear stress correlation associated with a profile of this shape will be between qualities having opposite signs and will thus always be negative.

FIG.4.19.SHEAR STRESS CORRELATION

taken to imply that the equilibrium flow regions for those flows start at L/H = 25 and L/H = 37 , respectively , it does indicate a generally quicker path to equilibrium in the cases where the vorticity accompanying the existence of a mean velocity profile is available to reiforce the propogation of turbulent shear stresses outwards from the walls.

Fig. (4.18) shows the distribution of turbulent shear stresses at various values of L/H for the triangular plow mixing device. Here the distribution is in the form of a reversed 's' shape in which the flow is credited with positive values of the shear stress correlation in each half of the duct. Referring back to the mean velocity profile for the triangular plow as shown in Fig. (4.10) an explanation of this unusual shear stress distribution is possible. The velocity profile is the wake type profile having a central velocity defect from y/H = 0.125 to y/H = 0.85 . In this central defect region the slope of the mean velocity profile is of the opposite sign to that of a normal velocity profile (say 1/7th power law) going first from negative , to zero at y/H = 0.4 , then to positive. Thus in terms of Prandtl's (see fig. (4.19)) explanation of the normal negative correlation of the fluctuating velocity components u and v for a boundary layer velocity profile we would expect a positive correlation in this defect region. This is indeed the case and from Fig. (4.18) we see a positive correlation from y/H = 0.15 to y/H = 0.8 with a zero value at y/H = 0.45 . The reason that the region of positive correlation is slightly narrower than would be expected is due to the effect of the propogation of the normal negative correlation outwards from the wall. The subsequent development of this distribution will continue to show positive regions of shear stress correlation whilst the velocity
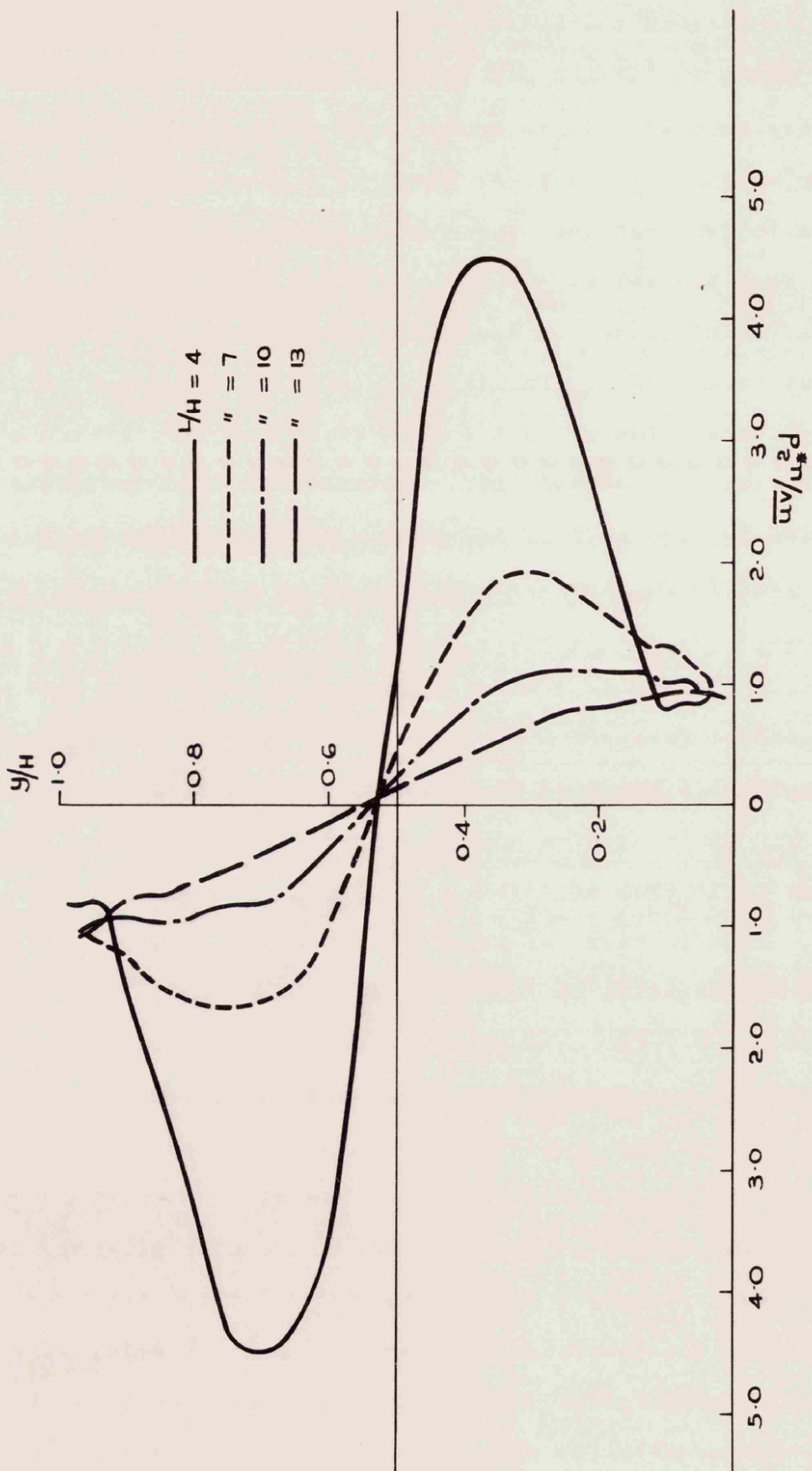
FIG. 4.20. REYNOLDS STRESS DEVELOPMENT BEHIND RAMP DEVICE
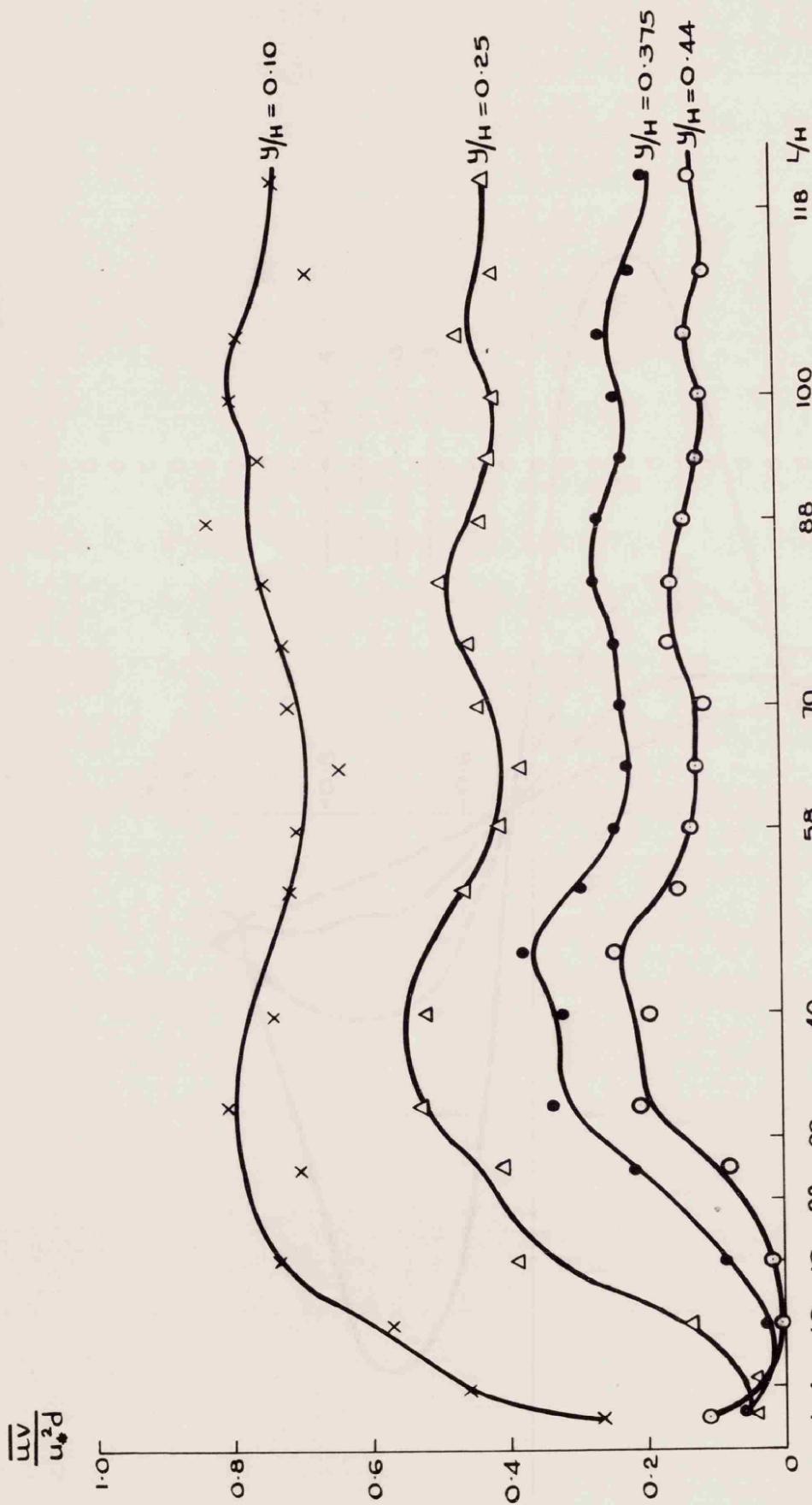
FIG.4.21.DEVELOPMENT OF REYNOLDS STRESSES BEHIND 1/7th P.L. GRID
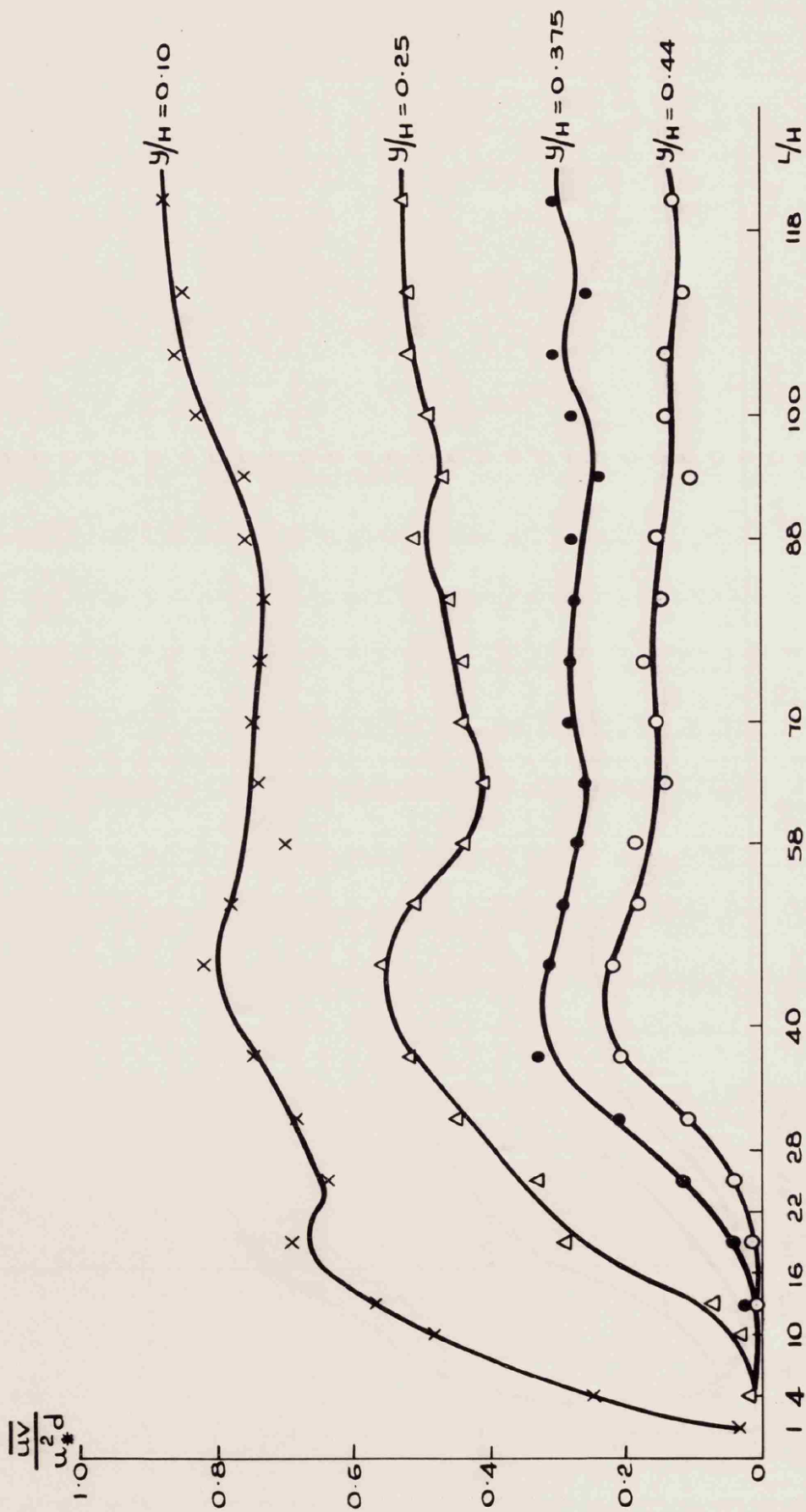
FIG.4.22.DEVELOPMENT OF REYNOLDS STRESSES BEHIND 1/12th P.L. GRID

$\dfrac{\overline{uv}}{u_*^2 \rho}$

$y/_H = 0.10$

$y/_H = 0.25$

$y/_H = 0.315$

$y/_H = 0.44$

$L/_H$
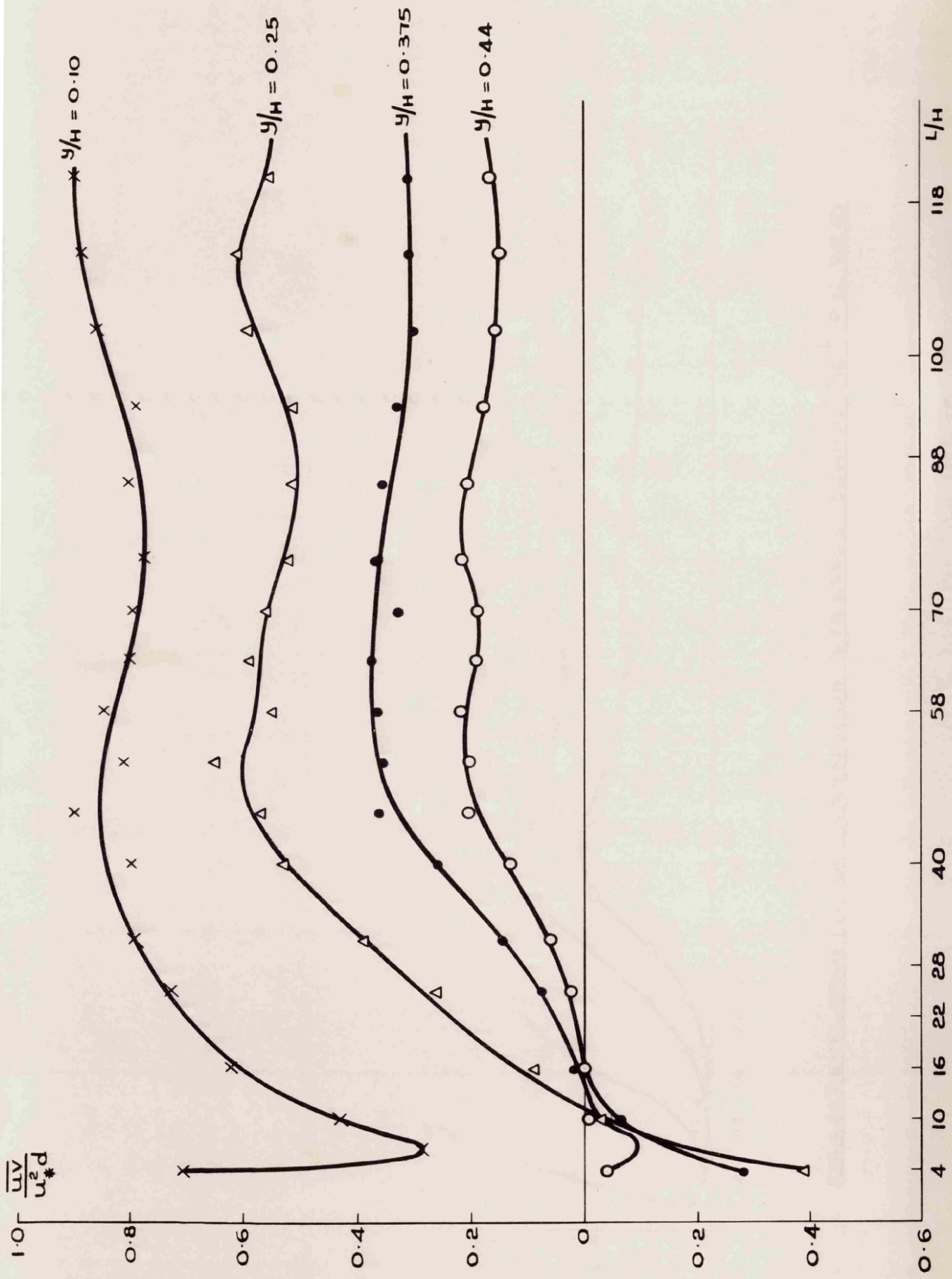
FIG. 4.23. DEVELOPMENT OF REYNOLDS STRESSES BEHIND TRIPLOW DEVICES

y/H = 0·10

y/H = 0·25

y/H = 0·375

y/H = 0·44

L/H

4 10 16 22 28 40 52 70 88 100 118

$\dfrac{\overline{p'^2}}{\frac{1}{2}\rho U^2}$

1·2 1·0 0·8 0·6 0·4 0·2 0
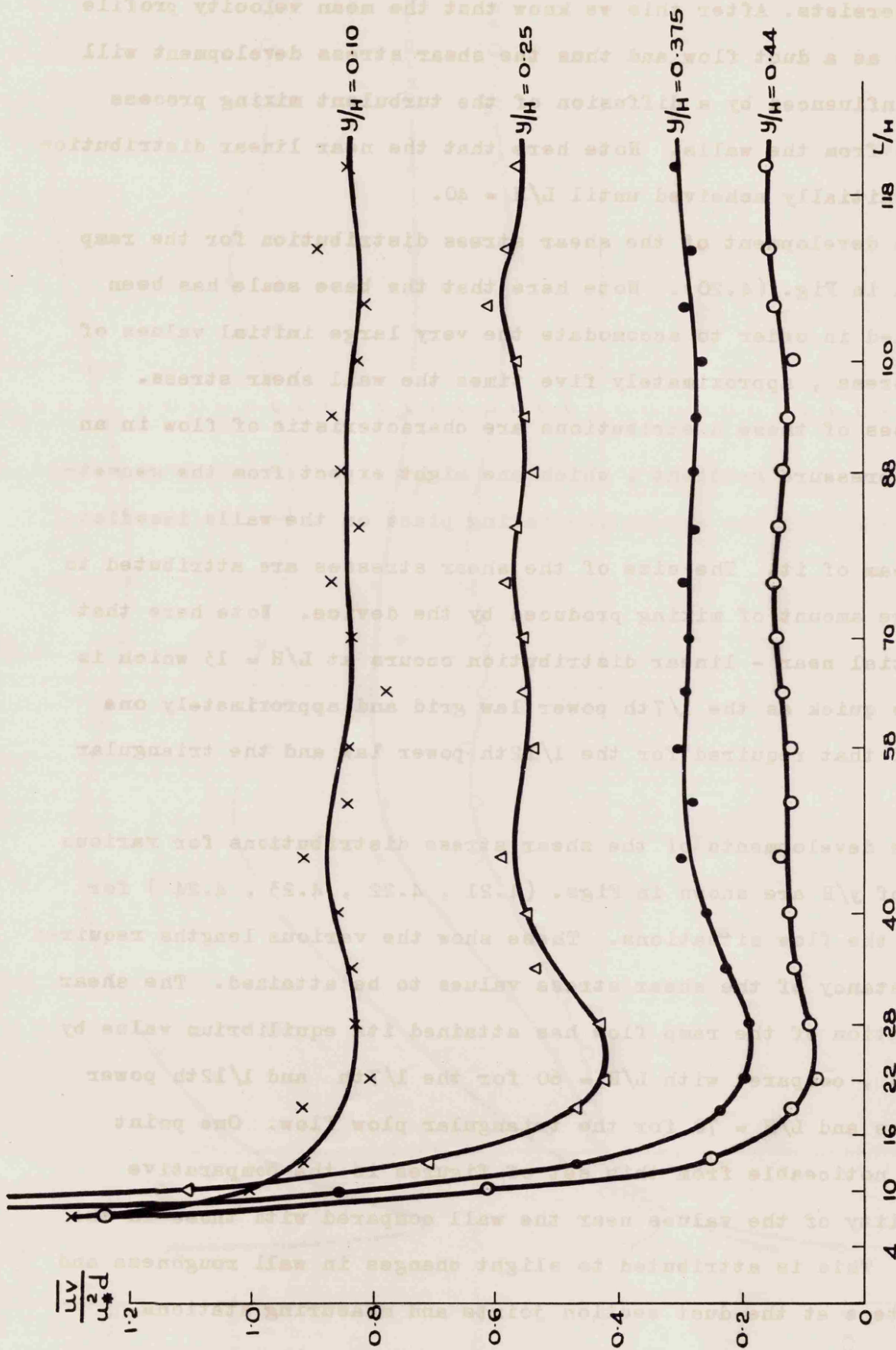
FIG. 4.24. DEVELOPMENT OF REYNOLDS STRESSES BEHIND RAMP DEVICES

defect persists. After this we know that the mean velocity profile develops as a duct flow and thus the shear stress development will be one influenced by a diffusion of the turbulent mixing process outwards from the walls. Note here that the near linear distribution is not initially acheived until L/H = 40.

The development of the shear stress distribution for the ramp is shown in Fig. (4.20). Note here that the base scale has been diminished in order to accomodate the very large initial values of shear stress , approximately five times the wall shear stress. The shapes of these distributions are characteristic of flow in an adverse pressure gradient , which one might expect from the geometry of the wedge and the separation taking place on the walls immediately downstream of it. The size of the shear stresses are attributed to the large amount of mixing produced by the device. Note here that the initial near - linear distribution occurs at L/H = 13 which is twice as quick as the 1/7th power law grid and approximately one third of that required for the 1/12th power law and the triangular plow.

The developments of the shear stress distributions for various values of y/H are shown in Figs. (4.21 , 4.22 , 4.23 , 4.24) for each of the flow situations. These show the various lengths required for constancy of the shear stress values to be attained. The shear distribution of the ramp flow has attained its equilibrium value by L/H = 40 , compared with L/H = 60 for the 1/7th and 1/12th power law flows and L/H = 70 for the triangular plow flow. One point readily noticeable from this set of figures is the comparative instability of the values near the wall compared with those in the centre. This is attributed to slight changes in wall roughness and small steps at the duct section joints and measuring stations.
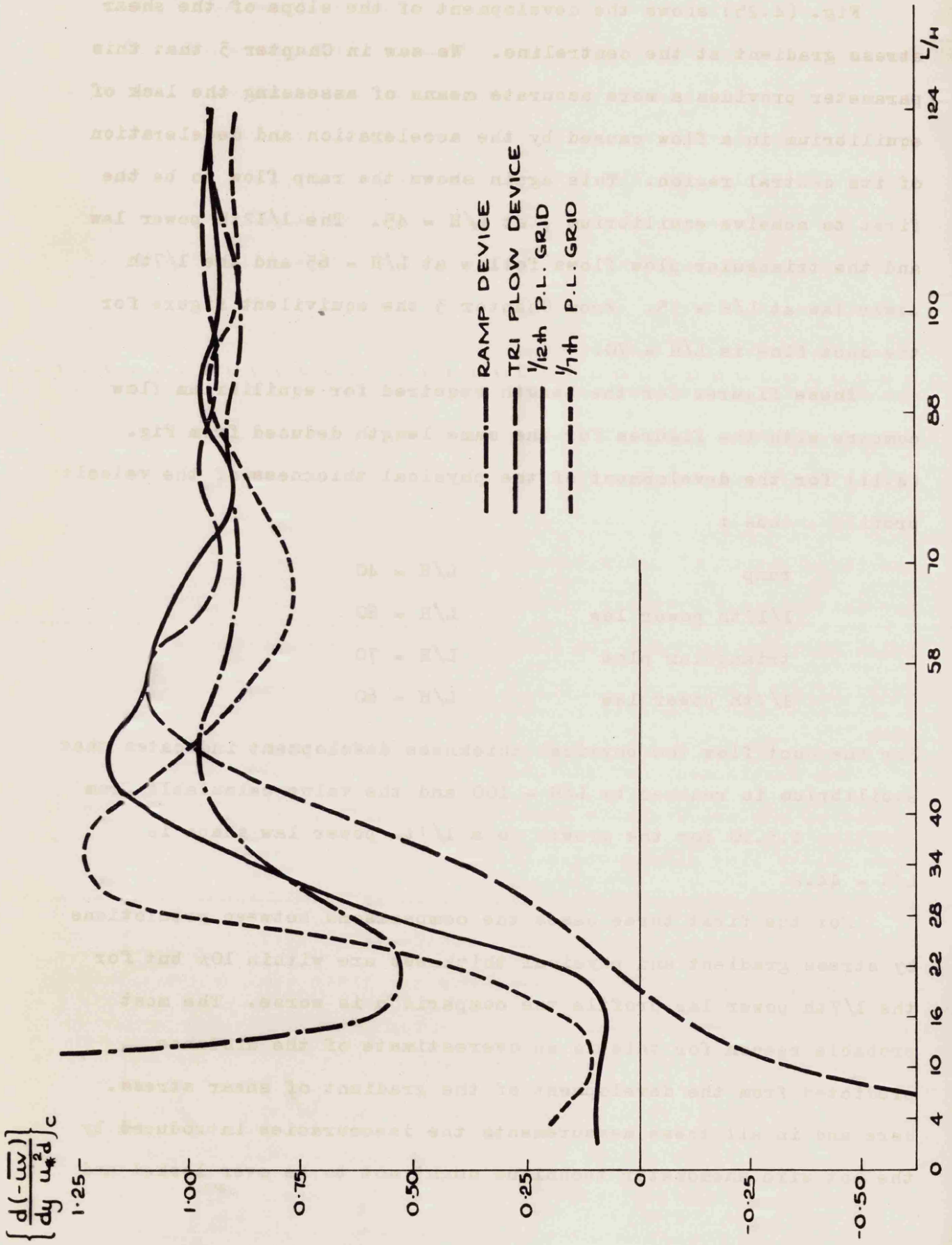
FIG.4.25.TURBULENT SHEAR STRESS GRADIENT ON CENTRELINE

$\left\{ \dfrac{d(-\overline{uv})}{dy\, u_*^2} \right\}_c$

1·25   1·00   0·75   0·50   0·25   0   -0·25   -0·50

L/H

0   4   10   16   22   28   34   40   58   70   88   100   124

Legend:
— · — RAMP DEVICE
— — — TRI FLOW DEVICE
———— 1/12th P.L. GRID
– – – 1/7th P.L. GRID

Fig. (4.25) shows the development of the slope of the shear stress gradient at the centreline. We saw in Chapter 3 that this parameter provides a more accurate means of assessing the lack of equilibrium in a flow caused by the acceleration and deceleration of its central region. This again shows the ramp flow to be the first to acheive equilibrium , at L/H = 45. The 1/12th power law and the triangular plow flows follow at L/H = 65 and the 1/7th power law at L/H = 75. From Chapter 3, the equivilent figure for the duct flow is L/H = 70.

These figures for the length required for equilibrium flow compare with the figures for the same length deduced from Fig. (4.11) for the development of the physical thickness of the velocity profile , thus :

ramp	L/H = 40
1/12th power law	L/H = 60
triangular plow	L/H = 70
1/7th power law	L/H = 60

For the duct flow the physical thickness defelopment indicates that equilibrium is reached by L/H = 100 and the value calculable from Equation 4.3.10 for the growth to a 1/7th power law shape is L/H = 44.2.

For the first three cases the comparisons between predictions by stress gradient and physical thickness are within 10% but for the 1/7th power law profile the comparison is worse. The most probable reason for this is an overestimate of the distance predicted from the development of the gradient of shear stress. Here and in all these measurements the inaccuracies introduced by the hot wire anemometer technique ought not to be over looked and
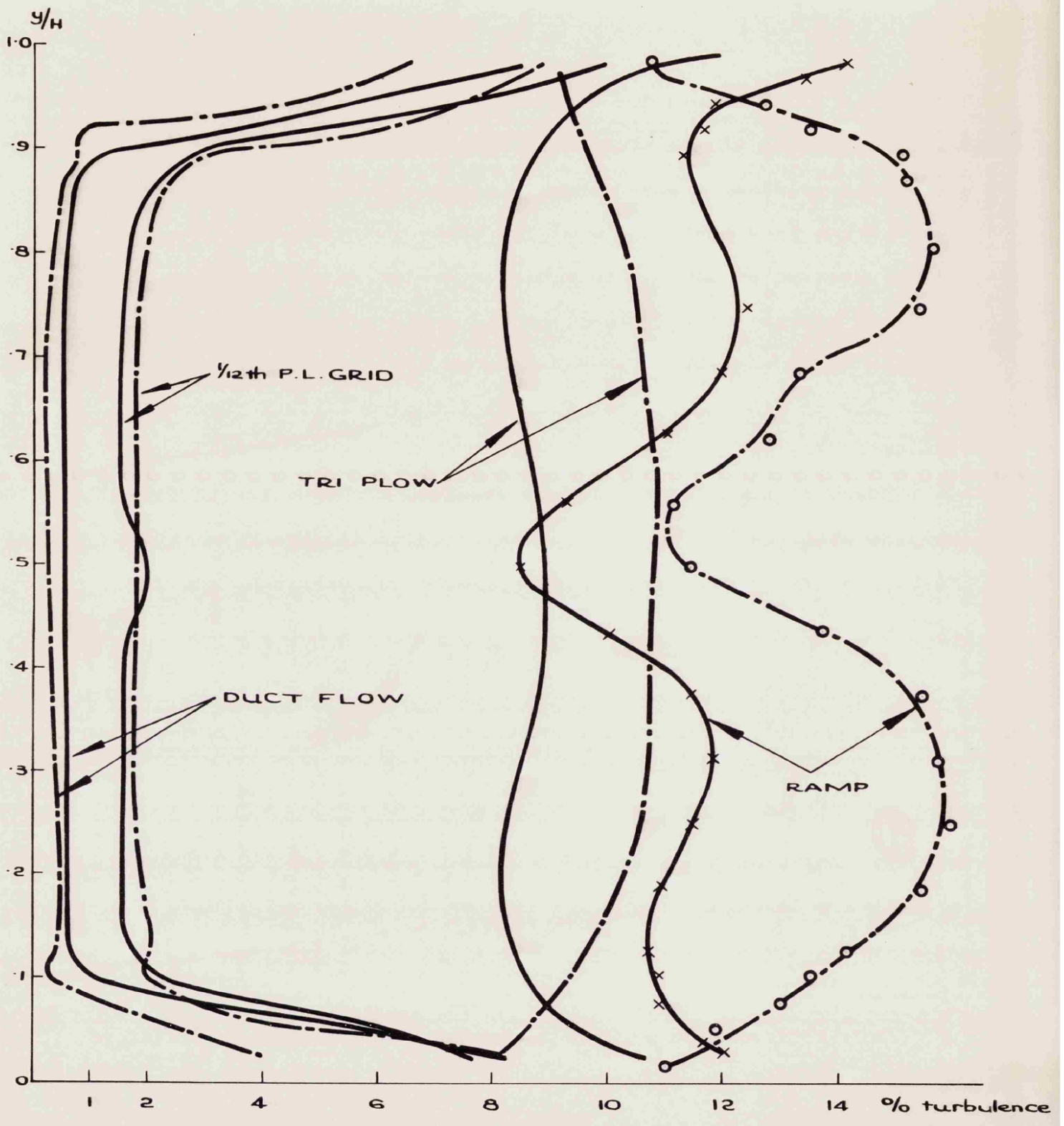
FIG.4.26.TURBULENCE INTENSITY DISTRIBUTION AT INLET

———————— LONGITUDINAL % $(\sqrt{\overline{u^2}}/U \times 100)$

—·—·—·— LATERAL % $(\sqrt{\overline{v^2}}/U \times 100)$

DUCT FLOW
1/7th P.L. GRID
1/12th P.L. GRID
TRI FLOW DEVICE
RAMP DEVICE

% turbulence

8 7 6 5 4 3 2 1 0

4 10 16 22 28 34 40 52 58 88 118 x/H
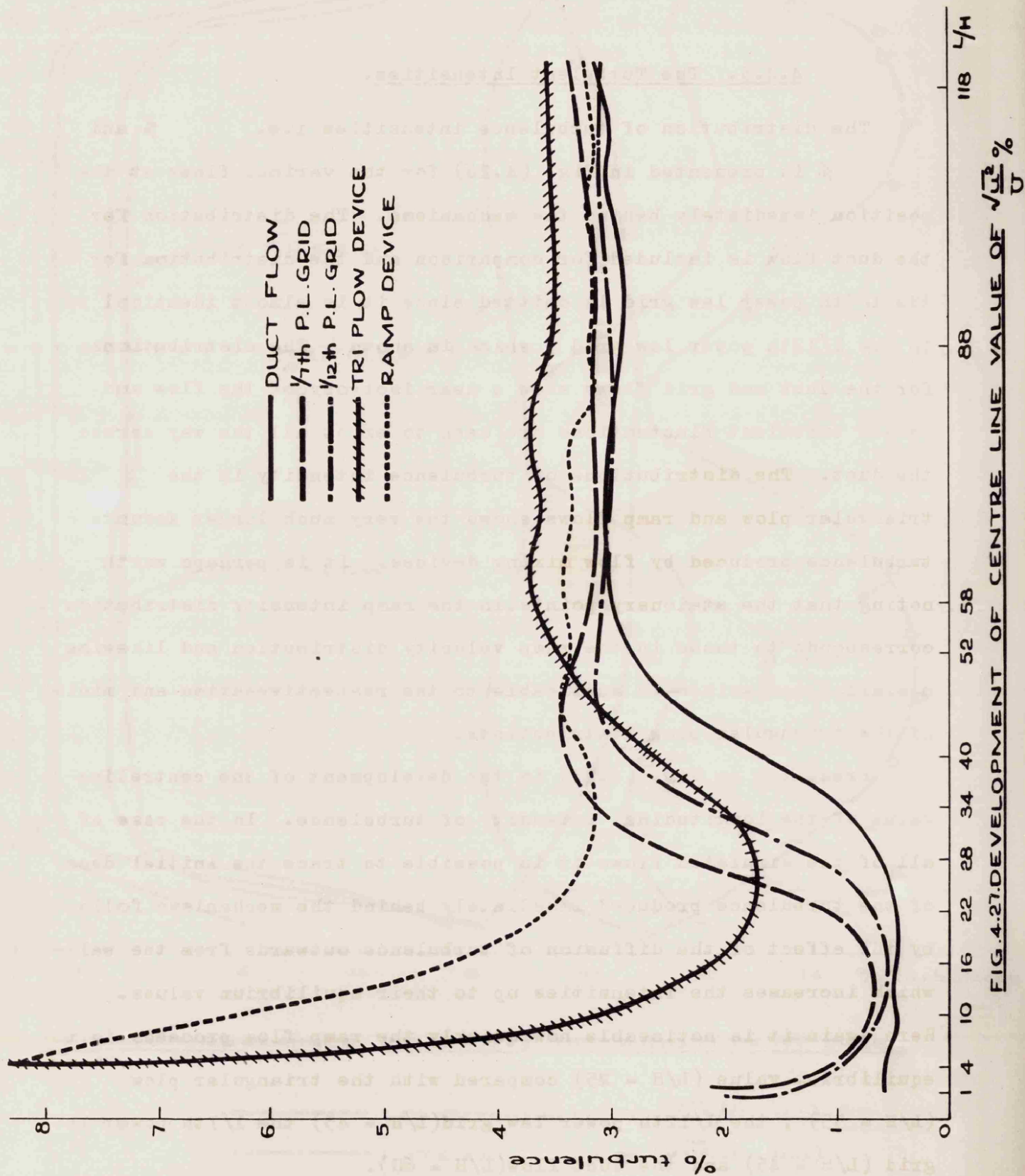
FIG.4.27.DEVELOPMENT OF CENTRE LINE VALUE OF $\frac{\sqrt{\overline{u^2}}}{U}$ %

and this is probably the underlying cause of the present discrepancy.

4.4.3. The Turbulent Intensities.

The distribution of turbulence intensities i.e. $\frac{\sqrt{\overline{w^2}}}{U}$ % and $\frac{\sqrt{\overline{v^2}}}{U}$ % is presented in Fig. (4.26) for the various flows at the position immediately behind the mechanisms. The distribution for the duct flow is included for comparison and the distribution for the 1/7th power law grid is omitted since it is almost identical to to the 1/12th power law grid , which is shown. The distributions for the duct and grid flows show a near isotropy of the flow and indeed turbulent fluctuations are seen to exist all the way across the duct. The distributions of turbulence intensity in the triangular plow and ramp flows shows the very much larger amounts of turbulence produced by flow mixing devices. It is perhaps worth noting that the staionary points in the ramp intensity distribution corresponds to those in the ramp velocity distribution and likewise a similar comparison is applicable to the respectivemaxima and minima of the triangular plow distributions.

Presented in Fig. (4.27) is the development of the centreline value of the longitudinal intensity of turbulence. In the case of all of the simulated flows it is possible to trace the initial decay of the turbulence produced immediately behind the mechanisms followed by the effect of the diffusion of turbulence outwards from the walls, which increases the intensities up to their equilibrium values. Here again it is noticeable how quickly the ramp flow proceeds to its equilibrium value (L/H = 25) compared with the triangular plow (L/H = 55) , the 1/12th power law grid(L/H = 45) the 1/7th power law grid (L/H = 45) and the duct flow(L/H = 60).

The initial decay of the turbulence produced by the grids is
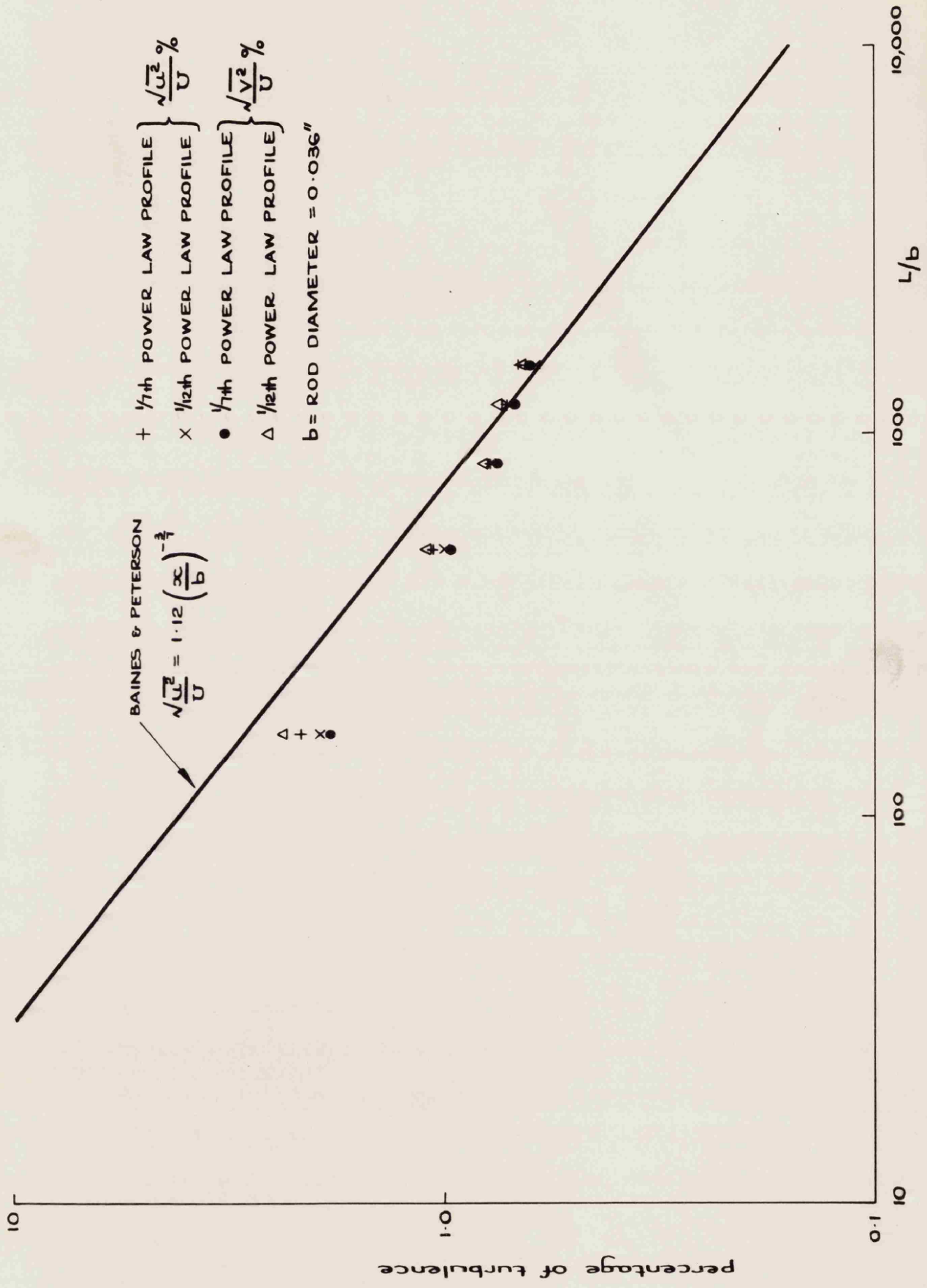
FIG. 4.28.   DECAY OF TURBULENCE BEHIND VELOCITY PROFILE SIMULATOR GRIDS
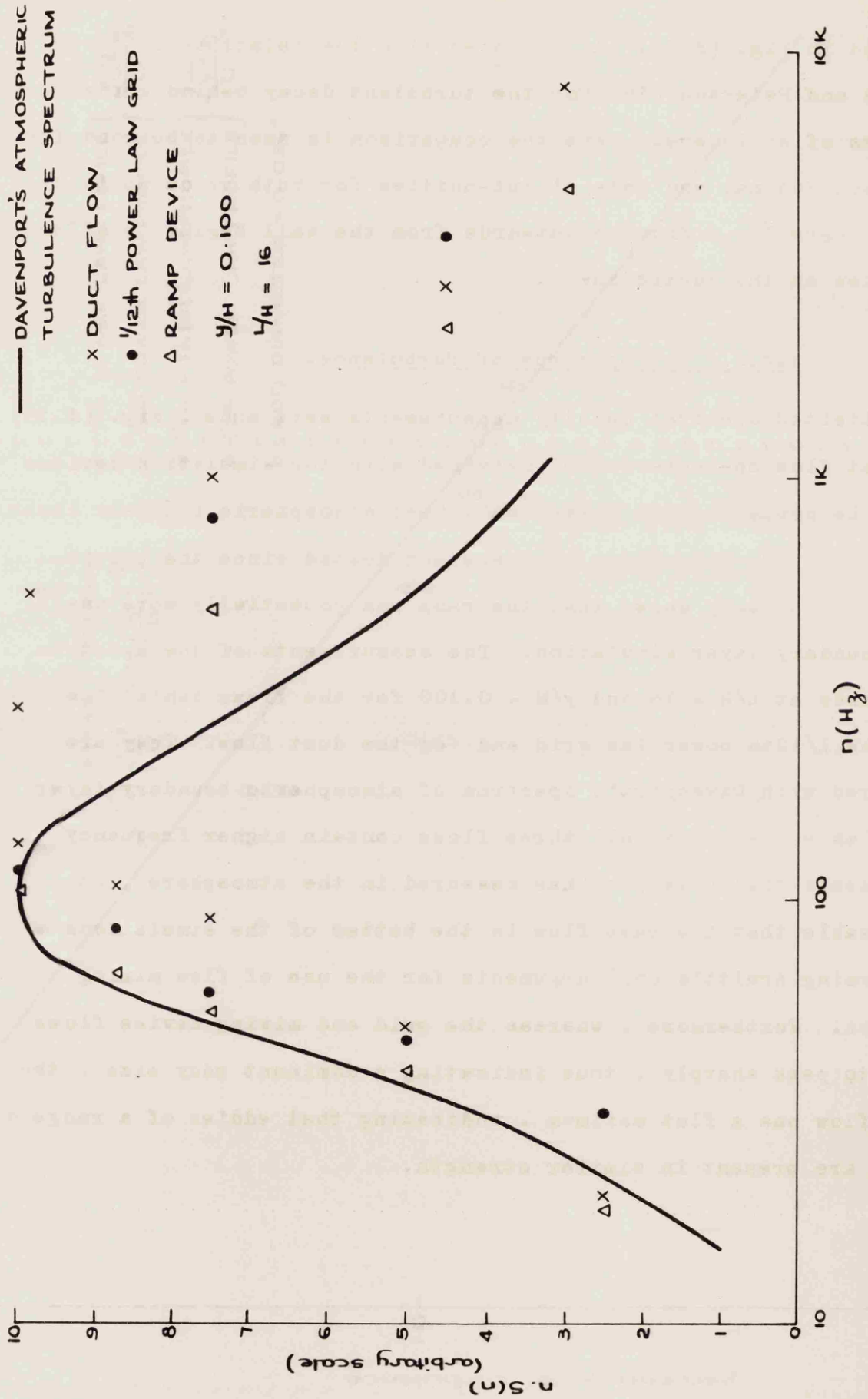
FIG.4.29. SPECTRUM OF THE LONGITUDINAL INTENSITY OF TURBULENCE ($\sqrt{u^2}$)

plotted in Fig. (4.28) and compared with the relationship given by
Baines and Peterson (36) for the turbulent decay behind grids formed
by rows of cylinders. Here the comparison is seen to be good for
the longitudinal and lateral intensities for both grids up to the
point where the diffusion outwards from the wall begins to affect
the flow on the centreline.

4.4.4. The Spectrum of Turbulence.

Limited spectral density measurements were made , Fig. (4.29),
so that flow characteristics obtained with the simulation devices
could be compared with Davenport's (66) atmospheric boundary layer
spectrum. The triangular plow was not tested since the previous
tests had already shown that the ramp was potentially more useful
for boundary layer simulation. The measurements of the spectrum
were made at $L/H = 16$ and $y/H = 0.100$ for the flows behind the ramp
and the 1/12th power law grid and for the duct flow. They are
compared with Davenport's spectrum of atmospheric boundary layer
turbulence. Although all three flows contain higher frequency
components than Davenport has measured in the atmosphere , it is
noticeable that the ramp flow is the better of the simulations , thus
confirming Armitt's (61) arguments for the use of flow mixing
devices. Furthermore , whereas the grid and mixing device flows
seem to peak sharply , thus indicating a dominant eddy size , the
duct flow has a flat maximum , indicating that eddies of a range of
sizes are present in similar strength.

4.5. Discussion and Conclusion.

There are a large number of possible methods which may be utilized for the production of a velocity profile. Some are better than others but all of them have their drawbacks regarding the flows they produce and the practical difficulties involved in their use. The use of wall roughness often requires a prohibitive length of wind tunnel. The effect of gauzes of rectangular mesh , whether they are curved or linear can only be predicted by complex mathematics and their practical difficulties are many. Honeycomb simulators are easy to use but little data is available on their accompanying turbulence production. The use of flow mixing devices is very much on a trial and error basis and the momentum balance theories used to relate their resistance to the resultant flow is of doubtful merit without reference to the resulting turbulence. The use of grids of rods is the most practical method and is frequently used. The early theories used to enable the grids to be designed in terms of the required flow are shown to contain questionable assumptions and the use of a simple theory which attempts to model the physics is recommended.

From the results presented in the foregoing section it would seem possible to arrive at differing conclusions regarding the stability of the flow depending on the particular parameter chosen as the basis for such a criterion. The best judge of the state of development of a flow would appear to be the centreline shear stress gradient.

The production of a stable flow is seen to depend very much more on the mechanism's ability to produce turbulent shear stresses than to produce the right velocity profile. The more linear the

distribution of shear stress produced then the sooner the flow will tend to stability and for this reason the ramp flow mixing device is the best of those tested.

Grids produce a stable velocity profile for a short distance downstream of the mechanisms , but as the turbulence diffuses out--wards from the wall they suffer changes. The grids produce very little turbulence and the current practise of their use in atmospheric model testing is regarded with suspicion. In the region close to the wall i.e. $0 < y/H < 0.2$ the gradient of shear stress can be up to three times that for a stable flow in the same region.

It has been found that the design value of the power law exponent for grid produced profiles is not fulfilled. Allowance for this shortcoming should be made by designing th grid to produce an exponent in which n is of the order of 15% higher than that required.

Chapter 5.

The Application of an Integral Method of
Boundary Layer Calculation to Duct Flow.

The prime objective of any method of boundary layer prediction
is to derive the values of certain mean properties of the flow as
it develops. With some of the more recent methods of boundary
layer prediction it may also be possible to obtain some information
about the turbulence structure. The difficulty and importance
of adequately predicting the behaviour of turbulent boundary layers
in adverse pressure gradients perhaps explains the predominance of
this type of flow in the literature available concerning prediction
methods and experimental comparisons. Nevertheless , the ability to
predict flow development in internal situations is also important
particularly in systems having varying cross sections and deviations
of centreline. It is for this reason that an attempt is presented
to apply an integral method of flow prediction to internal duct
flows. In the present example a two - dimensional prediction method
is given for flow between parallel plates but it is simply
extendable to the case of straight walled two - dimensional diffusers,
and to axisymmetric flow.

5.1. Calculation Methods.

No attempt will be made here to give a survey of all the calculation methods available in the literature since this is adequately done elsewhere.

In his critical review of turbulent boundary layer prediction methods Thompson (67) notes that they give rise to very different solutions and none of them , with the exception of Head (68) , provides a satisfactory agreement with more than half of the available experimental data at present used as a basis for comparison. Reynolds (69) in his introduction to the 1968 Stanford Conference on Boundary Layer Prediction also notes that the physical content of the available methods varies greatly and that the choice of physical input can often be a clue to the success of a method. Methods using the relevant physics should be relatively insensitive to the details of assumptions , whilst methods which use correct but physically irrelevant equations are likely to be more sensitive to particular assumptions.

The method of using integral equations was originally employed for the systematic reduction of the partial differential equations, which are derived from the Navier Stokes equations , to a few coupled ordinary differential equations so as to speed the numerical solution by hand calculations. Nowadays with high speed computers the main advantage of integral methods lies in the implicit and global manner in which the effects of turbulence can be incorporated.

As detailed in Hinze (14) Ch.7 , we can write down the differential equations of motion as derived from the Navier Stokes Equations by decomposition of the velocity terms into a mean and a fluctuating part , by time averaging and by making the usual

order - of-magnitude boundary layer approximation as follows:

For the x direction momentum

$$U\frac{\partial U}{\partial x} + V\frac{\partial U}{\partial y} + \frac{\partial \overline{u^2}}{\partial x} + \frac{\partial \overline{uv}}{\partial y} = -\frac{1}{\rho}\frac{\partial p}{\partial x} + \vartheta\frac{\partial^2 U}{\partial y^2} \qquad 5.1.1.$$

For the y direction momentum

$$\frac{\partial \overline{v^2}}{\partial y} = -\frac{1}{\rho}\frac{\partial p}{\partial y} \qquad 5.1.2.$$

Continuity

$$\frac{\partial U}{\partial x} + \frac{\partial V}{\partial y} = 0 \qquad 5.1.3.$$

By combining the first and second equations to get the momentum equation and using the continuity equation we are left with two equations and three unknowns , U , V and the shear stress , even assuming that we know the free stream or centreline velocity distribution to give the pressure term and that we neglect the normal stress terms. It is at this point , the choice of a third equation that variations in integral prediction methods arise. This third equation must be derived either empirically or from the partial differential form of the momentum equation. In this second category three possible methods of deriving a third equation are:-

(i) by multiplying the momentum equation by $U^n y^m$ and integrating across the boundary layer. For various integer value combinations of n and m it is possible to derive equations considered to have some physical significance,

  e.g.   n = 0 , m = 0 yields the momentum integral equation.

     n = 1 , m = 0 yields the energy integral equation.

n = 0 , m = 1 yields the moment of momentum integral equation

(ii) by dividing the boundary layer into strips and integrating the momentum equation or some other equation formed from it , across them.

(iii) by satisfying the momentum equation in its differential form at certain points within the boundary layer.

All of these methods require some knowlege of the distribution of the turbulent shear stress within the boundary layer. Various approximations ranging from simple eddy viscosity ideas to attempts to solve the turbulence energy equation have been made to describe the shear stresses but , as we have seen in the preceeding chapters, if local relationshps are used , then neglect of the effects of flow history will prevent more elaborate integration approaches being used to their proper advantage. This fact probably accounts for the attraction of many prediction methods to comparisons with similar or self - preserving flows which have a well defined history in terms of local parameters.

The concept of self - preserving flows or equilibrium * flows was put forward by Clauser (4, 70) who expressed the factors affecting the history of the flow in the following term:

$$\frac{S^*}{\tau_w} \frac{dp}{dx}$$

and stated that when this term has any constant value the velocity defect relationship $\left(\dfrac{U - U_{max}}{U_*} \right)$ v $\, y/\delta$

will remain fixed independently of the skin friction coefficient thus giving the flow a constant history.

* This definition of equilibrium is not to be confused with equilibrium pipe flow defined in Chapter 3 although a similarity exists.

In the prediction method outlined here the way in which the third equation is obtained is by (ii) above , the strip integral method. The description of the shear stress distribution is provided by the experimental data obtained in the tests described in Chapter 3.

5.2. Present Use of the Strip Method of Boundary Layer
Prediction.

As stated in the Introduction , the integral method of boundary layer calculation to be used was one into which the experimental data of the turbulent shear stress distribution could be fed in order to satisfy the requirement of accounting for flow history.

The method adopted was one initially proposed by Moses (71) in which the third equation needed for a solution was the momentum equation integrated across a strip of the boundary layer. This was chosen because of its simplicity when compared with the two other most likely choices , the energy integral equation and the moment of momentum equation. These both entail the evaluation of a shear stress integral term whereas the strip method merely requires the value of the shear stress at the strip boundary , furthermore it is possible to eliminate the wall shear stress term by subtraction of the strip momentum equation from the momentum equation.

The input data used was derived from the experimental tests described in Chapter 3 and the predictions are compared with the experimentally derived values of the mean flow parameters.

5.2.1. Derivation of the Momentum Equations.

The basic equations , detailed in section 5.1. , are as follows:

For the x direction momentum ,

$$U \frac{\partial U}{\partial x} + V \frac{\partial U}{\partial y} + \frac{\partial \overline{u^2}}{\partial x} + \frac{\partial \overline{uv}}{\partial y} = -\frac{1}{\rho} \frac{\partial p}{\partial x} + \nu \frac{\partial^2 U}{\partial y^2} \qquad 5.1.1$$

For the y direction momentum

$$\frac{\partial \bar{v}^2}{\partial y} = -\frac{1}{\rho}\frac{\partial p}{\partial y}$$

From continuity

$$\frac{\partial U}{\partial x} + \frac{\partial V}{\partial y} = 0$$

Integrating equation 5.1.2. with respect to y gives

$$\bar{v}^2 = -\frac{p}{\rho} + \text{Constant}.$$

which evaluated on the centreline of the duct , is

Thus

$$\bar{v}_c^2 = -\frac{p_c}{\rho} + \text{Constant}$$

$$-\frac{p}{\rho} = -\frac{p_c}{\rho} + \left(\bar{v}^2 - \bar{v}_c^2\right)$$

Differentiating this with respect to x gives

$$-\frac{1}{\rho}\frac{\partial p}{\partial x} = -\frac{1}{\rho}\frac{\partial p_c}{\partial x} + \frac{\partial}{\partial x}\left(\bar{v}^2 - \bar{v}_c^2\right)$$

Bernoulli's Equation on the duct centreline is

$$\tfrac{1}{2}\rho\bar{U}_c^2 + P_c = \text{Const.} + \triangle p_c$$

Now in order to use this and equation 5.2.1. to evaluate the pressure term in equation 5.1.1. the pressure drop term $\triangle p_c$ must be determined.

Equation 5.1.1. can be rewritten as

$$U\frac{\partial U}{\partial x} + V\frac{\partial U}{\partial y} = -\frac{1}{\rho}\frac{\partial p}{\partial x} + \frac{1}{\rho}\frac{\partial \tau}{\partial y} - \frac{\partial (\bar{u}^2)}{\partial x} + V\left(\frac{\partial V}{\partial x} - \frac{\partial U}{\partial y}\right)$$

which is

$$\frac{\partial (U^2)}{\partial x} + \frac{1}{\rho}\frac{\partial p}{\partial x} = \frac{1}{\rho}\frac{\partial \tau}{\partial y} - \frac{\partial}{\partial x}(\overline{u^2}) + V_S \qquad 5.2.3.$$

where

$$U^2 = U^2 + V^2$$

If the last two terms in equation 5.2.3. are assumed to be neglectable on the duct centreline we can write it as

$$\frac{1}{\rho}\frac{d \Delta p_c}{dx} = \frac{1}{\rho}\left(\frac{d\tau}{dy}\right)_c \qquad 5.2.4.$$

If we differentiate Bernoulli's Equation 5.2.2. and substitue in equation 5.2.4. we get

$$-\frac{1}{\rho}\frac{dP_c}{dx} = U_c\frac{dU_c}{dx} - \frac{1}{\rho}\left(\frac{d\tau}{dy}\right)_c$$

which , on substitution in equation 5.2.1. , gives

$$-\frac{1}{\rho}\frac{\partial p}{\partial x} = U_c\frac{dU_c}{dx} - \frac{1}{\rho}\left(\frac{d\tau}{dy}\right)_c + \frac{\partial}{\partial x}(\overline{v^2} - \overline{v_c^2}) \qquad 5.2.5.$$

This we can now substitute back into equation 5.1.1. to give the momentum equation for two-dimensional duct flow.

$$U\frac{\partial U}{\partial x} + V\frac{\partial U}{\partial y} = U_c\frac{dU_c}{dx} - \frac{1}{\rho}\left(\frac{d\tau}{dy}\right)_c + \frac{1}{\rho}\frac{d\tau}{dy}$$
$$\left. - \frac{\partial}{\partial x}(\overline{u^2} + \overline{v_c^2} - \overline{v^2}) \right\} \qquad 5.2.6.$$

By combining equations 5.1.3. and 5.2.6. , the continuity and momentum equations , and integrating the resultant from y = 0 to y = y_1 we get

$$\int_{o}^{y_{1}} \frac{\partial}{\partial x} U^{2} dy \; - \; U_{y_{1}} \int_{o}^{y_{1}} \frac{\partial U}{\partial x} \cdot dy \; = \; U_{c} \frac{dU_{c}}{dx}$$

<div align="right">5.2.7</div>

$$-\frac{1}{\rho} \left(\frac{d\tau}{dy} \right)_{c} y_{1} + \frac{1}{\rho} \left(\tau_{y_{1}} - \tau_{w} \right) - \int_{o}^{y_{1}} \frac{\partial}{\partial x} \left(\bar{u}^{2} + \bar{v}_{c}^{2} - \bar{v}^{2} \right) dy$$

This is then the momentum integral equation when y_1 = S ,
where S is the height of the boundary layer or in this case
half the duct height.

The third equation is obtained by putting y_1 = $S/2$. As
Moses (71) remarks in his introduction of the strip method , the
third equation could equally well be obtained by putting y_1 = 0.4 S
or 0.6 S . He tried different values of y_1 with no difference in
the final predicted results. If the third equation is obtained by
integrating from $S/2$ to S , i.e. across the outer half of the
boundary layer then there is no wall shear stress term and hence
it is not possible to dispose of τ_w by subtraction of one
integral equation from the other.

5.2.2. The Mean Velocity Profile.

A one-parameter power law velocity profile was used in
conjunction with the two momentum integral equations to effect a
solution. The adoption of power law velocity profiles has been
criticised for its use in flows with adverse pressure gradients,
but it is considered acceptable in this case , since its original
postulation was based on experimental observations of pipe flows.

The power law velocity profile may be written

$$\frac{U}{U_c} = \left(\frac{y}{\delta}\right)^{1/n}$$

5.2.8.

It then follows that the mean flow quantities to be predicted are determinable in terms of the parameter n , thus ,

the displacement thickness

$$\delta^* = \int_0^\delta \left(1 - \frac{U}{U_c}\right).dy = \frac{\delta}{1+n}$$

the momentum thickness

5.2.9

$$\theta = \int_0^\delta \frac{U}{U_c}\left(1 - \frac{U}{U_c}\right)dy = \frac{\delta n}{(n+1)(n+2)}$$

the shape factor

$$H = \frac{\delta^*}{\theta} = \frac{2+n}{n}$$

5.2.3. Derivation of the Differential Equations for Computation.

We can derive the momentum integral equation and the Strip momentum integral equation 5.2.7. by putting y_1 equal to δ and $\delta/2$ respectively.

$$\frac{d}{dx}\int_0^\delta U(U_c-U)dy - \frac{dU_c}{dx}.\int_0^\delta U dy + \delta U_c \frac{dU_c}{dx}$$

$$= \frac{\tau_w}{\rho} + \frac{\delta}{\rho}\left(\frac{d\tau}{dy}\right)_c$$

5.2.10

and

$$\frac{d}{dx}\int_0^{\delta/2} U(U_{\delta/2}-U)dy - \frac{dU_{\delta/2}}{dx}\int_0^{\delta/2} U.dy + \frac{\delta}{2}U_c\frac{dU_c}{dx}$$

$$= \frac{\tau_w}{\rho} - \frac{\tau_{\delta/2}}{\rho} + \frac{\delta}{2\rho}\left(\frac{d\tau}{dy}\right)_c$$

5.2.11

Here the normal stress terms have been neglected , since they have been shown (see Goldberg (72) , Hinze (14) , Rotta (2)) only to have an appreciable effect near to separation.

By subtracting equation 5.2.11. from equation 5.2.10 and using the power law velocity profile equation 5.2.8. it is possible to derive the differential equation required for computation as follows:

$$\frac{dn}{dx} = \left\{ \frac{\tau_{s/2}}{S\rho U_c^2} + \frac{1}{2\rho U_c^2}\left(\frac{d\tau}{dy}\right)_c - \frac{1}{U_c}\frac{dU_c}{dx}\left[A_1\right] \right\} \Big/ \left[B_1\right] \qquad 5.2.12.$$

where

$$A_1 = \left[\frac{n^2}{(n+1)(n+2)}\left(2^{-1-2/n} - 1 \right) + \frac{1}{2} \right]$$

and

$$B_1 = \frac{1}{(n+1)(n+2)}\left[\frac{(2-n^2)}{(n+1)(n+2)}\left(1 - 2^{-1-2/n}\right) + 2^{-1-2/n}\ln 2 \right] \qquad 5.2.13$$

Thus we have a differential equation for the velocity profile parameter n in terms of x . In order to solve it , the shear stress terms and the centreline velocity term will be evaluated from experimental data.

If we chose to ignore the effects of flow history and tried to determine an expression for the shear stress at $\tau_{s/2}$ from a polynomial representation of the shear stress distribution (in the manner originally proposed by Fediaevsky (73)) then it would still be necessary to provide expressions for the slope of the shear stress at the centreline and the wall shear stress , which again would have to be derived from experimental data. This is also a consequence of using an eddy viscosity or mixing length formula for the determination of $\tau_{s/2}$.

Since δ has been taken as being constant in the derivation of equation 5.2.12 it then follows that this method of prediction is limited to application after the boundary layers have merged. In order to predict the entire flow development it would be necessary to derive a pair of simultaneous differential equations in n and δ and then to make some stipulation concerning $\frac{d\delta}{dx}$ in the region before the boundary layers merge. The extension of this method to straight walled two-dimensional diffusers which follow a duct in which the boundary layers have merged does not necessitate the derivation of a further differential equation , but that a linear relationship between δ and x be used instead of a constant value of δ .

5.3. Data Input.

5.3.1. Error Analysis.

The differential equation to be computed , equation 5.2.12 , can be written as follows.

$$\frac{dn}{dx} = \frac{CA - CB.A_1}{B_1} \qquad\qquad 5.3.1.$$

where

$$\left.\begin{array}{c} CA = \frac{1}{U_c^2}\left[\frac{(-\overline{uv})_{\delta/2}}{\delta} + \frac{1}{2}\left(\frac{d(-\overline{uv})}{dy}\right)_c\right] \\[3em] \text{and} \\[1em] CB = \frac{1}{U_c}\frac{dU_c}{dx} \end{array}\right\} \qquad 5.3.2.$$

where the contribution to the shear stresses from viscosity has been neglected in CA.

For the purpose of compiling the input data the values of CA and CB were calculated from the experimental data at every measurement point down the length of the duct. Now since CA is zero in a flow in which the shear stress distribution is linear across the duct and the errors in the measurement of the two terms in CA are not negligible then any small departure from linearity in the stress distribution might be masked by errors. Because of this , an analysis of the errors in CA was conducted to determine what degree of uncertainty was tolerable in CA.

If we write CA as

$$CA = \left(a\gamma - b\phi\right)\frac{1}{U_c^2}$$

then the error in CA can be written

$$\mathcal{E}_{CA} = \frac{dCA}{CA} = \frac{\mathcal{E}_{\tau}\left(1 - \frac{a\tau}{b\phi}\right) + \mathcal{E}_{\phi}\left(1 - \frac{b\phi}{a\tau}\right)}{\left(2 - \frac{a\tau}{b\phi} - \frac{b\phi}{a\tau}\right)} - \mathcal{E}_{U_c}$$

If the average error in the measurement of $- \overline{uv}$ is assumed to be

$2\frac{1}{2}\%$ and in $\left(\frac{d\overline{uv}}{dy}\right)_c$ to be 5% and the error in the measurement of

U_c is neglected by virtue of its comparitive size , then the error

in CA becomes a function of the relative sizes of the two shear

stress terms.

If $\qquad \frac{a\tau}{b\phi} = \tau$

then $\qquad \mathcal{E}_{CA} = 0.025 \frac{(2\tau - 1)}{(\tau - 1)}$

thus when $r = 1$, i.e. the condition for a linear shear stress

profile , then $\mathcal{E}_{CA}$ becomes infinite and CA is zero. It can be

shown that for any value of r in the range

$$0.85 < r < 1.25$$

there will be an uncertainty in the evaluation of CA of greater

than 10%.

Using this analysis the graphs of CA against x derived directly

from the experimental data were smoothed in such a manner that the

line then lay within the limits of the uncertainty in CA. This

procedure gave a smoother set of input data for CA.

In the case of the CB term the error in CB can be expressed as

$$\mathcal{E}_{CB} = \mathcal{E}\left(\frac{dU_c}{dx}\right) - \mathcal{E}_{U_c}$$

Now since the evaluation of $\frac{dU_c}{dx}$ is based on two measurements of

U_c it has twice the error of the latter. Thus the error in CB is

the same as the error in U_c , and the experimental data was smoothed

accordingly.

5.3.2. Curve Fitting.

Since the values of the functions CA and CB must be capable of being evaluated at any point in the x direction , in order to get a solution using the computer programme chosen , it was necessary to express the data in the form of an equation in x and not in its present graphical or tabular form. A Lagrangian curve fitting method was adopted for this purpose , and is illustrated as follows. If the data exists in the tabular form

x	x_0	x_1	x_2	---	x_r	---	x_n
CA	CA_0	CA_1	CA_2	---	CA_r	---	CA_n

then to express it in the form

$$CA\ (x)\ =\ a_0\ +\ a_1 x\ +\ a_2 x^2\ ---\ a_r x^r\ ---\ a_n x^n$$

we can put

$$CA\ (x)\ =\ L_0 \cdot CA_0 + L_1 \cdot CA_1 + L_2 \cdot CA_2\ ---\ L_r \cdot CA_r\ ---\ L_n \cdot CA_n$$

where

$$L_r = \frac{(x - x_0)(x - x_1)(x - x_2)\ ---\ (x - x_{r-1})(x - x_{r+1})\ ---(x - x_n)}{(x_r - x_0)(x_r - x_1)\ ----(x_r - x_{r-1})(x_r - x_{r+1})\ ---\ (x_r - x_n)}$$

This method , adopted for all the input data , was used with a value of n = 6 and with a constant interval in x equal to unity.

The accuracy of this technique was tested by comparing the curve derived from the tabulated data with the original curve from the experimental data. No errors exceeding 5% were found.

5.4. The Computer Programme.

The basis of the method adopted for solving the differential
equation is that due to Adams-Bashforth , further details of which
are in Interpolation and Allied Tables (74). This is a numerical
method of solution by means of a step by step procedure using a
pair of equations for predicting and correcting the value of the
dependent variable at a point. The way in which the Adams-Bashforth
method has been used is due to Hirst and Reynolds (75).

The programme consists of a driver (MAIN) and three subroutines
(ADAMS , PRFLE , and DERIV). The input data is read in MAIN which
then prints out the headings on the first page of the output. MAIN
then calls ADAMS to solve the differential equation and after the
calculations have been completed control is returned to MAIN and
then terminated. Although ADAMS uses a four point predictor -
correcter pair only one initial point is fed in as data. A simple
predictor formula is used to determine a second point and these
two are then used by a two point predictor correcter pair to
determine the next two points. After this , four points are avail-
-able and the Adams-Bashforth scheme is then used.

Besides performing numerical integrations ADAMS is also
responsible for keeping errors within certain bounds. The programme
is set up so that the accumulated relative error for the entire
boundary layer is less than the value of a preset size. If the
error becomes too large ADAMS automatically reduces the step size
until the equations can be solved to the desired accuracy. If the
step size must be reduced too often or if too many points are
required between printing points then the calculation is terminated
and an error message is printed out.

To perform the integrations ADAMS calls DERIV twice (for the
predictor and the corrector) for each step forward. DERIV

determines the derivative at any point , given the local values of the dependent variables. When ADAMS has sucessfully integrated up to a printing point , PRFLE computes the various integral parameters from the dependent variable and prints them out.

The computer programme is listed in Appendix 3.
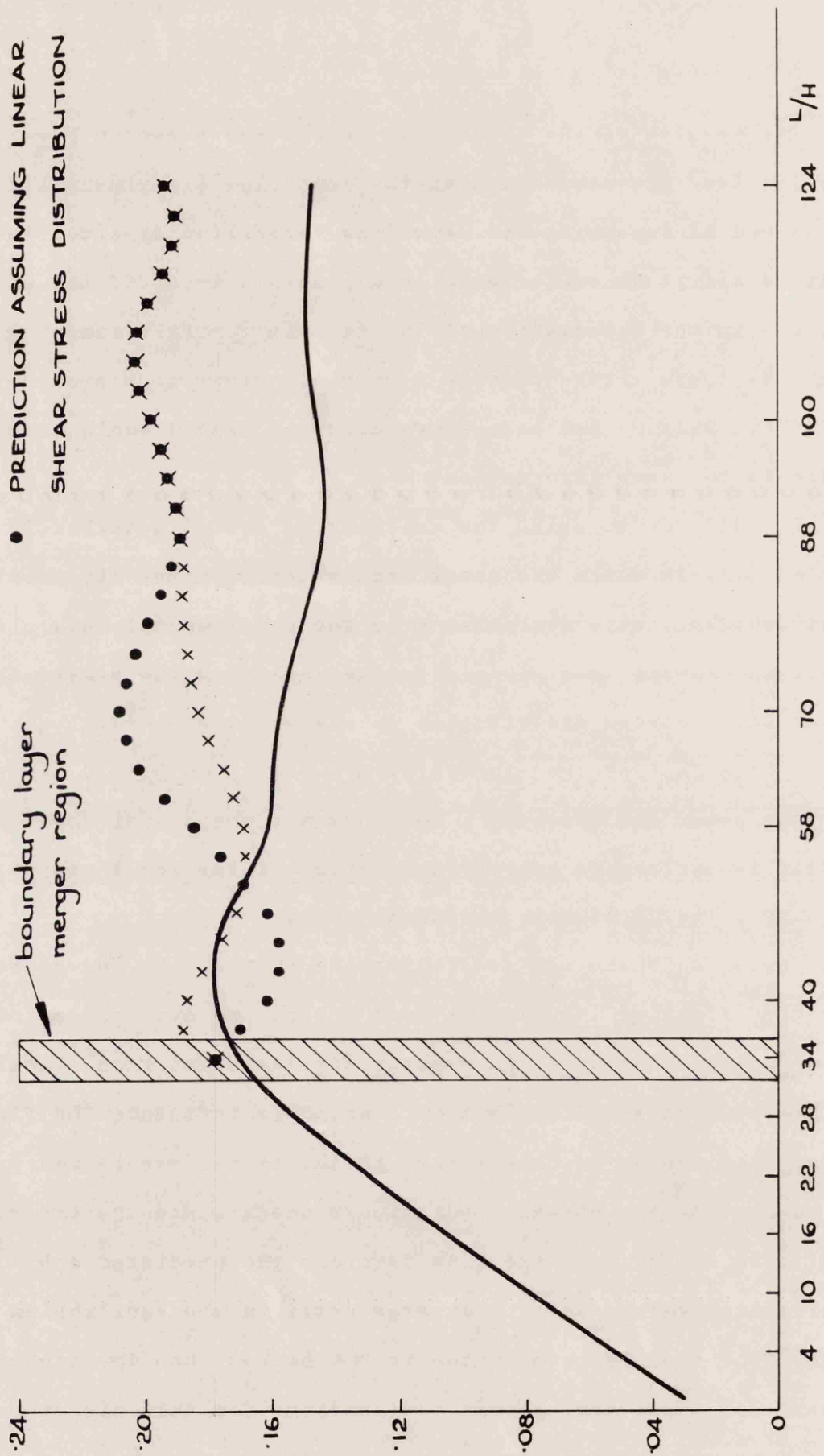
FIG.5.1. PREDICTION OF THE DEVELOPMENT OF θ FOR DUCT FLOW

5.5. Results and Discussion.

The results of the prediction method are shown in Figure (5.1) in which they are compared with the duct flow experimental data. The method of measuring the mean flow velocities by pitot tube and inclined spirit manometer entails a possible error of the order of 1% , and in the calculation of the velocity profile momentum thickness these errors produce a possible error of approximately 3% in θ . Only θ has been shown since δ^* and H would merely duplicate the same information.

In addition to using the calculation method detailed in Section 5.2. in which the shear stress terms in the differential equation5.2.12. were evaluated from the experimental data , the calculation method was also undertaken assuming the existence of a linear shear stress distribution as one might expect in eqilibrium flow. This implies that the CA term in equation 5.3.1. is zero and that the power law exponent , and thus the shape , of the velocity profile is influenced only by a function of the local centreline velocity , the CB term in equation 5.3.1.

Comparing these two predictions in Figure 1 it can be seen that the effect of the CA term does not become negligible until L/H = 90 and that up to this point the deviation from linearity of the shear stress distribution , which is influenced by flow history , plays an important part in the normal prediction procedure.

Comparing the normal prediction procedure and the experimental results we see that as the flow develops the predicted and experimental values of θ diverge until in the equilibrium region of the flow the predicted value is 20% higher than the experimental value. The three most common explanations for this disagreement between experiment and two dimensional theory are:-

(i) Inaccuracy of the description of the shear stress
distribution.

(ii) Neglection of the normal stress terms.

(iii) Presence of three dimensional effects in the experimental
boundary layers.

The first reason given cannot be entirely discounted since
although the description of the shear stress distribution is
provided by the experimental data and will thus contain the effects
of flow history , the curve fitting technique is only an
approximation. This curve fitting procedure would be better if
more of the available tabulated data were used in the derivation
of the polynomial in x used to describe the CA term in equation
5.3.1. Furthermore the shear stress measurements were made using
inclined hot wire anemometers and thus are subject to the measure-
-ment errors discussed in Chapter 2.

Concerning the second reason , it was considered justifiable
to neglect the normal stress terms in the mild favourable pressure
gradient flow characteristic of the present work.

It is the third reason that is probably the major cause of the
discrepancy. As the flow develops , the sidewall boundary layers
grow and thus accelerate the central flow to a higher equilibrium
flow Reynolds Number than would be the case for an infinite aspect
ratio duct. The effect of this higher than two dimensional
Reynolds Number is to increase the power law exponent n and thus
decrease the momentum thickness.

CONCLUSIONS.

1.   An assessment of the possible errors involved in the
measurement of turbulence by hot-wire anemometers is presented.
It is shown that the major errors arise from the presence of high
intensities of turbulence and from the assumption of the cosine
law of directional sensitivity when using inclined wires. The
former may give rise to errors of up to +5% in the flow regions
near the walls and behind the flow mixing , and the latter to
errors of up to - 10% .

2.   An explanation of the 'overshoot' phenomenon observed in the
development of velocity profile thickness parameters in duct flow
is presented. This explanation is in terms of a momentum balance
in which the acceleration and deceleration of the central region of
the flow is shown to be governed by the turbulent shear stress
gradient. Since the shear stresses in the central region of the
flow have their origins at points on the wall upstream of their
present position , the 'overshoot' is shown to be a function of
the history of the flow.

3.   Although the boundary layers growing on opposite walls of the
duct merge in the region $31 < L/H < 37$ the flow is not stable
(i.e. unchanging with increasing distance) until a value of $L/H = 90$
is reached.

4.   A discussion on the use of various methods of simulating
velocity profiles is presented. For simplicity of analysis and
ease of structural support the use of a grid of rods or a row of

flow mixing devices is suggested. Some possible consequences of
the use of these mechanisms is outlined.

5. An examination of the basic principles whereby velocity
profiles are produced , and the effect that constraints placed in
the flow have on the length required for their production is
presented. This is shown to produce a realistic estimate of the
length required for the production of a 1/7th Power Law profile
for flow over smooth walls , this estimate being L/H = 44.2 .

6. The ability of a simulator mechanism to produce a stable
velocity profile is shown to depend on the size and shape of the
turbulent shear stress distribution produced immediately downstream.
The larger and more nearly linear the stress distribution , the
sooner will the flow become stable. Thus the flow pattern produced
by the ramp flow mixing device becomes stable more quickly than
those produced by the grid of rods.

7. The design values of the velocity profile parameters for grid
produced flows are found not to be complied with in practice.
Allowance for this can be made by increasing the required power
law exponent by 15% .

8. By application of an integral method of boundary layer
calculation to duct flows the effect of flow history is demonstrated.
The solution obtained using experimental values of the turbulent
shear stresses may be compared with that obtained assuming the
stress distribution to be linear. This shows the effect of flow
history to be appreciable up to L/H = 90 , a figure which is

compatible with those obtained from observation of the mean

velocity profile development.

9. Based on experimental observations an equation is suggested

for the development of the mixing length distribution in duct flows.

The relationship is

$$\ell_m = K_1 \, y + K_2 \, y$$

where the first term is effective in the range $0 < y < y_1$ and the

second in the range $y_1 < y < H/2$. The development of the

parameters y_1 , K_1 and K_2 with respect to x is presented graphically.

Appendix 1.

Mixing Length Theories.

As we have seen in Chapter 5 it is necessary to be able to relate the turbulent shear stresses in the flow to other flow properties in order to obtain a solution to the momentum equation. for flow calculations.

In an analysis of turbulent flow the concept of mixing length is often used to relate the mean velocity profile to the turbulent shear stresses , and although such formulations often lack a rigorous physical basis they have been found to be useful in treating equilibrium turbulent flows. Perhaps a better reason for looking at mixing length theories concerns the recent reinterpretation of the mixing length as a dissipation length scale. The basis of this idea was advanced by Townsend (76) who used equations governing the local balance of kinetic energy of the turbulent fluctuations to modify the mixing length so as to account for the pressure - velocity diffusion of energy near a wall.. This idea has subsequently been developed by Bradshaw et. al. (78) and McDonald (79) in their boundary layer calculation methods.

A.1.1. Mixing Length Formulations.

The classical theories for turbulent flow are Prandtl's mixing length theory , Von Karman's similarity hypothesis and Taylor's vorticity transport theory.

Since Taylor's theory is primarily applicable to free turbulence it will not be covered here. A further theory developed more recently than these is due to Rotta.

(i) Prandtl's Mixing Length Theory.

Prandtl hypothesized that the turbulent mixing motion was composed of moving eddies of fluid such that an eddy in a layer at y could move to a layer at $y + \ell$. He then assumed that the eddy preserved its momentum as it moves along the path ℓ , and at $y + \ell$ the eddy has a different velocity associated with it than the other eddies in this layer.

The difference in velocity between the eddy and the layer at $y + \ell$ may be written

$$\Delta U = \ell \cdot \frac{dU}{dy} \qquad \qquad \text{A.1.1.}$$

if ℓ is assumed to be small and higher order terms are neglected. This difference may be interpreted as the fluctuating velocity at $y + \ell$ and thus

$$|u| = \ell \frac{dU}{dy} \qquad \qquad \text{A.1.2.}$$

Prandtl further assumed

$$|v| = K_1 |u| \qquad \qquad \text{A.1.3.}$$

and thus $\quad \overline{uv} = -K_2 |u||v| \qquad \qquad$ A.1.4.

since the correlation of u and v has been shown to be negative, and where K_2 is a positive constant. Thus

$$\overline{uv} = -K_1 K_2 \ell^2 \left(\frac{dU}{dy}\right)^2$$

or

$$\overline{uv} = -\ell_{PR}^2 \left(\frac{dU}{dy}\right)^2 \qquad \qquad \text{A.1.5.}$$

where ℓ_{PR} is Prandtl's mixing length.
Since the turbulent shear stress

$$\tau = -\rho\overline{uv}$$

then

$$\tau = \rho \ell_{PR}^2 \left(\frac{dU}{dy}\right)^2 \qquad \qquad \text{A.1.6.}$$

Except in the small region adjacent to the wall where viscosity is dominant the mixing length ℓ_{PR} is regarded as a local function.

In order to make use of Equation A.1.6. Prandtl assumed the mixing length to be given by

$$\ell_{PR} = K_3 \, y \qquad \qquad \text{A.1.7.}$$

where K_3 is a constant.

(ii) Von Karman's Similarity Hypothesis.

Von Karman assumed that the turbulent fluctuations are similar at all points in the flow field and that only the time and length

scales differ. He also assumed that the mechanism of turbulence was independent of viscosity. Consequently from the similarity assumption we get:

$$|u| \sim |v| \sim l_1 \frac{dU}{dy}$$

or

$$\overline{uv} = -l_1^2 \left(\frac{dU}{dy}\right)^2 \qquad\qquad \text{A.1.8.}$$

This result is identical with that derived from the Prandtl mixing length theory , the difference in the theories being that the similarity hypothesis is independent of any special flow models. If it is assumed that l_1 (a similarity scale rather than a mixing length) is dependent not upon distance from the wall but upon the velocity distribution then

$$l_1 = f\left(\frac{dU}{dy} , \frac{d^2U}{dy^2} , ----\right)$$

and thus the simplest derivable length is

$$l_1 = K_4 \frac{dU/dy}{d^2U/dy^2} \qquad\qquad \text{A.1.9}$$

thus it follows

$$\tau = -\rho\overline{uv} = \rho K_4^2 \frac{\left(dU/dy\right)^4}{\left(d^2U/dy^2\right)^2} \qquad\qquad \text{A.1.10.}$$

With the assumption of constant shear stress both theories give identical velocity profiles.

<u>(iii) Rotta's Theory for a Length Scale of Turbulence.</u>

Briefly , Rotta (79) has developed a differential equation for the length scale of turbulence , l_s , which is derived from the Navier-Stokes equations. This differential equation consists of the following four terms.

(a) the substantive derivative of l_s , Dl_s/Dt .

(b) the rate of growth of l_s as a result of the dissapation. of energy

(c) the tendency of the shear stresses to reduce l_s by rupturing large eddies.

(d) the diffusion of eddy size as a result of the gradient in

l_s

This theory of Rotta has been succesfully used by Spalding to account for the similarity of spreading characteristics in various types of jet flow.

Batchelor (5) presents a discussion on the formulation ,merits and disadvantages of the concept of mixing length theories. The more notable defects of this type of formulation are as follows:-

(a) In reality the turbulence transfer coefficient derived from the mixing length does not become zero at $\frac{dU}{dy} = 0$ as the theory would indicate.

(b) The implication that l_{PR} is small compared with the dimensions of the mean flow is not confirmed when the theory is checked against various types of flow.

(c) the theory takes no account of conditions at the boundaries of free turbulent flows.

(d) The theory leads to inaccurate predictions regarding the distribution of turbulence energy.

Furthermore there is a lack of guidance for postulations concerning the variation of the mixing length across the flow.
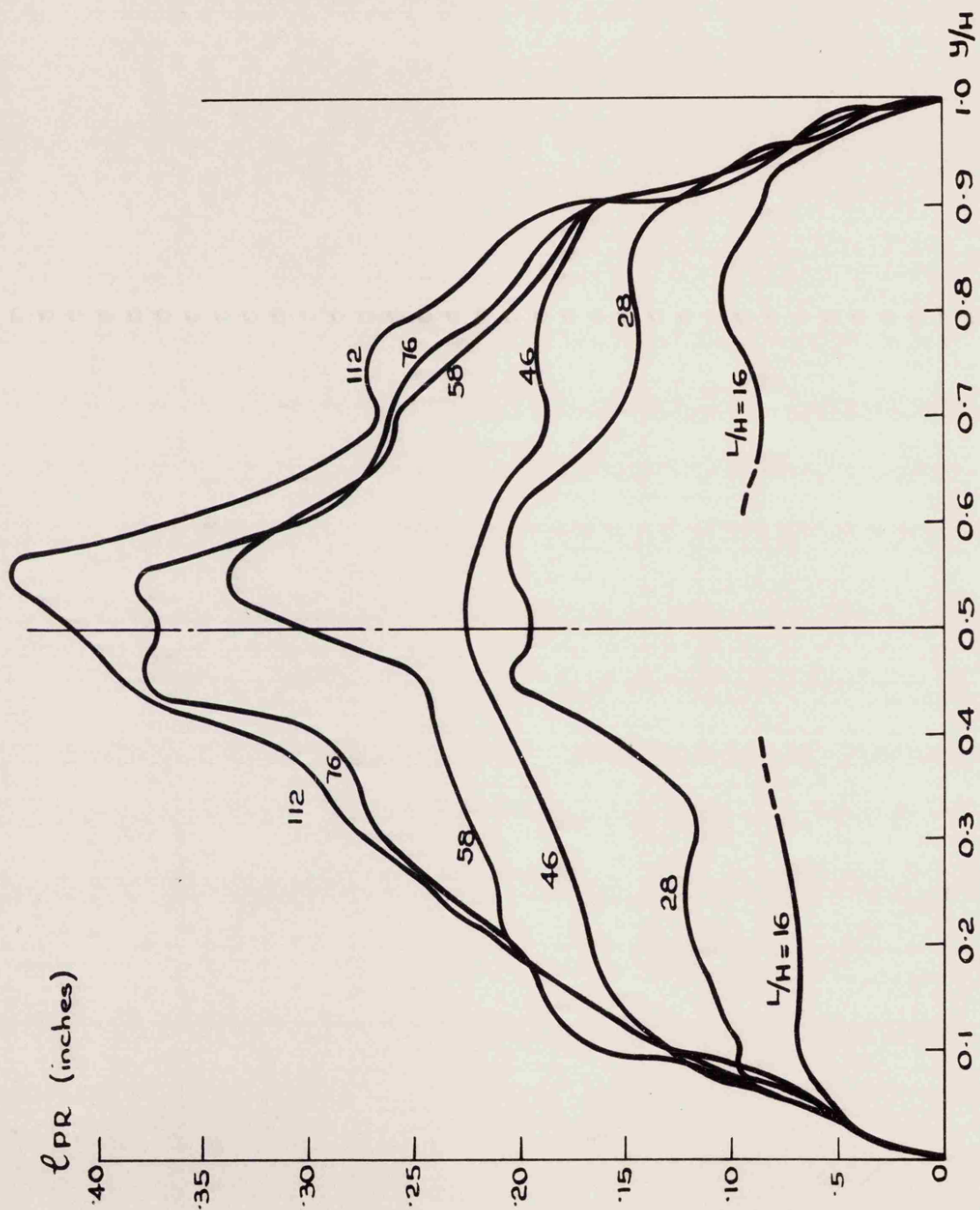
FIG. A.11. DISTRIBUTION OF ℓ_{PR} IN DUCT FLOW
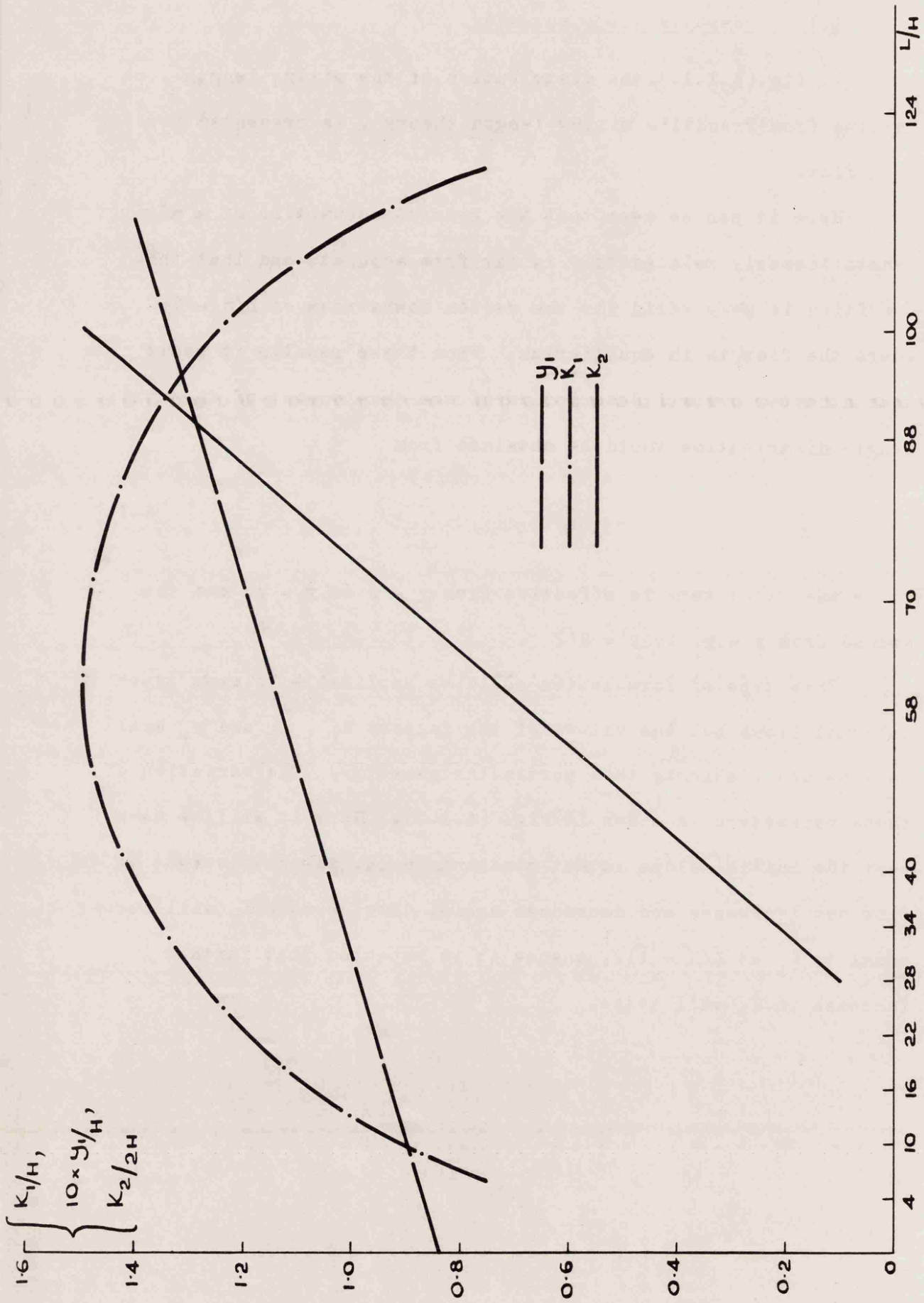
FIG. AI.2. DEVELOPMENT OF PARAMETERS y_1, K_1 AND K_2 IN MIXING LENGTH FORMULATION

A.1.2. Results and Discussion.

In fig.(A.1.1.) the distribution of the mixing length , as derived from Prandtl's mixing length theory , is presented for the Duct Flow.

Here it can be seen that the general assumption of a mixing length linearly related to y is far from accurate and that this condition is only valid for the region downstream of L/H = 76 , where the flow is in equilibrium. From these results it would seem that a better overall description of the development of the mixing length distribution would be obtained from

$$ \ell_{PR} = K_1 y + K_2 y $$ A.1.11.

where the first term is effective from y = 0 to y = y_1 and the second from y = y_1 to y = H/2

This type of formulation could be applicable to many types of internal flows but the values of the factors K_1 , K_2 and y_1 would only be applicable to this particular geometry. The variation of these parameters is shown in Fig. (A.1.2). Here it will be seen that the initial slope is not constant during the development of the flow but increases and decreases again. Furthermore K_2 will become equal to K_1 at L/H = 112, whence it is expected that further increase in K_2 will cease.

Appendix II

In turbulent flow it is considered that the motion may be separated into a mean flow and a superimposed fluctuating flow. The fluctuating velocity components give rise to shear stresses,(the so called Reynolds stresses) and the total shear stress may be considered to be the sum of that due to molecular viscosity and the Reynolds stresses. Hence

$$\tau = \mu \frac{dU}{dy} - \rho \overline{uv} \qquad \text{A.2.1.}$$

Bossinesq (80) assumed that the Reynolds stresses , like the viscous ones , were proportional to the mean velocity gradient and introduced the concept of an eddy viscosity , ϵ_m , such that

$$\tau = \left(\mu + \rho \epsilon_m \right) \frac{dU}{dy} \qquad \text{A.2.2.}$$

thus

$$\epsilon_m = -\overline{uv} \left/ \frac{dU}{dy} \right. \qquad \text{A.2.3.}$$

According to Boussineq , the eddy viscosity has a constant scalar value , but this we know now to be untrue. The following section presents some of the theories that have been put forward for the behaviour of ϵ_m .

A.2.1. The Behaviour of ϵ_m.

A.2.1.1. The Constancy of ϵ_m .

The most common assumption regarding the distribution of eddy

viscosity in a boundary layer concerns its constancy over at least

part of the outer region of the flow (typically $y^+ >$ 1000). This

assumption leads to the result that the velocity profile will be

parabolic in regions of linear shear stress distribution as is

stable laminar flow.

Clauser (70) stated that the eddy viscosity might be considered

to be constant over the outer 80% of the boundary layer in similar

or self preserving flows. In this region he stipulates that

$$\epsilon_m = K . U_\infty . \delta^*$$
A.2.4.

where K is a function of the turbulent Reynolds Number and U_∞

is the free stream velocity. For the inner region of such a flow,

where $\tau = \tau_w$ he gives a suitable relationship as

$$\epsilon_m = \kappa . u^* . y$$
A.2.5.

where κ is Von Karman's constant , equal to 0.41 .

This approach to a hypothesis for an eddy viscosity distribution

is followed by Mellor and Gibson (81) and developed further by

Mellor (82).

Commenting on this approach , Townsend (76) states that although

there seems no physical grounds for its validity , the assumption

of a constant eddy viscosity leads to an accurate description of

the mean velocity distribution in self-preserving flows , and is

a useful hypothesis to use when the nature of turbulence is not

concerned.

In an earlier paper however , Townsend (83) outlines an idea
concerning an equilibrium theory of eddy viscosity . This is
that the eddy viscosity is a parameter describing a balance set up
between the orientating effect of the shear forces and the
disorientating effect of the turbulent transfer process. This idea
could be readily tested by observing the attainment of isotropy in
an initially anisotropic flow.

A.2.1.2. ϵ_m Distributions based on a Velocity Profile.

If we assume the effect of molecular viscosity is negligible
then Equation A.2.2. can be written

$$\tau = \rho \, \epsilon_m \, \frac{dU}{dy}$$

Now by assuming a known distribution of shear stress within the
boundary layer and a velocity profile shape , the eddy viscosity
distribution is simply calculated. If we take a linear shear
stress distribution

$$\frac{\tau}{\tau_w} = y/\delta$$

and a 1/7th Power Law velocity profile

$$\frac{U}{U_{max}} = \left(y/\delta \right)^{1/7}$$

then the eddy viscosity distribution can be
written as

$$\epsilon_m = 7 \frac{\tau_w}{\rho} \left(U_{max} \right)^{-1} y \cdot \left(y/\delta \right)^{6/7} \qquad\qquad \text{A.2.6.}$$

If the logarithmic velocity profile

$$\frac{U}{U_*} = 2.5 \log \frac{y U_*}{\vartheta} + C \qquad /$$

is used then the eddy viscosity distribution becomes

$$\mathcal{E}_m = \frac{\mathcal{T}_w}{\rho \cdot \delta} \cdot \frac{y}{U_*} \frac{(\delta-y)}{2.5} \qquad A.2.7.$$

Rapier (84) , who discussed a number of variations using this approach , produced eddy viscosity variations for two types of velocity profile. This led him to recommend the assumption of a constant $\mathcal{E}_m$ whose value is given by

$$\mathcal{E}_{m+2} = \frac{U_* y_{max}}{10} \qquad A.2.8.$$

This method is also adopted by Bennet (85) who used a universal velocity profile in conjunction with a linear shear stress variation to give distributions of $\mathcal{E}_m$ applicable to pipe , annulas and parallel plate flow.

A.2.1.3. $\mathcal{E}_m$ Formulations based on Mean Velocity Parameters

The majority of the theories concerning the distribution of $\mathcal{E}_m$ are formulated only in terms of mean velocity parameters. Although this limits their potential , many of them have been shown to produce satisfactory results.

From a hypothesis in which the flux density of turbulent diffus-ion , $\frac{d\mathcal{E}_m}{dy}$, is equated to an adverse flux produced by the effective macroscopic velocity fluctuations corresponding to

$$U_* \left\{ \frac{\sqrt{\overline{u^2}}}{U_*} - \left(\frac{\sqrt{\overline{u^2}}}{U_*}\right)_c \right\}$$

Gosse (86) produces the following eddy viscosity relationship

$$\frac{\epsilon_m}{\epsilon_{m_c}} = 1 - \left(\frac{H_{/2} - y}{H_{/2}}\right)^2 \qquad \text{A.2.16}$$

for duct flow. In a later report Gosse (87) gives an evaluation of the eddy viscosity at the duct centreline

$$\frac{\epsilon_{m_c}}{\vartheta} = 0.0656 \left(\frac{u_* \cdot H_{/2}}{\vartheta}\right) \qquad \text{A.2.17}$$

In order to proceed with an analysis of free turbulent mixing processes Schetz and Jannore (88) discuss the use of the eddy viscosity models of Clauser (70), Prandtl (89) , Schlichting (22) and Townsend (76). They conclude that for their particular application the various formulations are equivalent and could be expressed as

$$\epsilon_m = \kappa \cdot U_\infty \cdot \vartheta \qquad \text{A.2.18}$$

Deissler (90) in an investigation into heat transfer in turbulent fluid flow deduces the following expression for the distribution of eddy viscosity in a duct from dimensional arguments

$$\epsilon_m = n^2 \, U \cdot y \qquad \text{A.2.19}$$

where n is a constant of proportionality.

In order to calculate the rate of hear transfer from a heated wall to a fluid , a knowledge of the eddy viscosity near the wall is required. Sleicher (91) shows that the criteria of Reichardt (92) that

$$\frac{\epsilon_m}{\vartheta} \, \alpha \, y^3 \qquad \text{A.2.20}$$

and of Elrod (93) that

$$\frac{\epsilon_m}{\nu} \propto y^4 \qquad \text{A.2.21}$$

are not critical and that acceptable results are obtained in the wall region (i.e. $0 < y^+ < 20$) with a square law relationship.

Kleinstein (94) also presents an eddy viscosity model for flow in the wall region. Based on a logarithmic velocity distribution and a turbulent shear stress variation proportion to the cubic power of the wall distance , his expression can be written

$$\frac{\epsilon_m}{\nu} = \left(\frac{\tau(y)}{\tau_w}\right)^{1/2} \cdot \frac{K_1}{K_2} \left\{ e^{K_1 U_K} - 1 + K_1 U_K + \frac{1}{2} K_2^2 U_K^2 \right\} \qquad \text{A.2.22}$$

where $K_1 = 0.41$

$K_2 = 7.7$

$$U_K = \int_0^{U/u_*} \left(\frac{\tau_w}{\tau(y)}\right)^{1/2} d\left(\frac{U}{u_*}\right)$$

A.2.1.4. The Inclusion of Turbulence Parameters in ϵ_m

The majority of theories which attempt to qualify the behaviour of ϵ_m contain no reference to the turbulence structure of the flow. This then would seem an area for some improvement , but the few formulations which do include an allowance for the state of the turbulence have not yet been widely accepted.

Glushko (95) shows that the effective viscosity arising from the turbulent shear stresses is a function only of the Reynolds Number of the turbulence , where

$$Re_{turb} = \tau = \frac{\sqrt{\bar{q}^2} \cdot L_s}{\nu} \qquad \text{A.2.9}$$

and L_s in the scale of the turbulence.

This he shows to be universal for turbulent flows of the boundary layer type and not to depend on the presence of a pressure gradient. From theoretical considerations of the Reynolds Equations the following relationship for ϵ_m is obtained ,

$$\epsilon_m = \frac{\tau^2}{(\tau + \beta)(\tau + \gamma)}$$ A.2.10

where β and γ are constants. An analysis of the available experimental data gives the piece-wise function

$$\epsilon_m = H(\tau) \cdot \alpha \cdot \tau$$ A.2.11

where for

$0 < r/ro < 0.75$	$H(r) = r/ro$
$0.75 < r/ro < 1.25$	$H(r) = r/ro - (r/ro - 0.75)^2$
$1.25 < r/ro < \infty$	$H(r) = 1$

r_o is an arbitrary constant , taken by Glushko to be equal to 110

For their method of boundary layer calculation Patanker and Spalding (96) require an eddy viscosity distribution. Amongst others , they refer to the use of the formulation originally derived independently by Kolmogorov (97) and Prandtl (98) , thus

$$\epsilon_m = l_k \cdot \sqrt{\overline{q^2}}$$ A.2.12

Here l_k is a length scale associated with the mean kinetic energy of the turbulent motion.

Tyulpanov (99) has also produced an expression for the assessment of the eddy viscosity , based upon the flow's turbulence characteristics. For near - isotropic flow in rough tubes he

writes the eddy viscosity as

$$\mathcal{E}_m = c \cdot \frac{U^2 \cdot \overline{q^2}}{f}$$

A.2.13

in which c is a constant and f is defined as the fundamental

frequency of the stream velocity fluctuations. No further information

is given on the evaluation of f , but it could well be that its

value is that defined by the maximum point in an n S(n) v. n

spectrum graph (e.g. Fig. 4.29)

Phillips (100) proposes a relationship for the gradient of the

turbulent shear stresses. He notes that recent experiments have

shown the practise of seeking local relationships between the mean

velocity gradient and the shear stresses to be erroneous in principle

since these are not local properties but of the whole flow field.

It has been found that the turbulent shear stress is associated with

the energy containing components of turbulence , whose length scales

are of the same order as the scale of mean velocity variation .

Over these distances the turbulent shear stress varies as does the

mean velocity gradient; indeed it is the variation of the turbulent

shear stress and not the stress itself which features in the

boundary layer calculation equations. Thus Phillips sought a relat-

-ionship between the variations in mean velocity gradient and

turbulent shear stress. The expression he derived can be expressed

as

$$\frac{d\tau}{dy} = \mu_e \frac{d^2 U}{dy^2}$$

A.2.14

The 'apparent' eddy viscosity μ_e is

$$\mu_e(y) = A \cdot \rho \cdot \overline{v^2} \cdot \theta \qquad \text{A.2.15}$$

where A is a dimensionless constant

and θ is the integral time scale of the lateral velocity

fluctuations.

The major advantage of these methods of deriving an eddy

viscosity relationship is that unlike the formulations based only

on mean velocity parameters , they are capable of making an allowance

for the flow history either by way of a time or length scale or by

means of a frequency characteristic. It is unfortunate that these

mehtods are all of too recent vintage to be well tried in comparison

with experiment , but any improvement in eddy viscosity formulations

must surely come from this direction.
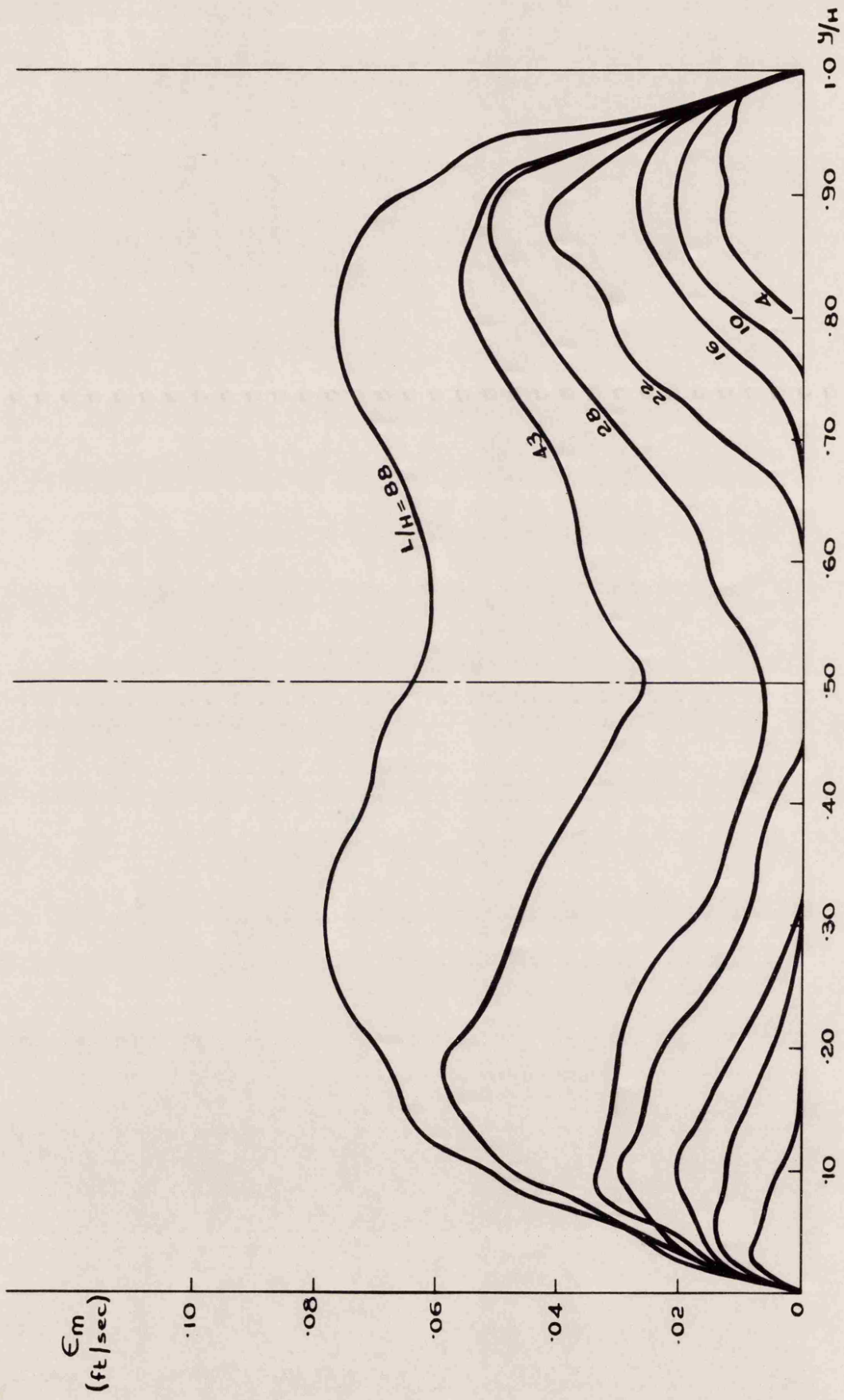
FIG. A.2.1. EDDY VISCOSITY DISTRIBUTION IN DUCT FLOW
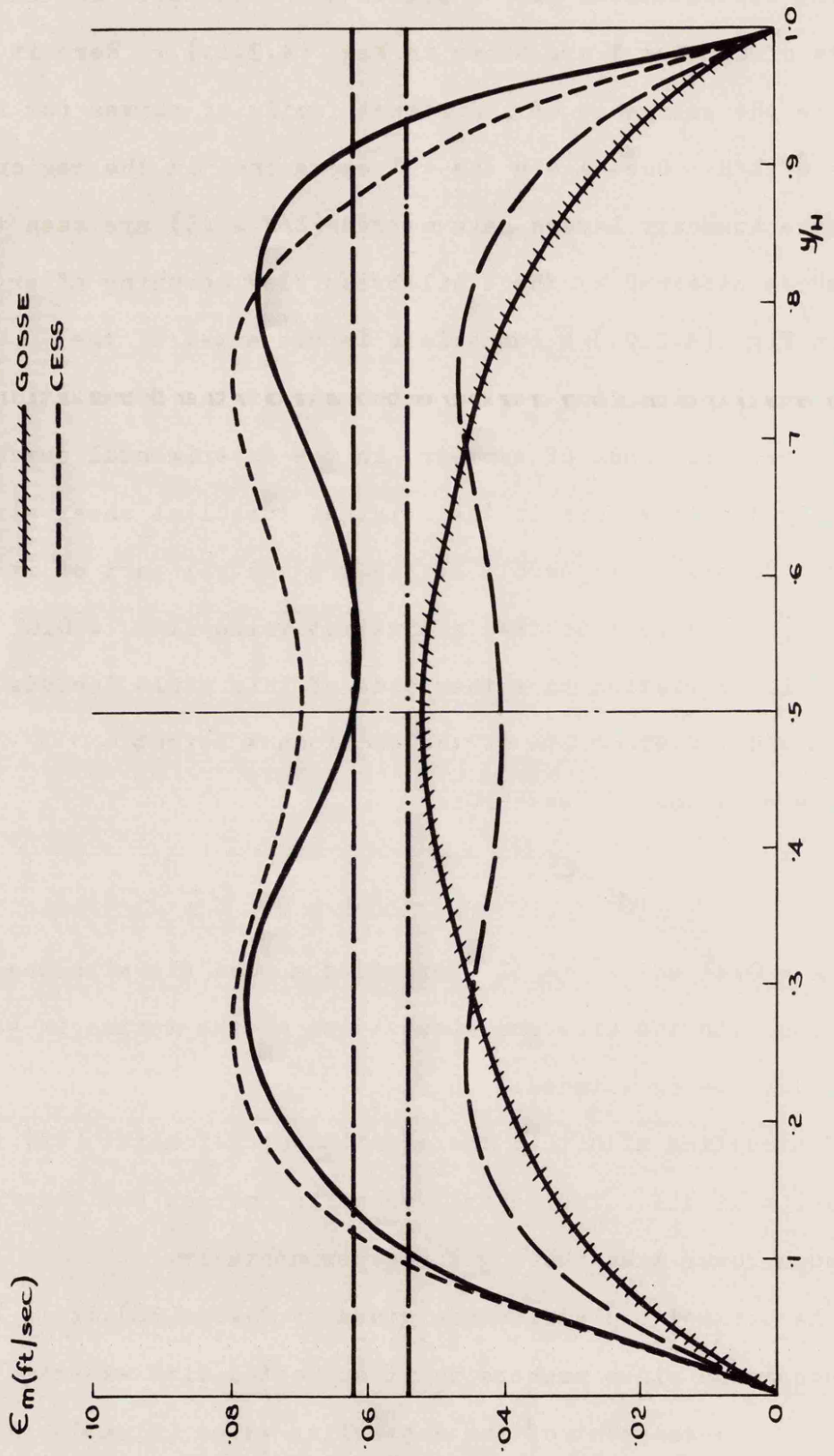
FIG. A22. COMPARISON OF EDDY VISCOSITY DISTRIBUTIONS

A.2.2. Results and Discussion.

The distributions of $\mathcal{E}_m$ across the duct based on the experimental results of Chapter 3 are shown in Fig. (A.2.1.) . Here it is possible to trace the emergence of a distinct family of curves for increasing values of L/H. Once again the values reached in the region just after the boundary layers have merged (L/H = 43) are seen to be less than those attained by the equilibrium flow occuring after L/H = 88.

In Fig. (A.2.2.) a comparison is presented of the $\mathcal{E}_m$ distribution in the equilibrium flow region with some of the formulations in the literature. The lack of symmetry in the experimental curve is primarily due to errors in the original turbulent shear stress data, but even so one could hardly define the central part of it as constant. However , if we were to take a constant value at $\mathcal{E}_m$ = 0.07 ft²/sec then a 10% variation to either side of this would include the range 0.14 $<$ y/H $<$ 0.91 or 77% of the total duct height.

The equation of Cess (101)

$$\frac{\mathcal{E}_m}{\nu} = \frac{1}{2}\left[1 + \frac{K^2 R_e^2}{144} \cdot \frac{f \cdot Y}{2}\left(2-Y\right)^2\left(3-4Y+2Y^2\right)^2\left\{1-e^{-\frac{YR_e}{4A^+}\sqrt{f/2}}\right\}\right]^{1/2} - \frac{1}{2}$$

where K = 0.41 and A⁺ = 31 , provides a good fit with the experimental data with both the size and disposition of the maxima in each half of the duct being matched.

Contrasting with this the equation of Reichardt (92) is not a good fit at all. The general shape is correct but the values are very much lower than those given experimentally.

The parabolic distribution given by Gosse (86) is to be regarded with suspicion since nowhere is it supported with experimental proof. However the assessment of the centreline value (Equation A.2.17.) compares favourably.

The constant values given by Rapier (84) and Corcoran et.al. (102) are both low but would appear better if compared with the ε_m distribution at a lower value of L/H. This leads one to suspect that their formulation may have been based on pipe flow data taken at the end of the inlet region rather than in the equilibrium flow.region.

Appendix III

Computer Programme for the Prediction of

Flows in Ducts.

The computer programme , listed overleaf , is written in
FORTRAN 1VA for use on an Elliot 4130 digital computer. The
average time taken for the calculation of a flow is 30 seconds.

```
  &JOB;ENG200BEL;SCMPL;
SWOP


&FORTRAN;


&LIST;
      REAL NI
      COMMON DEL,E1,E2,E3,E4,E5,E6,E7,F1,F2,F3,F4,F5,F6,F7,M
C     INPUT DATA.1ST CAR DATA SERIES NO,TEST CASE NO (INTEGERS )
C     2ND &3RD CARDS.COEFFICENTS OF THE CA CURVE
C     4TH & 5TH CARDS.COEFFICIENTS OF THE CB CURVE
C     6TH CARD.INITIAL VALUE OF POWER LAW EXPONENT N.NON DIMENSIONAL X
C     7TH CARD.X0,DX,XMAX,DELTA (ALL IN FEET)
      READ(7,100)J,K
  100 FORMAT(2I10)
      READ(7,200)E1,E2,E3,E4,E5,E6
  200 FORMAT(6F11.6)
      READ(7,300)E7
  300 FORMAT(F11.6)
      READ(7,400)F1,F2,F3,F4,F5,F6
  400 FORMAT(6F11.6)
      READ(7,500)F7
  500 FORMAT(F11.6)
      READ(7,600)NI,M
  600 FORMAT(F10.2,I1)
      READ(7,700)X0,DX,XMAX,DEL
  700 FORMAT(F10.2,F10.6,F10.2,F10.6)
      WRITE(2,800)NI,X0,K,J
  800 FORMAT(1H1,33X,66HSTRIP INTEGRAL CALCULATION OF CHANNEL FLOW USING
     1 POWER LAW PROFILE/10X,21HINITIAL VALUE OF N = ,F5.2,/10X,23HCALCU
     2LATION STARTED AT ,F4.2,4HFEET/10X,13HTEST CASE NO.,I2,/10X,8HDATA
     3 NO.,I2,//10X,5HX FT.,10X,1HN,10X,6HDS FT.,10X,6HTH FT.,10X,1HH)
      ERR=0.50
      ABE=0.0025*NI
      CALL ADAMS(1,NI,X0,XMAX,DX,1,2,ERR,ABE)
      STOP
      END


      SUBROUTINE PRFLE(N,X)
      REAL N
      COMMON DEL,E1,E2,E3,E4,E5,E6,E7,F1,F2,F3,F4,F5,F6,F7,M
      DS=DEL/(1.0+N)
      TH=DEL*N/((1.0+N)*(2.0+N))
      H=DS/TH
      WRITE(2,100)X,N,DS,TH,H
  100 FORMAT(1H ,10X,F5.2,7X,F6.3,10X,F5.3,10X,F5.3,7X,F5.3)
      RETURN
      END


      SUBROUTINE DERIV(X,N,DN)
      REAL N
      COMMON DEL,E1,E2,E3,E4,E5,E6,E7,F1,F2,F3,F4,F5,F6,F7,M
```

```
      CA=(E1+E2*X+E3*X*X+E4*(X**3.0)+E5*(X**4.0)+E6*(X**5.0)+E7*(X**6.0)
     1)*10.0**(-3.0)
      CB=(F1+F2*X+F3*X*X+F4*(X**3.0)+F5*(X**4.0)+F6*(X**5.0)+F7*(X**6.0)
     1)*10.0**(-3.0)
      A1=(N*N*(2.0**(-1.0-2.0/N)-1.0)/((N+1.0)*(N+2.0)))+0.5
      B1=1.0/((N+1.0)*(N+2.0))*(((2.0-N*N)*(1.0-2.0**(-1.0-2.0/N)))/((N+
     11.0)*(N+2.0))+2.0**(-1.0-2.0/N)*ALOG(2.0))
      WRITE(2,100)X,N,CA,CB,A1,B1
  100 FORMAT(1H ,6F15.10)
      WRITE(2,999)M
  999 FORMAT(I1)
      DN=(CA-CB*A1)/B1*M
      RETURN
      END


      SUBROUTINE ADAMS (N,Y,X0,XMAX,HP,ECV,EOP,ERR,ABE)
C     THIS SUBROUTINE SOLVES A SYSTEM OF UP TO 10 FIRST ORDER ORDINARY
C     DIFFERENTIAL EQUATIONS. N= NO OF EQNS, Y IS THE ARRAY OF DEPENDENT
C     VARIABLES, D IS THE NAME OF A SUBROUTINE WHICH COMPUTES THE
C     DERIVATIV ES
C     X0 IS THE STARTING VALUE OF THE INDEPENDENT VARIABLE, XMAX IS THE
C     FINAL VALUE OF THE IND. VARIABLE.
C     ECV,EOP,ERR,ABE ARE USED FOR ERROR CONTROL
C     ERR IS THE RELATIVE ERROR CONTROL, ABE IS THE ABSOLUTE ERR CONTROL
C     IDENT IS USED FOR IDENTIFICATION OF THE OUTPUT
C     HP IS THE INTERVAL FOR PRINTING OUTPUT
C     N13 CONTROLS THE SKIPPING OF PAGES IN OUTPUT
C     NALG = 1 FOR STARTING  NALG= 2 FOR 4 POINT SCHEME
C     NC INDICATES CHANGES IN STEP SIZE
C     N14 CONTAINS ALPHAMERIC INFORMATION WHICH GETS WRITTEN OUT AS THE
C     HEA DING
      REAL Y(1),F(6,1),Y0(1),Y1(1),G(1)
      REAL NC
      INTEGER EOP,ECV
C     Y1 = INITIAL VALUES OF DEPENDENT VARIABLE
      DO 10 I = 1,N
   10 Y1(I) = Y(I)
C     INITIALIZE EVERYTHING IN SIGHT
      X = X0
      XP = X0 - 0.0004*HP
      H = HP
C     ERP IS THE MAX ERROR AT EACH POINT
      ERP = ABS(ERR*H/(XMAX-X0))
      HO24 = H/24.0
      N13 = 5
      NSTEP = 0
      NODES = 0
      NODXP = 0
      NALG = 1
      NC = 1.0
  100 IF (NODES-NODXP .GT.100)GO TO 485
C     LOOP POINT TEST FOR PRINTING
      IF (X -XP) 120,106,106
  106 N13 = N13 + 1
      NODXP = NODES
      IF (N13 .LE. 60) GO TO 108
      N13 = 0
  108 CALL PRFLE (Y(1),X)
C     PROFILE TAKES CARE OF PRINTING THE OUTPUT
```

```
      XP = XP + HP
C     TEST FOR STEP AHEAD
  120 IF (X- XMAX) 200,700,700
C     MARCH AHEAD - 1,2,3,4
  200 DO 202 I = 1,N
  202 YO(I) = Y(I)
      CALL DERIV(X,Y,G)
C     X= IND VARIABLE, Y= DEP VARIABLE (ARRAY) G=ARRAY OF DERIVATIVES
C     COMPUTED BY SUBROUTINE D
      DO 210 I =1,N
C     STORE DERIVATES IN F(1,I)
  210 F(1,I) = G(I)
      GO TO (220,240),NALG
C     TWO POINT PREDICTOR FOR STARTING
  220 DO 222 I = 1,N
  222 Y(I) = YO(I) + F(1,I)*H
      GO TO 250
C     FOUR POINT PREDICTOR FROM AMS P896
  240 DO 242 I = 1,N
  242 Y(I) = YO(I) + HO24*(55.0*F(1,I) -59.0*F(2,I) +37.0*F(3,I)
     1 -9.0*F(4,I))
  250 XN = X + H
      CALL DERIV(XN,Y,G)
      GO TO (260,270),NALG
C     TWO POINT CORRECTOR FOR STARTING
  260 DO 262 I = 1,N
  262 G(I) = YO(I) +0.5*H*(G(I) + F(1,I))
      GO TO 300
C     FOUR POINT CORRECTOR FROM AMS P896
  270 DO 272 I = 1,N
  272 G(I) = YO(I) +HO24*(9.0*G(I) +19.0*F(1,I) -5.0*F(2,I) +F(3,I))
C     ERROR CONTROL TEST
C     IF ECV = 0 CHECK IS ON SUM ABS(ERRORS) OTHERWISE ON THEKTH
C     VARIABLE
  300 IF (ECV) 302,302,319
  302 S = 0.0
      S1 = 0.0
      DO 308 I = 1,N
      IF (ABS(G(I)) .LT. 1.0E-4) N11 = 1
      IF (ABS(G(I)) .LT. 1.0E-5) GO TO 308
C     T IS THE DIFFERENCE BETWEEN THE PREDICTED AND CORRECTED VALUES
C     OF Y
  304 T = G(I) - Y(I)
C     S= ERROR TEST
      S = S + ABS(T/G(I))
  308 S1 = S1 + ABS(T)
      GO TO (318,310),NALG
  310 S = 0.25*S
  318 S = 0.25*S
C     CHECKS ON SIZE OF ERROR
      IF (S-ERP) 338,400,400
C     IF EOP = 1 ABSOLUTE VALUE OF ERROR MAINTEINED LE ABE
C     IF EOP=2 PERCENT ERROR LE ERP IF EOP=3 NO MESH SIZE CHANGE
  319 GO TO (320,330,600),EOP
C     VALUE OF ERROR BOUNDED
  320 S1 = ABS(G(ECV) -Y(ECV))
      N11 = 1
      S = 1000.0*ERP
      GO TO 331
C     PERCENT ERROR MAINTAINED
```

```
    330 IF (ABS(G(ECV)) .LT. 1.0E-5) GO TO 320
        N11 = 2
        S = ABS((G(ECV) - Y(ECV))/G(ECV))
        S1 = ABS(G(ECV) - Y(ECV))
    331 GO TO (334,332) , NALG
    332 S = 0.25*S
    334 S = 0.25*S
C       CHECKS ON SIZE OF ERROR
        IF (S -ERP) 338,400,400
    338 IF (S-0.005*ERP) 500,600,600
C       HALVE THE MESH SIZE- WILL TRAVEL
    400 IF (N11 .NE. 1) GO TO 403
        N11 = 4
        IF (S1 - ABE) 338,403,403
    403 IF (H/HP .LT. 2.0E-6) GO TO 480
    401 GO TO (402,420),NALG
C       TWO POINT SCHEME CUT OUT AND START OVER
C       SET Y EQUAL TO ITS INITIAL VALUES
    402 DO 404 I =1,N
    404 Y(I) = Y1(I)
        X = X0
        NSTEP = 0
        GO TO 430
C       FOUR POINT INTERPOLATION SCHEME   AMS P879
    420 DO 428 I =1,N
        F(5,I) = F(3,I)
        F(3,I) = F(2,I)
        F(2,I) = (15.0*F(1,I) +45.0*F(3,I) -15.0*F(5,I) +3.0*F(4,I))/48.0
        F(6,I) =(15.0*F(4,I) +45.0*F(5,I) -15.0*F(3,I) +3.0*F(1,I))/48.0
        F(4,I) =(-3.0*(F(4,I) +F(1,I)) +27.0*(F(5,I) +F(3,I)))/48.0
    428 Y(I) = Y0(I)
    430 H = 0.5*H
        HO24 = HO24*0.5
        NC = 2.0*NC
        GO TO (432,434) ,NALG
    434 ERP = 0.5*ERP
    432 GO TO 200
    485 WRITE (2,498)
    498 FORMAT (1H0,29HTOO MANY MESH POINTS REQUIRED/)
    480 WRITE (2,499) H,X
    499 FORMAT (13H0MESH SIZE H=,E12.3, 3X, 15HTOO SMALL AT X=, E12.3)
        GO TO 700
C       POSSIBLE MESH SIZE INCREASE
C       NC INSURES THAT H IS NOT MADE GREATER THAN HP
    500 IF (NC - 1.0) 600,600,502
C       NSTEP CHECKS TO SEE IF ENOUGH POINTS ARE AVAILABLE TO DOUBLE THE
C       MESH SIZE
    502 IF (NSTEP -5) 600,504,504
C       MESH SIZE IS DOUBLED ONLY AT PRINTING POINTS (XP)
    504 IF (XN - XP) 600,506,506
    506 DO 508 I = 1,N
C       DOUBLE MESH SIZE
        Y(I) = G(I)
        F (3,I) = F(4,I)
    508 F(4,I) = F(6,I)
        X = XN
        NSTEP = 2
        NC = NC/2.0
        ERP = 2.0*ERP
        H = 2.0*H
```

```
      HO24   = 2.0*HO24
      GO TO 607
C     THE NEW POINT IS SATISFACTORY  GET READY TO DO THE NEXT POINT
  600 DO 606  I = 1,N
      Y(I) = G(I)
      DO 606 J = 1,5
      K = 6-J
  606 F(K+1,I) = F(K,I)
      X = XN
  607 NODES = NODES + 1
  610 NSTEP = NSTEP + 1
C     DO WE HAVE ENOUGH POINTS TO USE THE 4 POINT SCHEME
      IF (NSTEP - 3) 620,612,612
  612 NALG = 2
      HO24 = H/24.0
  620 GO TO 100
  700 WRITE (2,720) X,ECV,EOP,ERR,ABE,H,S,NODES
      RETURN
  720 FORMAT (17HOTERMINATED AT X=,1PE10.3,3X,35HERROR PARAMETERS,ECV,EO
     1P,ERR,ABE,H=,2I4,3E13.3/1H , 10X,17HEST ERROR AT END=,E10.3,I10,2X
     2,5HSTEPS)
      END
```

References.

1. Cockrell D.J. , Diamond M.J. and Jones G.D. " The Diffuser
    Inlet Flow Parameter".   Jnl. Roy. Aero. Soc. ,V.69 ,May 1965

2. Rotta J.C. " The Turbulent Boundary Layer in Incompressible
    Flow ". Prog. Aero. Sci. , V.2 , Pt. 1 , 1962.

3. Jacobs W. Zeits. f. angew. Math. u Mech. , V.19 , 1939
    Translation : NACA T.M. 951 , 1940

4. Clauser F.H. "The Turbulent Boundary Layer " Advances in
    Applied Mechanics , V4 , 1956 , Academic Press , New York.

5. Batchelor G.K. " A Note on Free Turbulent Flows "
    Jnl. Aero. Sci. , V.17 , 1950

6. Hoagland L.C. " Fully Developed Turbulent Flow in Straight
    Rectangular Ducts ". M.I.T. Tech. Report No.2 on Contract
    D.A. 19 - 020 - ORD - 4538. Sept 1960

7. Bradshaw P. & Hellens G.E. " The N.P.L. 59" x 9" Boundary
    Layer Tunnel ". N.P.L. Aero. Report 1119 , Oct. 1964.

8. Tracy H.J. " Turbulent Flow in a Three dimensional Channel "
    Proc. A.S.C.E. , HY.6 , V.91 , Pt. 1 , Nov. 1965.

9. Pankhurst & Holder   " Wind Tunnel Techniques ".
    Pitman , 1956.

10. Goldstein S. " Modern Developments in Fluid Mechanics ".
    O.U.P. 1938.

11. Cooper & Tulin N.P. " Turbulence Measurements with a Hot Wire
    Anemometer ". AGARDograph No. 12 , 1955.

12. Collis D.C. " The Dust Problem in Hot Wire Anemometry ".
    Aero. Quart. , Vol.4 , 1952.

13. Dryden H.L. & Kuethe A.M. " The Measurement of Fluctuations of Air Speed by the Hot Wire Anemometer ". N.A.C.A. Report No. 320 , 1929.

14. Hinze J.O. " Turbulence ". McGraw - Hill , 1959.

15. Betchov R. Proc. Kon. Ned. Akad. Wetenschap Vol.51 , 1948.

16. Frenkiel F.H. " Effects of Wire Length in Turbulence Investigations with a Hot Wire Anemometer ". Aero.Quart., Vol.5 , 1954.

17. Champagne F.H. "Turbulence Measurements with Inclined Hot Wires ". Boeing Sci. Res. Labs. , Flight Sci. Lab. Report No. 103 , 1965.

18. Webster C.A.G. Jnl. Fl. Mech. , Vol.13 , 1962.

19. Dueller J.W. " Flow Direction Measurement by Hot Wire Anemometry ". Proc. A.S.C.E. , Eng. Mech. Div. , 1967.

20. Schubauer G.B. & Klebanoff P.S. "Theory and Application of Hot Wire Instruments ". N.A.C.A. Wartime Report W-86 , 1946.

21. Chu W.T. Annual Progress Report No.42. , Inst. for Aerospace Studies , Toronto Univ. , 1964.

22. Schlichting. "Boundary Layer Theory ". McGraw-Hill , 1962.

23. Ross D. " Turbulent Flow in the Entrance Region of a Smooth Pipe ". Trans. A.S.M.E. , Vol.78 , 1956.

24. Lakshamana R. " A General Method to Calculate the Settling Length for Pipe Flow ". Proc. "2nd. Australasian Conf. on Hyd and Fl. Mech. , N.Z. , 1965.

25. Bowlus D.A. & Brighton J.A. " Incompressible Turbulent Flow in the Inlet Region of a Pipe". Jnl. Basic Eng., Sept.1968.

26. Cockrell D.J. " The Development of Turbulent Boundary

Layers in the Inlet Region of Smooth Ducts and Pipes ".

To be published.

27. Hirst E. & Reynolds W. "An Integral Prediction Method for

Turbulent Boundary Layers using the Kinetic Energy Equation"

Report MD-21 , Dept.of Mech.Eng. , Stanford Univ., 1968.

28. Barbin A.R. & Jones J.B. " Turbulent Flow in the Inlet Region

of Smooth Pipes". Jnl. Basic Eng. , March 1963.

29. Comte - Belliot G. " Contribution a l'etude de la Turbulence

de Conduite " D.Sc. Thesis , Grenoble University , 1963.

30. Schubauer G.B. "Turbulent Processes as Observed in Boundary

Layer and Pipe". Jnl. App. Phys. , Vol.25 , 1954.

31. Holdhusen J.S. "The Turbulent Boundary Layer in the Inlet

Region of a Smooth Pipe" Ph.D. Thesis , Minnesota Univ.,1952.

32. Prandtl L. " The Essentials of Fluid Dynamics "

(Trans) Blackie , 1952.

33. Ludweig H. & Tillman W. "Investigations of the Wall Shearing

Stress in Turbulent Boundary Layers". N.A.C.A. , T.M.1285,

May 1950

34. Schultz & Grunow. " Neues Reibungswiderstandsgesetz für glatte

Platten ". Luftfahrtforschung Vol.17 , 1940.

35. Olson R.H. "Essentials of Engineering Fluid Mechanics ".

International Textbook Co. Ltd. , 1966.

36. Baines & Peterson. "An Investigation of Flow Through Screens"

Trans. A.S.M.E. , Vol.73 , 1951.

37. <u>Nikuradse J.</u> " The Principle of Turbulent Flow in Smooth
   Pipes". Forschung. Arb. Ing. Wessen. , No.356 , 1932.

38. <u>Franck N.</u> "The Model Law and Experimental Technique for the
   Determination of Wind Loads on Buildings ". Paper 15 , N.P.L.
   Symposium No.16 , June 1963.

39. <u>Torrance V.B.</u> Paper 31 , Loughborough Univ. Symp. on Wind
   Effects on Buildings and Structures , 1968.

40. <u>Klebanoff P.S. & Diehl Z.W.</u> " Some Features of Artificially
   Thickened Fully Developed Turbulent Boundary Layers ".
   N.A.C.A. Report 1110 , 1952.

41. <u>Logan E. & Jones J.B.</u> "Flow in a Pipe Through an Abrupt
   Increase in Surface Roughness". Jnl. Basic.Eng. , March 1963

42. <u>Jenson & Frank N.</u> "Model Scale Tests in the Turbulent Wind"
   Danish Technical Press , Copenhagen , 1963.

43. <u>Brighton J.A.</u> "Artificially Thickened Turbulent Boundary
   Layers by Means of Wires" A.S.M.E. , WA - FE - 29 , 1965.

44. <u>Elder J.W.</u> " Steady Flow Through Non - Uniform Gauzes of
   Arbitrary Shape" J.F.M. , Vol.5. , 1959.

45. <u>McCarthy J.H.</u> "Steady Flow Past Non-Uniform Wire Grids "
   J.F.M. , Vol.19 , 1964.

46. <u>Cockrell D.J. & Lee B.E.</u> "The Production of Shear Profiles in
   A Wind Tunnel" Jnl. R. Ae. Soc. , July 1966.

47. <u>Owen P.R. & Zienkiewicz H.K.</u> "The Production of Uniform Shear
   Flows in a Wind Tunnel" J.F.M. , Vol.2 , 1957.

48. <u>Rose W.G.</u> "The Results of an Attempt to Generate a Homogenious
   Turbulent Shear Flow" J.F.M. , Vol.22 , 1966.

49. Livesey J.L. & Turner J.T. "The Generation of Symmetrical
   Duct Velocity Profiles of High Uniform Shear". J.F.M. ,
   Vol.20 , 1964.

50. Wolf & Johnson J.P. "The Effect of Non-Uniform Inlet Velocity
   Profiles on Flow Regimes and Performance of a Two Dimensional
   Diffuser" Dept. of Mech. Eng., Stanford Univ., 1968.

51. Cowdrey C.F. "A Simple Method for the Design of Wind Tunnel
   Velocity Profile Grids " N.P.L. Aero. Note 1055 , 1967.

52. O'Neill P.G.G. " Experiments to Simulate a Natural Wind Velocity
   Gradient ". N.P.L. Aero. Note No.313 1956.

53. Brighton J.A. " Artificially Produced Boundary Layers ".
   Jnl. Basic Eng. , Vol. 87 , 1965.

54. Lau Y.L. " The Flow of Stratified and Homogenous Fluids
   through Curved Screens." T.P. 6604 , Dept. of Mech.Eng.
   Toronto Univ. , 1966.

55. Baines D.W. " The Effects of Velocity Distribution on Wind
   Loads." N.P.L. Symposium No.16 , 1963.

56. Turner J.T. " A Computational Method for the Flow Through
   Non-Uniform Gauzes." J.F.M. , Vol.36 , 1969.

57. Bonneville J.& Harper D. " An Analysis and Investigation of
   Two Dimensional Flow Through Screens." M.Sc. Thesis , Dept.
   of Mech. Eng. , M.I.T. , 1951.

58. Kotansky D.R. " The Use of Honeycombs for Shear Flow Generation"
   A.I.A.A. Jnl. , Vol.4 , 1966.

59. Schubauer G.B. & Spandenburg W.S. " Forced Mixing in Boundary
   Layers." J.F.M. , Vol.8 , 1960.

60. Taylor H.D. " Summary Report on Vortex Generators ."
   Rep. United Aircraft Corp. , No. R - 05280 - 9 , 1950.

61. <u>Armitt J.</u> " The Simulation of the Atmospheric Boundary Layer in a Wind Tunnel." C.E.R.L. , 1966.

62. <u>Counihan J.</u> " An Integral Method of Simulating an Atmospheric Boundary Layer." Atmospheric Environment Jnl. , Vol3 ,1969.

63. <u>Weighardt K.E.</u> " On the Resistance of Screens." Aero. Quart. , Vol. 4 , 1953.

64. <u>Collar A.R.</u> " The Effect of a Gauze on the Velocity Distribution in a Uniform Duct." A.R.C. , R. & M. 1867 , 1939.

65. <u>Taylor G.I. & Batchelor G.K.</u> " The Effect of a Wire Gauze on Small Disturbances in a Uniform Stream." Quart.Jnl. Mech. App. Math. , Vol.2 , 1949.

66. <u>Davenport</u> " The Relationship of Wind Structure to Wind Loading." N.P.L. Symposium No.16 , 1963.

67. <u>Thompson B.G.J.</u> "A Critical Review of Existing Methods of Calculating the Turbulent Boundary Layer." A.R.C., R. & M. 3447 , 1964.

68. <u>Head M.R.</u> " Entrainment in the Turbulent Boundary Layer." A.R.C. , R. & M. 3152 , 1958.

69. <u>Reynolds W.C.</u> "A Morphology of Prediction Methods." A.F.O.S.R. - I.F.P. - STANFORD. , Conf. on Turb. B.L. Pred., Stanford Univ. , 1968.

70. <u>Clauser F.H.</u> " Turbulent Boundary Layers in Adverse Pressure Gradients." J. Aero. Sci., Vol.21 , 1954.

71. <u>Moses H.L.</u> " The Behaviour of Turbulent Boundary Layers in Adverse Pressure Gradients." M.I.T. , 1964.

72. Goldberg P. "Upstream History and Apparent Shear Stress in Turbulent Boundary Layers." Gas Turbine Lab. M.I.T. Report No. 85 , 1966.

73. Fediavesky K. "The Turbulent Boundary Layer on an Airfoil " (Trans) N.A.C.A. , T.M. 822 , 1937.

74. Interpolation and Allied Tables. H.M.S.O. , 1955.

75. Hirst E. & Reynolds W. " An Integral Prediction Method for Turbulent Boundary Layers." Report M.I.-21 , Dept. of Mech. Eng. Stanford Univ. 1968.

76. Townsend A.A. "The Structure of Turbulent Shear Flow" C.U.P. , 1962.

77. Bradshaw P.,Ferris D.H. & Atwell N.P. "The Calculation of Boundary Layer Development using the Turbulent Energy Equation" N.P.L. Aero, Report 1182 , 1966.

78. McDonald H. "The Departure from Equilibrium of Turbulent Boundary Layers." Aero. Quart., Vol. 19 , 1968.

79. Rotta J. " Statistische Theorie Mehthomogener Turbulenz " Z. fur Physik , Vol. 131 , 1951.

80. Bossinesq J. "Theorie de l'ecoulement Tourbillant " Mem. pres. par. div. Savants a l'Acad. Sci., Paris , Vol.23 , 1877.

81. Mellor G. & Gibson D. "Equilibrium Turbulent Boundary Layers" FLD No.13 , Dept. of Aerospace and Mech. Sci., Priceton Univ. 1963.

82. Mellor G. "The Effect of Pressure Gradients on Turbulent Flow near a Smooth Wall." FLD No.14 , Dept. of Aerospace and Mech. Sci., Princeton Univ. , 1964.

83. Townsend A.A. "The Eddy Viscosity in Turbulent Shear Flow"
Phil. Mag. , Vol.41 , 1950.

84. Rapier A.C. "Forced Convection Heat Transfer in Passages
with Varying Roughness." Proc. I. Mech. E. ,Vol.178,1963-64.

85. Bennet E.J. "A Study of Turbulent Flow in Simple Ducts."
C.E.G.B. , Berkley Labs. , RD/B/N630 , 1966.

86. Gosse J. "A Discussion of the Variation of Eddy Viscosity"
C.R. Acad. Sci. (France), Vol.253 , 1961.

87. Gosse J. "Established Turbulent Flow in Pipes."
C.R. Acad. Sci.(France) , Vol 257 , 1963

88. Schetz J. & Jannore U. "Planar Free Turbulent Mixing with an
Axial Pressure Gradient" Jnl. Basic.Eng., Dec. 1967.

89. Prandtl L. Z.A.M.M. , Vol 22 , 1942.

90. Deissler R.G. "An Investigation of Turbulent Flow and Heat
Transfer in Smooth Pipes." Trans. A.S.M.E., Vol.73 , 1951.

91. Sleicher C.A. Jnr. "Experimental Velocity and Temperature
Profiles for Air in Turbulent Pipe Flow." Trans. A.S.M.E.
Vol. 80 , 1958.

92. Reichardt H. "The Principles of Turbulent Heat Transfer."
(Trans) N.A.C.A. T.M. 1408 , 1957.

93. Elrod H.G. Jnr. "A Note on Turbulent Shear Stress near a
Wall." J. Aero. Sci. , Vol.24 , 1957.

94. Kleinstein G. "A Generalized Law of the Wall and Eddy
Viscosity Model for Wall Boundary Layers." A.I.A.A. Jnl.
Vol.5 , 1967.

95. Glushko G.S. "The Turbulent Boundary Layer on a Flat Plate"
Izv. Akad. Nauk. SSSR. Mekh., Vol.4 , 1965.

96. <u>Patanker S. & Spalding D.B</u>. "A Finite Difference Procedure
for Solving the Equations of the Two Dimensional Boundary
Layer." Int. Jnl. Heat Mass Transfer , Vol.10 , 1967.

97. <u>Kolmogorov A.N</u>. "Equations of the Turbulent Motion of an
Incompressible Fluid." Izv. Akad. Nauk. S.S.S.R., Ser.
Phys., Vol. 6(1/2) , 1942.

98. <u>Prandtl L</u>. "Üben ein neues Formelsystem für die ausgebildete
Turbulenz." Nachrichten der Akad. Wiss. , Gottingen , Math.,
Phys., Vol.6 , 1945.

99. <u>Tyulpanov R.S</u>. "Some Flow Peculiarities in Very Rough Tubes"
(Trans) Int. Chem. Eng. , Vol.5 , 1965.

100. <u>Phillips O.M</u>. " The Maintenance of Reynolds Stresses in
Turbulent Shear Flow." J.F.M. , Vol.27, 1967.

101. <u>Cess R.D</u>. "A Survey of the Literature on Heat Transfer."
Westinghouse Research Report No. 8-0529-R 24 , 1958

102. <u>Corcoran W.H., Opfell J.B. & Sage B.H</u>. "Momentum Transfer
In Fluids." Academic Press , New York , 1956.